REPORT DOCUMENTATION PAGE

Form Approved
OMB No. 0704-0188

(2)

AD-A231 848

2. REPORT DATE	3. REPORT TYPE AND DATES COVERED
Dec. 1990	Final 9-8-87 - 9-30-90

4. TITLE AND SUBTITLE

Focused Ion Beam Fabrication of Microelectronic Structures

5. FUNDING NUMBERS

DAAL03-87-K-0126

6. AUTHOR(S)

Dr. John Melngailis

7. PERFORMING ORGANIZATION NAME(S) AND ADDRESS(ES)

Research Laboratory of Electronics
Massachusetts Institute of Technology
77 Massachusetts Avenue
Cambridge, MA 02139

8. PERFORMING ORGANIZATION REPORT NUMBER

9. SPONSORING/MONITORING AGENCY NAME(S) AND ADDRESS(ES)

U.S. Army Research Office
P.O. Box 12211
Research Triangle Park, NC 27709

10. SPONSORING/MONITORING AGENCY REPORT NUMBER

ARO 24871.7-EL

11. SUPPLEMENTARY NOTES

The view, opinions and/or findings contained in this report are those of the author(s) and should not be construed as an official Department of the Army position, policy, or decision, unless so designated by other documentation.

12a. DISTRIBUTION/AVAILABILITY STATEMENT

Approved for public release; distribution unlimited.

12b. DISTRIBUTION CODE

13. ABSTRACT *(Maximum 200 words)*

The work of Dr. Melngailis and his collaborators is summarized here

14. SUBJECT TERMS	15. NUMBER OF PAGES
	16. PRICE CODE

17. SECURITY CLASSIFICATION OF REPORT	18. SECURITY CLASSIFICATION OF THIS PAGE	19. SECURITY CLASSIFICATION OF ABSTRACT	20. LIMITATION OF ABSTRACT
UNCLASSIFIED	UNCLASSIFIED	UNCLASSIFIED	UL

"Focused Ion Beam Fabrication of Microelectronic Structures"

Final Report

September 8, 1987 to September 30, 1990

U.S. Army Research Office

Contract DAAL03-87-K-0126

by

John Melngailis

Research Laboratory of Electronics

Massachusetts Institute of Technology

Table of Contents

ABSTRACT

The development of the capability focusing many species of ions to beam diameters well below 0.1 μm has led to many applications, from the repair of photomasks and integrated circuits to the fabrication of quantum effect devices. The work reported here has concentrated on ion induced deposition. This novel method of film growth combines patterning and deposition in a single step. It is used in repair processes to locally add material, and it may also be useful in making conductors and contacts in-situ, for example, on III-V compounds which cannot be exposed to the ambient between MBE growth steps. In ion induced deposition a local gas ambient of, for example, an organometallic , is created where the ion beam is incident. A film grows where the beam is scanned.

We have demonstrated, characterized, and developed focused ion beam induced deposition of gold and platinum. Features down to 0.1 μm line width have been written as well as, thick (~ 1 μm) features with steep sidewalls. The microstructure of the gold and platinum deposits has been studied by transmission electron microscopy (TEM). The Pt deposits were found to be amorphous while the gold growth begins as islands an becomes columnar. Measurements were made of the dependence of growth rate on average ion current, ion energy, ion species, and precursor gas pressure and a macroscopic and microscopic model of the process developed. The atomic mechanism of the process appears to consist of an excitation of the substrate by the collision cascade produced by the incoming ion which decomposes the adsorbed gas molecules in the excited area. We have successfully made circuit repairs by depositing jumpers between two existing conductors on an integrated circuit, and have made gold contacts directly on bare GaAs substrates. For the case of platinum we have measured the deposition rate as a function of angle of incidence. The results of this work have been described in eight published papers two of which were invited review papers.

I. INTRODUCTION

Activity in the field of focused ion beam microfabrication has increased steadily over the past decade. A recent bibliography shows a total of 1100 entries.[1] Numerous potential and already demonstrated applications are possible due to the fact that beams of many ion species can be focused to dimensions below 0.1 μm and that the ion-surface interaction is multifaceted. Energetic ions (the relevant range in this field has been 1-300 keV) incident on a surface will: a) sputter off material, b) implant the substrate, c) produce local damage or heating d) cause chemical reactions on the surface or in the bulk, and e) induce secondary electron emission. The ability to affect material in these many ways at dimensions used in microfabrication is clearly of interest.

The applications can be grouped into two categories each served by a somewhat different machines. Our program of research at MIT spans both categories, although this report concentrates on research done with the lower energy machine.

A. Higher Energy Columns with Mass Separation

Implantation and lithography are demanding applications and require columns at higher energies, with a choice of ion species, and with sophisticated, precision pattern writing. Such columns are available up to 150 kV accelerating potentials, with alloy liquid metal sources, and ExB mass separation in the column. Numerous ion species can be obtained including the main dopants of Si and GaAs. (e.g., B, As, Si, Be or Zn). Since some species are doubly ionized, incident ion energies on the sample up to 300 keV are available.[2]

This higher energy is often needed for implantation and for lithography in thick resist. Be^{++} ions at 300 keV could expose resist up to 1.2 μm thick. The advantage of ion lithography vs. e-beam is the absence of proximity effect i.e. the ions expose resist in a well defined volume surrounding the point of entry. For example, we have made x-ray masks with 50 nm features by exposing 0.3 μm thick PMMA with 280 keV Be^{++} ions. (Ref. 3)

Implantation with focused ion beams can be carried out without the use of mask and resist. In addition, one has point to point control of the dose. Thus, for example, one can make devices with lateral gradients of doping, or with implantation dose varied from device to device. For example, we have exploited this to make tunable Gunn diodes[4], unique high performance MOSFET's in silicon[5], and CCD's with a gradient of doping in the channels which increases the clocking frequency by 16 fold.[6]

B. Lower Energy Columns without Mass Separation

These columns usually operate in the range of 15-60 keV with Ga^{+} ions. Beam diameters down to 0.05 μm are attainable with current densities in the beam spot of $4A/cm^2$. The main commercial applications of these columns, namely, photomask repair and integrated circuit restructuring, diagnostics and repair, exploit sputtering and ion induced surface chemical reaction. Detection of the secondary electrons is used for imaging much like in a scanning electron microscope. Unwanted material such as an opaque defect on a photomask or an erratic electrical connection in an integrated circuit are simply milled off. Missing material such as a clear defect on a mask or a broken or omitted electrical connection is added with submicron resolution using ion induced deposition.

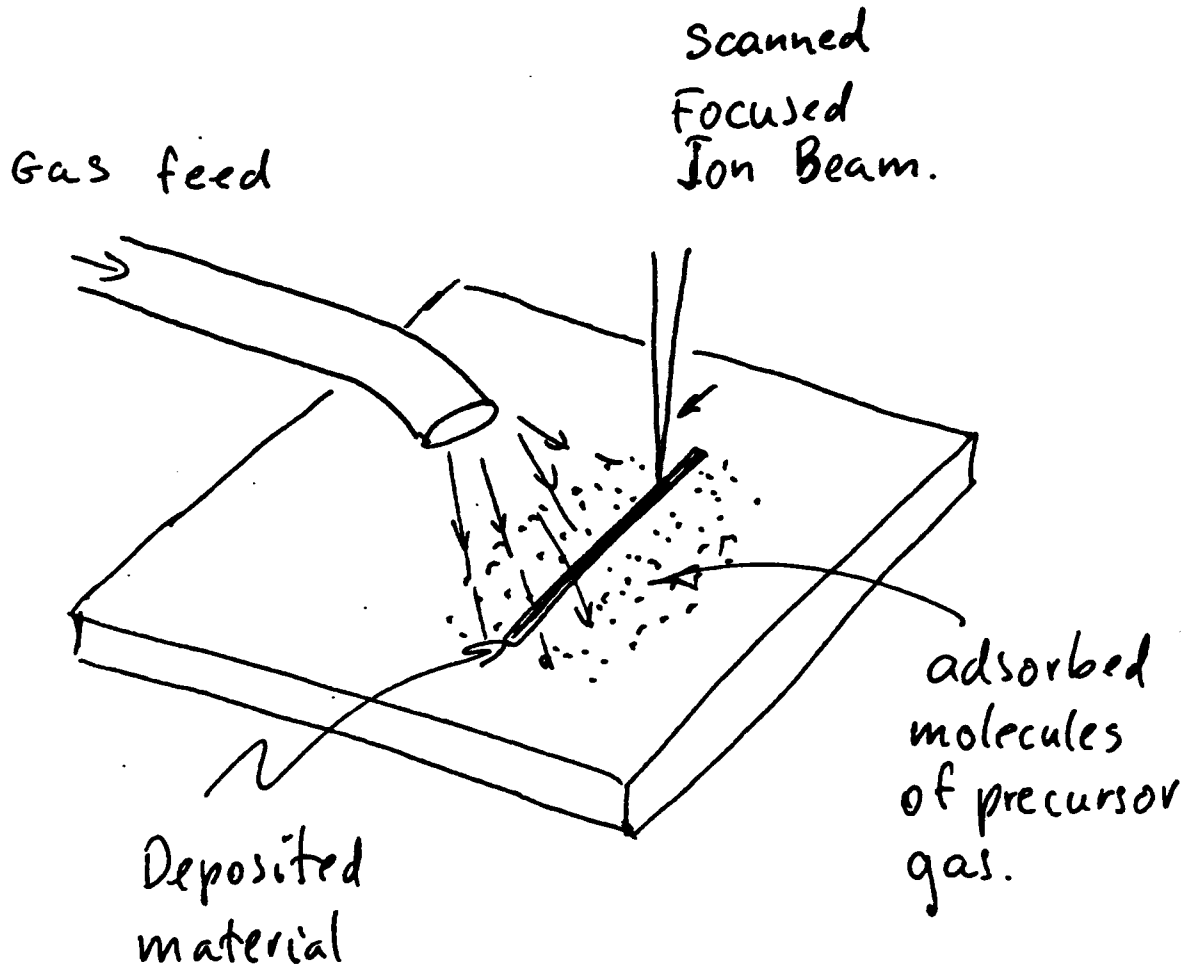

Fig. 1 Schematic of focused ion beam induced process.

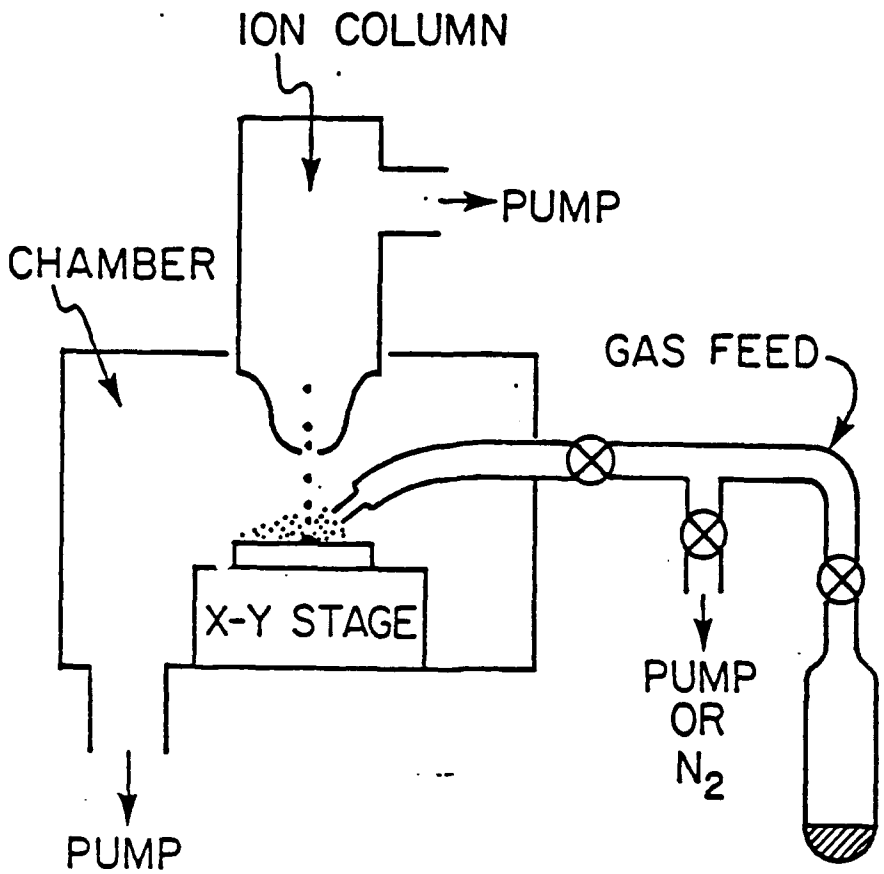

Fig. 2 Schematic of focused ion beam induced deposition apparatus showing a differentially pumped ion column. A gas feed creates a local gas ambient in the area scanned by the focused ion beam. When low vapor pressure materials are used as the gas source, such as $W(CO)_6$, the entire gas feed system may need to be heated.

Table 1. Ion Induced Deposition of Conducting Films

Gas (Reference)	Ion, Energy	"Yield" (atoms/ion)	Deposit Composition	Resistivity ($\mu\Omega$cm)
WF_6 (1)	Ar^+ 750 eV	5	W:O:C 90:5:5	350 (Bulk W = 4.6)
WF_6 (2)	Ar^+ 500 eV		W:F:C 93.3:4.4:2.3	15
$W(CO)_6$ (3)	Ga^+ 25 keV	2	W:C:Ga:O 75:10:10:5	150 - 225
$W(CO)_6$ (4) (40°C)	Ga/In/Sn 16 keV		W:C:O 50:40:10	100
$C_7H_7F_6O_2Au$ (5)	Ga^+ 40 KeV (room T)	3-8	Au:C:Ga 50:35:15	500-1500 (Bulk Au = 2.44)
$C_7H_7F_6O_2Au$ (6)	Ga^+ 40 KeV at 120°C	3	Au:C:Ga *80:10:10*	3-10
$C_9H_{17}Pt$ (7)	Ga^+ 35 KeV	0.2-30	Pt:C:Ga:O 45:24:28:3 24:55:19:2	70-700 (Bulk Pt = 10.4)

(1) H.Lezec, MIT (unpublished).
(2) Z. Xu T. Kosugi, K. Gamo, and S. Namba, J. Vac. Sci. Technol. B7, 1959 (1989).
(3) D.K. Stewart, L.A. Stern, and J.C. Morgan, SPIE (1989).
(4) Y. Madokoro, T. Ohnishi, and T. Ishitani, Riken Conf., Mar. 1989.
(5) P.G. Blauner, J.S. Ro, Y. Butt, and J. Melngailis, J. Vac. Sci. Technol. B7, 609 (1989).
(6) P.G. Blauner, Y. Butt, J.S. Ro, C.V. Thompson, and J. Melngailis, J. Vac. Sci. Technol. B7, 1816 (1989).
(7) T. Tao, J. Melngailis, Z. Xue, and H.D. Kaesz, EIPB 1990 and to be published J. Vac. Sci. Technol. (1990).

In this process a local ambient of a precursor gas, for example, an organometallic, is produced where the ion beam is scanned in a desired pattern. Adsorbed molecules are broken up by the incident ion beam (see Fig. 1 and Fig. 2) leading to deposition with submicrometer resolution.[7, 8] (Ref. 7 & 8 included as Appendix I and II).

This process is similar to laser induced deposition which can also be used for repair and circuit modification. The ion beam process, however, has the advantage that the beam diameter can be much smaller. For example, in ion lithography lines down to 15 nm width have been exposed in PMMA. (Ref. 9) So far 0.1 μm wide lines have been written by focused ion beam induced deposition[10] (Ref. 10 is Appendix V).

Electron beams have also been used to induce deposition[11, 12] and in principle are also capable of very fine dimensions. A practical drawback is that the same tool cannot be used for both material addition and material removal as conveniently, i.e. electrons do not sputter.

Since the first report of focused ion beam induced deposition[13], numerous materials have been deposited. A list of the more recent results is given in Table I. In some cases broad ion beams have also been used to study the phenomena, since at an atomic level the diameter of the beam is not an issue. One of the main problems of the deposited films has been their low purity and consequently high resistivity. Since the precursor gases in many cases contain carbon and oxygen as constituents, the deposited films often contain these elements as impurities. (As will be discussed below we have, in some cases been able to overcome this.)

C. Future Applications of Ion Induced Deposition

One of the challenging applications of focused ion beam induced deposition is x-ray mask repair. In x-ray masks the absorber must be of high Z material and must be of high aspect ratio. Deposition over existing topology will also be needed. Minimum linewidth being considered for production is 0.25 μm and feature height is between 0.3 and 1 μm depending on the energy of the x-rays used.[14] Since the masks are expected to have many millions of features, the probability of a few defects is high. Thus some repair process is needed. Focused ion beam induced deposition provides one of the most likely candidates for the rebuilding of missing absorber. As will be discussed below we have obtained some promising results, but much more work is still needed.

Another challenge is in the repair of integrated circuits, usually in the prototyping phase. In order to remake a missing connection in a circuit a good conductor is desirable. Many of the earlier attempts to deposit for example, Al and W led to very impure materials essentially, insulators, with high concentrations of carbon and oxygen.[15] This is partly due to the reactivity of those metals. Recently, as will be discussed below, low resistivity gold and platinum have been obtained.

The availability of good conductors opens the possibility of combining ion induced deposition with projection ion lithography.[16] In ion projection lithography line widths down to 0.15 μm have been demonstrated with fields of 3 x 3 mm. Noble gas ions, such as He, have been used. The current density is of order 10^{-3} A/cm^2. This if a yield of 10 atoms deposited per ion is assumed, a 0.1 μm thick film would be formed in 10 sec. This, in principle, would be an entire patterned film of conductors with 0.15 μm minimum linewidth over several millimeter size areas.

Perhaps the most exciting application of focused ion beam induced deposition is in the area of in-situ fabrication of contacts and conductors, particularly when combined with other vacuum processing such as MBE. There the ability to deposit metal in a fine submicron pattern without exposing the sample to the ambient will open the door to new device possibilities. The challenge is to deposit pure, low resistivity metal with submicron resolution and to avoid or mitigate the effects of ion implantation or ion damage to the substrate.

II. WORK PERFORMED

Focused ion beam induced deposition promises to be an important microfabrication technique. Our group's contributions to this field include: the first ion induced deposition of gold, the smallest reported linewidth, the lowest reported resistivity, macroscopic and microscopic models of the process, the first deposition of platinum, measurement of deposition yield as a function of angle of incidence, and the first actual circuit restructuring through a passivation layer. We have also made contacts to GaAs using ion induced deposition. Most of these results have been presented in detail in published papers which are included as appendices to this report. The highlights of the results will be described below.

A. Microstructure of Gold

In our first demonstration of the deposition of gold from dimethylgold hexafluoroacetylacetanate ($C_7H_7O_2F_6Au$) Auger analysis showed that the film contained substantial percentages of carbon.[17] Its resistivity was measured to be at least 200 times higher than bulk gold. This led us to investigate the microstructure of the films grown by ion induced deposition.

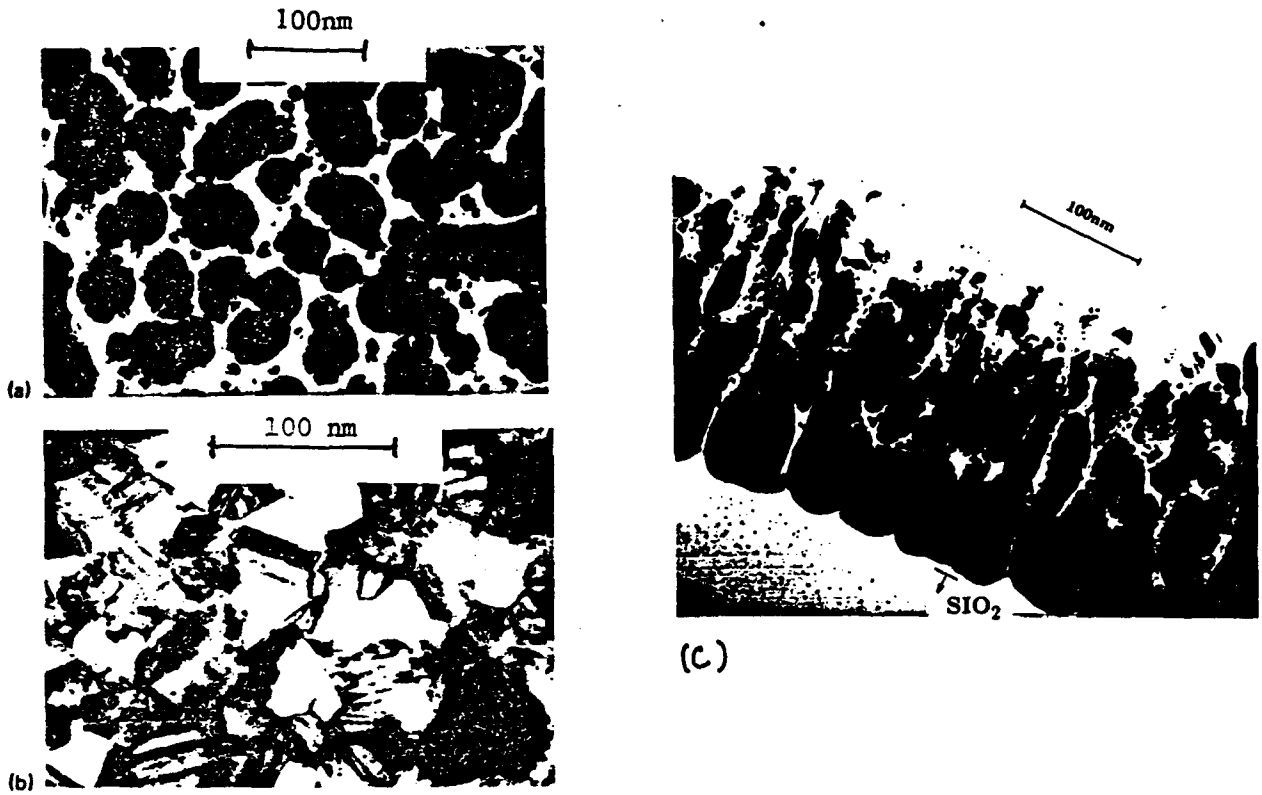

Fig. 3 Transmission electron micrographs of gold films grown by ion-induced deposition at two substrate temperatures: (a) Room temperature, nominal thickness 60 nm, 70 keV Ar^+ ions at 0.7 $\mu A/cm^2$, total dose $1x10^{16}/cm^2$. Film is seen to be made up of unconnected gold islands. This discontinuous columnar structure was observed by cross sectional TEM to persist even to 250 nm thicknesses. (b) 160°C, otherwise same conditions, thickness 100 nm. Film is seen to be continuous and has the microstructure typical of conventionally evaporated films. (c) Cross sectional TEM of a 250 nm thick film grown under the same conditions as (a) above. A columnar structure is seen to form.

The microstructure was investigated by transmission electron microscopy (TEM). To examine the early stages of growth the gold was deposited on a thin (~ 0.1 μm) membrane of SiO_2/SiN created by back-etching part of a Si wafer which has this membrane material grown on it. An Ar ion beam at 70 keV was used. The result was surprising. The film was found to grow as islands of gold in a carbon matrix. See Fig. 3. E-beam evaporated gold films of comparable thickness (60 nm) appear continuous and composed of polycrystalline grains. Thicker films were examined by TEM in cross section by very challenging potting and thinning techniques. Sample results are shown in Fig. 3. The island structure seen in the early stages of growth is found to become a columnar structure.[18] (Included as Appendix III). This is of intrinsic scientific interest and also of practical importance. The disconnected structure explains the high resistivity of the deposited films and points to possible diminution of x-ray opacity of the structures when they are used for x-ray mask repair.

We have also verified that the same kind of structures are produced when the gold films are deposited using a focused Ga ion beam.[19] (See Appendix IV). In addition with the Ga ions the average current density could be varied and we found that the island structure became coarser as the current was increased i.e. the average island size was 10 to 20 nm at 14μA/cm^2 and increased to 50 to 70 nm at 217 μA/cm^2. Reducing the local gas pressure at the point of deposition (by raising the tube in Fig. 1.) also increased the island size.[19] (See Appendix IV.)

Perhaps the most interesting result of these microstructure studies was that raising the temperature of the substrate to 100° C or above yielded continuous polycrystalline gold films with greatly reduced carbon content and with a resistivity which approached the bulk value.[18] (Appendix III) this

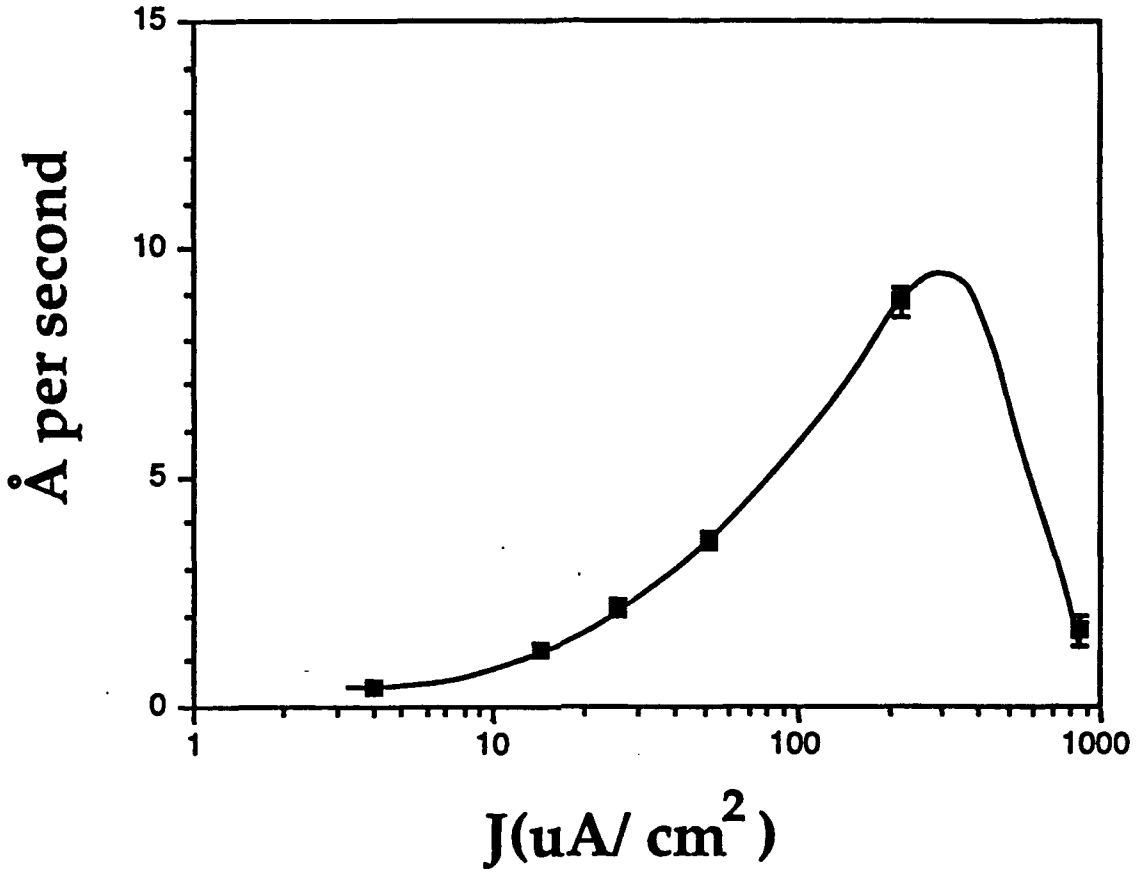

Fig. 4 The vertical growth rate of a gold film vs the average current density at a precursor gas pressure of 10 mTorr. The solid line merely serves to correct the points.

was first verified with the 70 keV Ar^+ ions, and later with Ga^+ ions as will be discussed below. The effect of raising the temperature is presumably to speed up the desorption of the carbon containing reaction products.

B. Macroscopic Models

Even in our earliest experiments we observed that the deposition yield decreased and became negative (i.e., sputtering resulted) if the focused ion beam was scanned too slowly.[17] A too high instantaneous flux of ions depletes the adsorbed gas film. The deposition rate of the gold film was, therefore, measured as a function of gas pressure and average current density, and a simple model of the process was fitted to the data.[10] (See Appendix V) To vary the gas flux to the surface in a controlled fashion the local pressure on the surface as a function of tube height was calibrated using a stagnation tube. Deposition experiments were then carried out at various tube heights and current densities. If one is interested in the total vertical growth rate of a film, then there is an optimum average current density of about 200 $\mu A/cm^2$. (See Fig. 4) A higher current density depletes the gas and enhances sputtering while for low current densities the growth rate is just proportional to the current density. In all of these experiments the focused ion beam was scanned over a given area fast enough so that beam transient effects played no role, i.e. the growth rate was independent of scan rate. The various values of average current density were obtained by adjusting the ion current and the scanned area.

C. Microscopic Models

The atomic mechanism by which an incident, energetic ion decomposes a number of adsorbed molecules has not been hitherto

understood. Direct ion-molecule impact cannot explain the high yields (sometimes of order 100) produced in monolayer adsorbates. The area over which an incoming ion decomposes the adsorbate can be of order 10 nm in diameter.

The first step in pinning down the atomic mechanism is to determine how the yield scales with ion energy and ion mass. We have measured the yield of gold deposited from dimethylgold hexafluoro acetylacetonate for noble gas ions from 2 kV to 10 kV and for 30 to 100 kV. For the lower range the deposition was carried on a special ion beam apparatus at IBM Research at Yorktown using a quartz crystal microbalance to measure in-situ both adsorbate film thickness vs pressure and gold film thickness deposited. (This work was performed by MIT graduate student A.D. Dubner who completed his Ph.D. thesis in July 1990, and was supported by IBM. It is included here to complete the picture).

One of the useful results of this work was the observation that at room temperature the adsorbate covers the surface with a monolayer over most of the pressure range of interest. Thicker films can be adsorbed by going to lower temperatures (say 10°C) and higher pressure (over 10 mtorr).[20] To make interpretation easier all measurements were taken in the monolayer regime.

The deposition occurs as a result of competition between the material addition by dissociation of the adsorbate and the sputtering of the gold film by the incoming ions. The net yield is directly measured, and the sputter yield is measured by turning off the adsorbate gas supply and noting the material removal rate. The sum of the net yield and the sputter yield is the total dissociaton yield, which is the quantity of interest in the microscopic modeling. The total yield increases with increasing mass and increasing ion energy.[21, 22] It correlates much better with the nuclear stopping power than

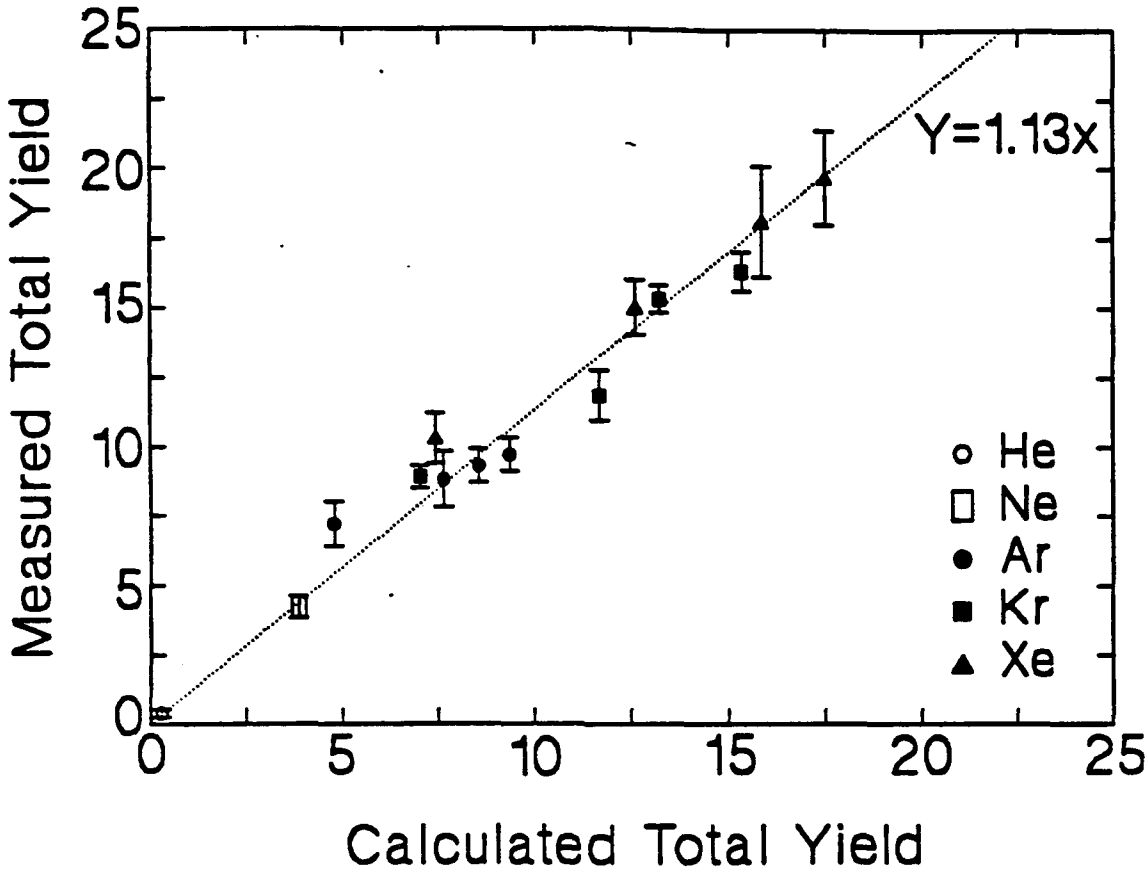

Fig. 5(a) A plot of the measured total decomposition yield vs. the calculated yield. The measurements were carried out at 25°C and 0.1 millitorr of $C_7H_7O_2F_6$ Au gas. The calculations were done with the collision cascade model. For each species of ion the different data points are for different energies: 2, 5, 9.5 and 10 kV. The dashed line is a least squares fit to the data forced through the origin. From Ref. 22.

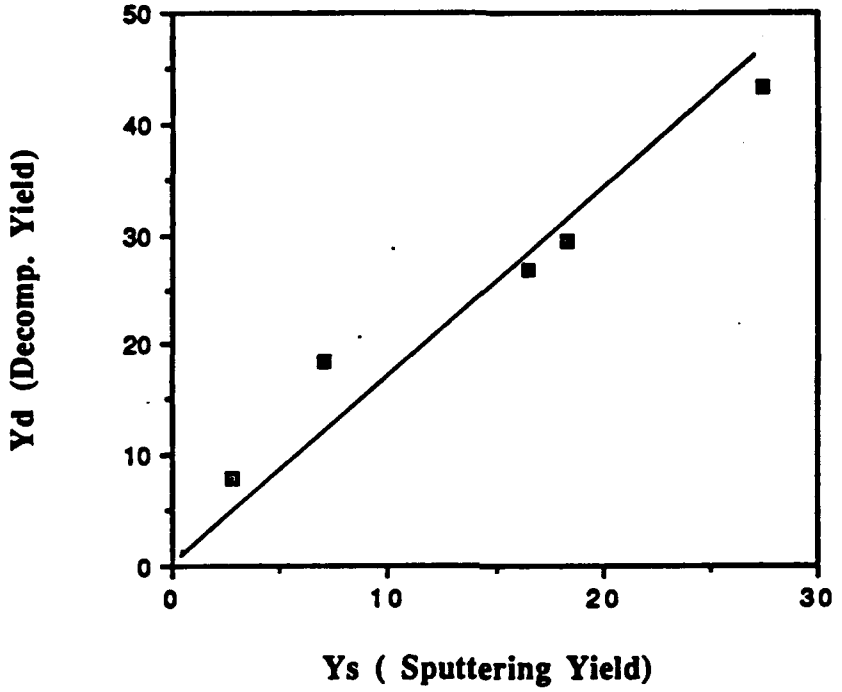

Fig. 5(b) A plot of the measured total decomposition yield vs the measured sputtering yield. The data points,in order of increasing yield, are for 50 keV Ne, 70 keV Ar, 45 keV Kr, 100 keV Kr, and 100 keV Xe. The fact that decomposition yield correlates with sputter yield indicates that the atomic collision cascade model which has been fitted to the low energy results will also fit to the high energy results, since the model is successful in predicting sputter yields. More data has recently been obtained and will be fitted to the collision cascade model.

with the electronic stopping power. A collision cascade model based on the Monte-Carlo simulation of ion penetration in the solid appears to fit the data well. In this model an ion penetrates the solid scattering atoms which in turn scatter other atoms. Some of these atoms reach the surface. Dissociation occurs when surface atoms have enough energy (0.95eV in this case) to break up the adsorbed molecules. (Sputtering, by the way, occurs if the gold surface atoms acquire enough energy to break all bonds and leave the solid. This takes about 3.8eV for gold.

The yield for the different ions species and energies used was calculated and compared to the measured total yield. The result is shown in Fig. 5(a). This covers the low energy range done on the special apparatus at IBM. The fit is seen to be quite good lending credence to this model of the atomic process.

The results at the higher energy range obtained at MIT are shown in Fig. 5(b). The same model will be fitted to these results as well as more recent results but this work is not yet complete.

D. Minimum dimensions and low resistivity

As the dimensions of microfabricated structures shrink the interest in any processes that can deposit material at 0.1 μm and below increases. In particular ion induced deposition is challenged by x-ray lithography mask repair where there is a need to deposit 0.25 μm dimension structures with 0.025 μm dimensional control. Similarly integrated circuit restructuring and repair will demand smaller dimensions. Our focused ion beam used for these experiments was able to achieve a beam diameter of about 60 nm, limited mainly by vibration. The narrowest line we were able to write with this beam was 0.1 μm, as shown in Fig. 6. By scanning the beam repeatedly over a

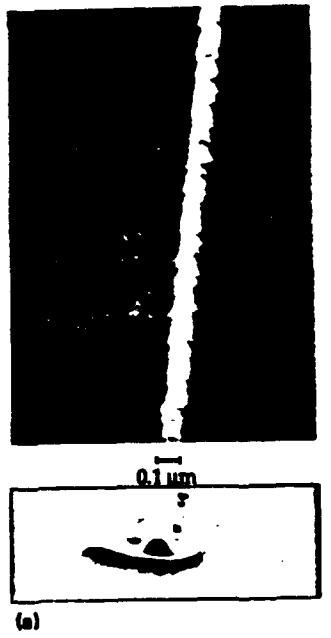

Fig. 6 SEM of deposited Au line shown in perspective (top) and in cross section (bottom). This line was written using a 50-pA 40-keV Ga^+ beam focused to <0.1μm diameter. The line is 25 μm long and was written in 30 s. The feature in the foreground of the cross section is an artifact of the beam not being blanked at the end of a line.

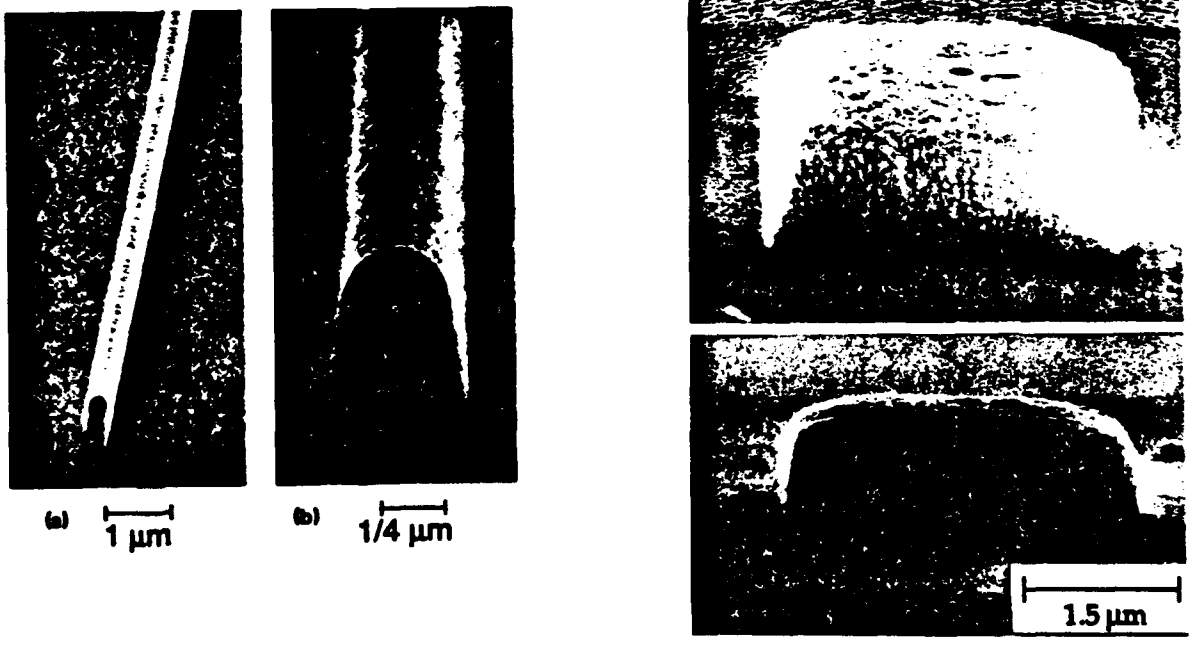

Fig. 7 Scanning electron micrographys of high aspect ratio deposits on the left (a) in perspective and (b) in cross section a line 100 μm long 0.75 μm high a rapidly scanned 20 pA 40 KV Ga ion beam was used. On the right a 3.4x3.4 μm deposit 1 μm thick, a structure of interest to x-ray mask repair.

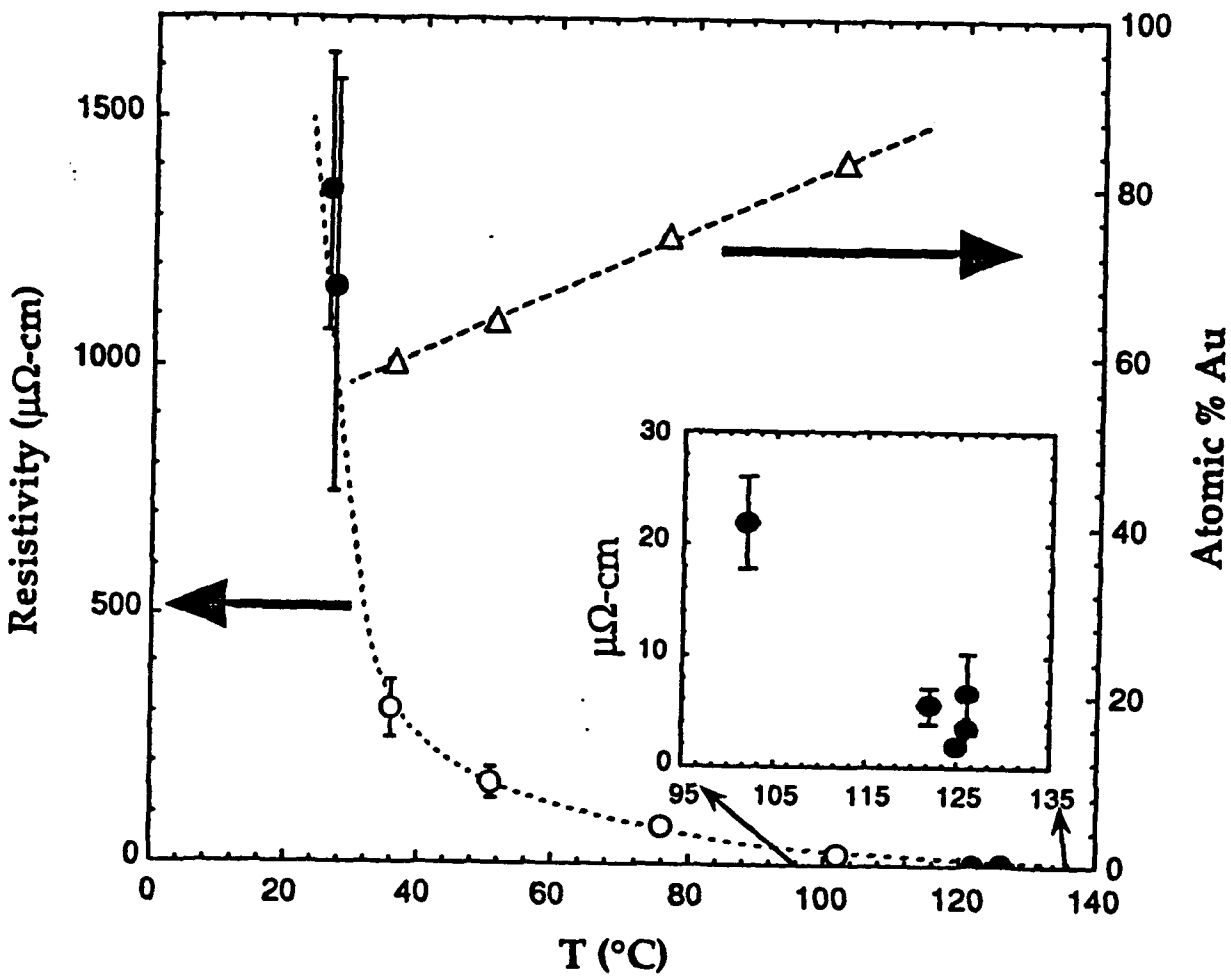

Fig. 8 Resistivity of gold film grown by ion induced deposition vs. temperature of substrate during growth. The resistivity of bulk gold is 2.44 μΩcm. On the right hand axis the atomic % of gold is shown. The film at 100°C had a composition of 80% Au, 10% C, 10% Ga.

7. (See Ref. 10, Appendix V). As also shown in Fig. 7, the best high aspect ratio single line we have written was 0.3 μm wide and 0.75 μm high.[23] (Appendix VI). Such high aspect ratio features are needed for x-ray lithography mask repair. All of these depositions were carried out at room temperature, and the "gold" films contained from 30 to 50% carbon. Their resistivities were typically over 100 μΩcm.

Prompted by the observation that the gold films deposited using Ar^+ ions at temperatures above 100°C had higher purity and lower resistance, we constructed a heated stage for our focused ion beam machine, and deposited gold films at substrate temperatures from 25°C to 135°C. These films were deposited across conducing fingers connected to probe pads and their resistivity was measured. The results are shown in Fig. 8. (See also Ref. 23, Appendix VI). The resistivity is seen to fall rapidly as a function of substrate temperature during deposition. The gold content is also seen to rise. The abrupt and large drop in resistivity is not merely due to increase in film purity but, we believe, largely due to a change in the crystal structure as observed previously (Ref. 17, Appendix III). At 120-125°C the resistivity is found to be about $5.5 \pm 3\mu\Omega$cm; i.e. within experimental error of the bulk gold value. This is the lowest resistivity reported by focused ion beam induced deposition by at least a factor of 20.

E. Platinum deposition

Focused ion beam induced deposition of plantinum has several attractions. Platinum is a slightly better x-ray absorber than gold or tungsten. It is preferred for integrated circuit repair because it is not a fast diffusing containment of silicon like gold is. We have achieved the first focused ion beam induced platinum deposition using (Methylcyclopentadienyl)-

CIRCUIT REWIRING BY FOCUSED ION BEAM INDUCED DEPOSITION

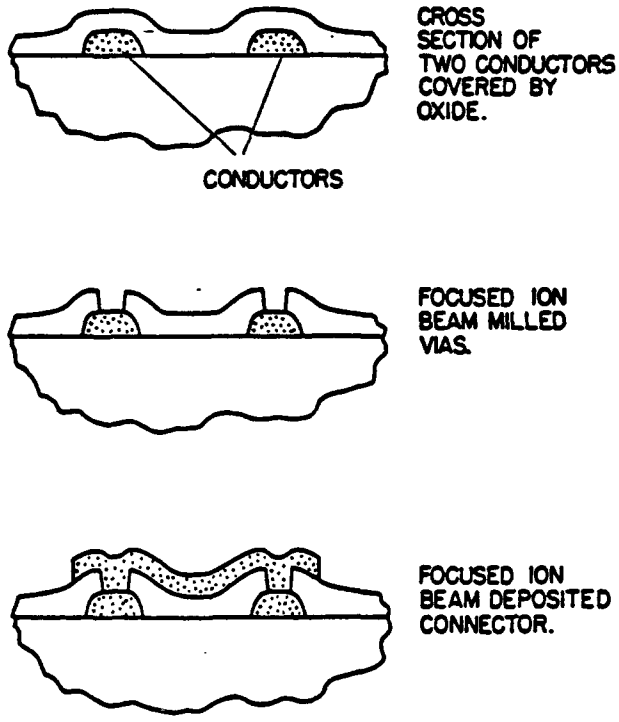

Fig. 9 (Top left) Schematic of circuit repair or restructuring. Two parallel conductors shown in top sketch in cross section need to be connected electrically. Vias are first milled with the focused ion beam by scanning small rectangles over the passivation until the metal is exposed. (Middle) Imaging in the scanning ion microscope mode can be used for end point detection since the secondary electron yield of the metal is usually higher than that of the passivating oxide. Finally (Bottom) a metal connector is made by focused ion beam induced deposition. (Bottom) SEM of a "jumper" of deposited Pt connecting two adjacent conductors, (done as shown schematically on the left). On the right is a closeup of one of the via milled and filled through the passivation.

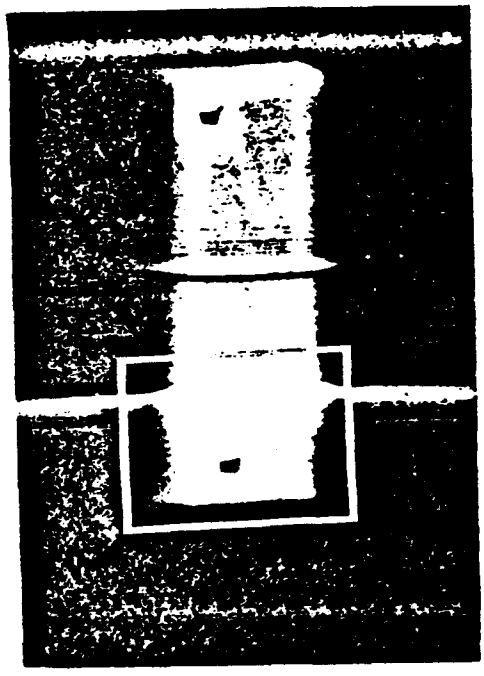

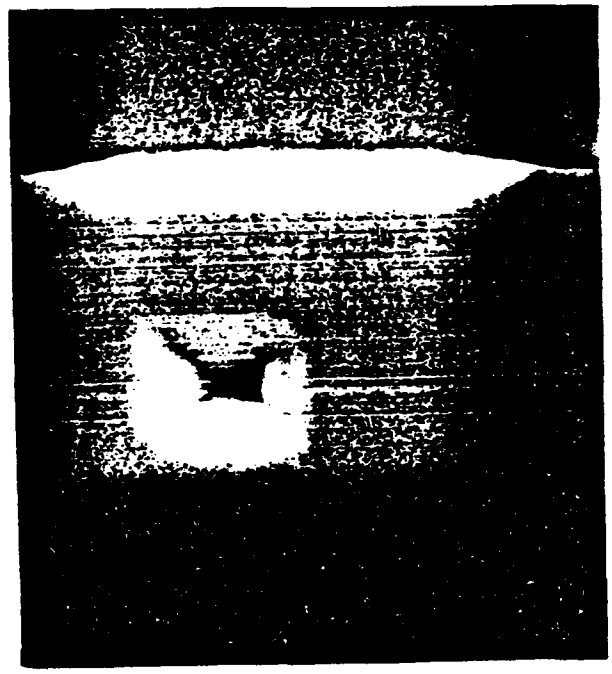

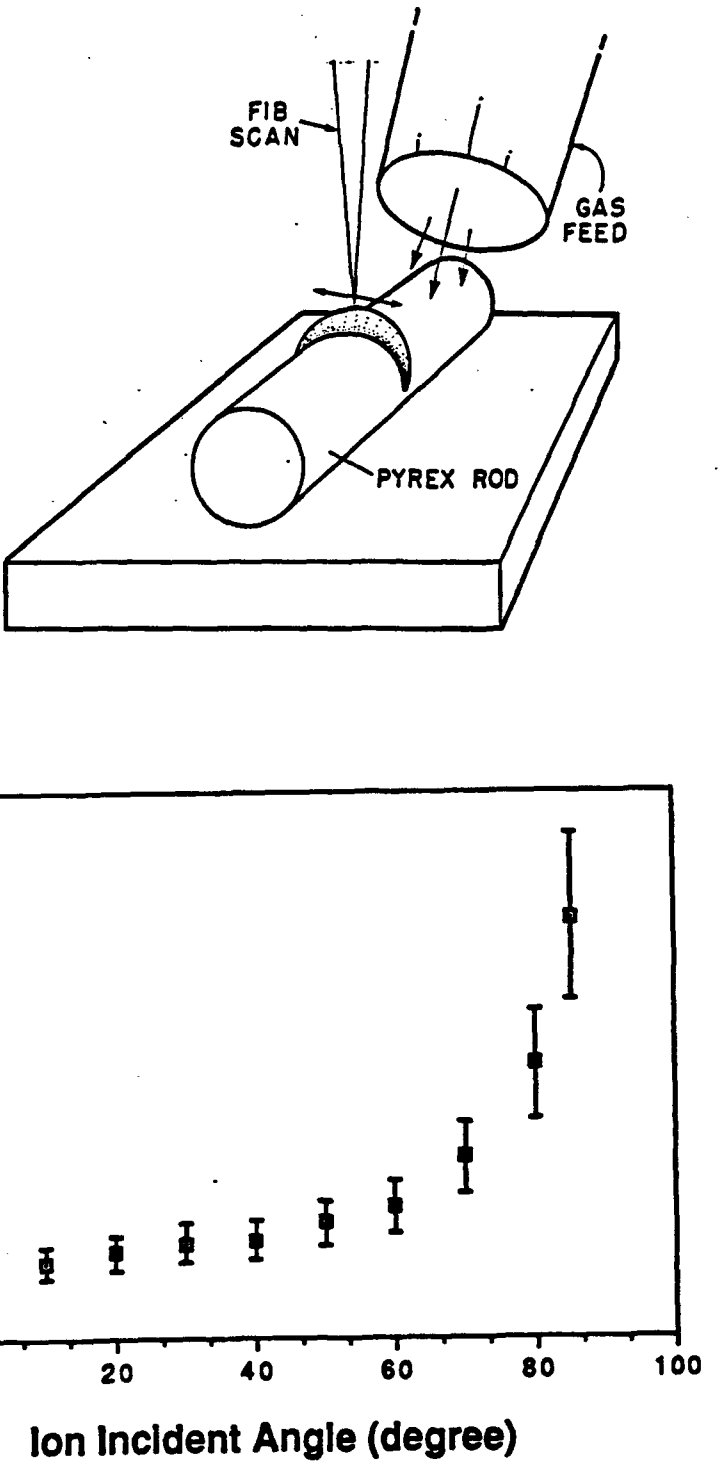

Fig. 10 Measurement of focused ion beam deposition yield as a function of incidence angle. The results were obtained by depositing over a pyrex fiber 3 μm in diameter as shown schematically (on the top). The yield is found to increase as the angle of incidence approaches 90°. Incidentally the sputtering yield similarly increases as grazing incidence is approached.

Platinumtrimethyl (Ref. 24, Appendix VII). This is a recent result, and the line width obtained so far was 0.3 μm. The beam diameter was not optimized, and this value is not expected to be a fundamental limit. The platinum, as in the case of room temperature deposited gold, was found by Auger analysis to contain high percentages of carbon. TEM examination quite surprisingly showed these films to be amorphous.

The platinum deposits were found to have resistivities as low as 70 μΩcm in spite of the high carbon content. And were used in actual integrated circuit repair. (Ref. 25, Appendix VIII) In addition filling of previously ion milled grooves and vias was found to occur more rapidly than growth on a flat surface, i.e. the yield (atoms deposited per incident ion) was found to be over 30 inside a 0.65 μm deep, 0.4 μm wide groove vs 5 on a flat surface. In addition we have made actual circuit repairs by milling vias and depositing plantinum "jumpers". See Fig. 9.

In many of the repair processes the deposition is not on a flat surface. This is particularly true in x-ray mask prepair. Thus to make our observation of increased deposition yield in vias more quantitative we measured the deposition yield as a function of the angle of incidence. This was done simply by depositing plantinum over a small glass fiber. The arrangement and the results are shown in Fig. 10. (Ref. 25, Appendix VIII).

F. Contacts to GaAs

One of the potentially most fruitful applications of focused ion beams is to in-situ processing. Numerous novel devices can be envisaged if patterning, e.g. by focused ion beam, and material growth, e.g. MBE, are combined in a single vacuum chamber. Such apparatus was assembled at the Optoelectronics Joint Research Laboratory largely for implantation and MBE

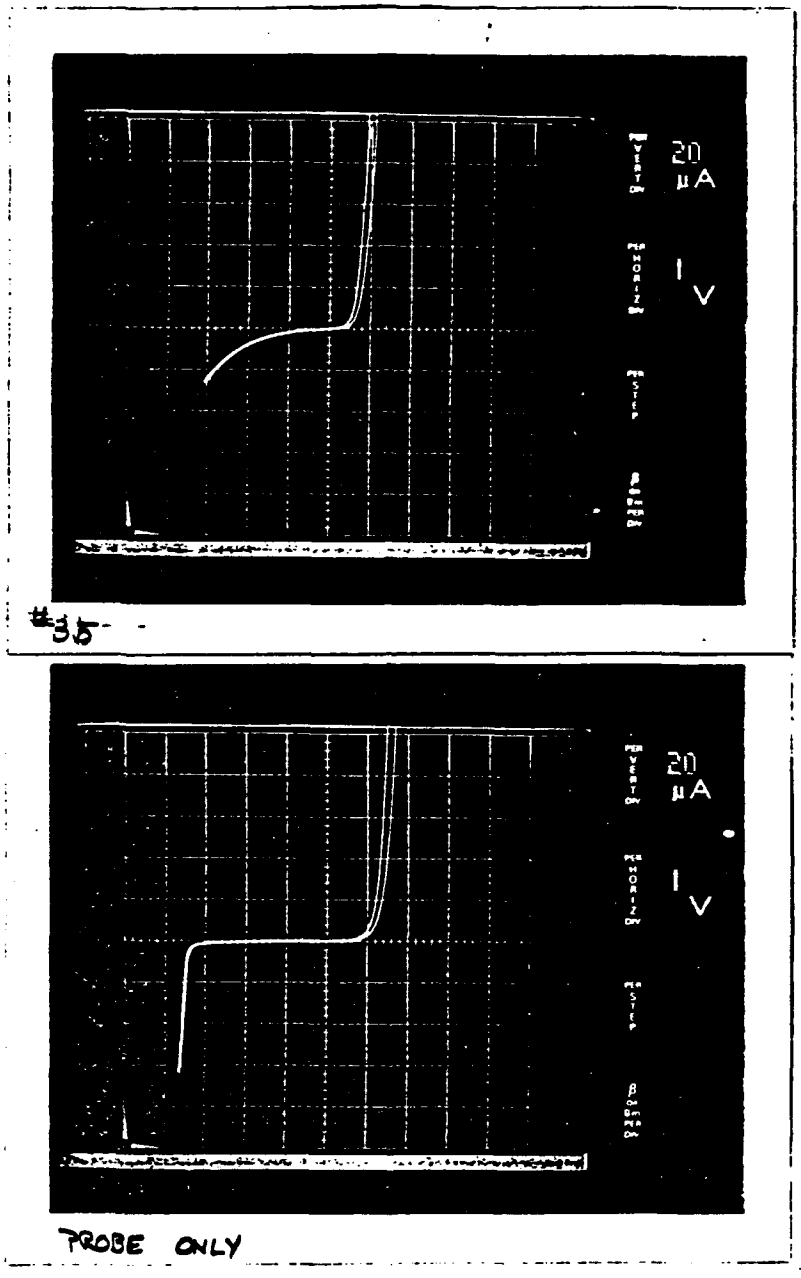

Fig. 11 (Top) I-V characteristics of a gold contact 15 x 15 μm deposited at 10 keV with Ga^+ ions. (Bottom) I-V characteristics of a gold probe pressed to the bare GaAs sample adjacent to the deposited contact, for comparison.

overgrowth,[26] and now at Fujitsu.[27] A low energy focused ion beam system combined with MBE has ben used at ATT Bell Laboratories to etch III-V compounds in-situ and then overgrow with MBE.[28] If focused ion beam induced deposition were combined with MBE, in-situ contacts or other conductor structures may be made. To test this possibility we have deposited some contact on GaAs. (not in-situ)

In the first experiments Ar ions were used at 50 and 100 keV with the sample held at 100°C. As discussed above this yields relatively pure gold with low resistivity. Patches 2 mm in diameter were deposited. Ohmic contacts were made to the back side of the sample. The patches showed poor diode characteristics with the 50 keV result being somewhat better, i.e. the reverse I-V characteristic rolls off so that at -1.5v the current is 500 μA. Next gold patches 15 x 15 μm were deposited with a Ga ion beam at 40 and 10kV with and without pre-etching. (Pre-etching implies bombarding the surface with Ga^+ ions for cleaning purposes before the $C_7H_7O_2F_6$ Au gas is introduced). The pre-etched patches showed somewhat poorer characteristics than those that were not, and the 10kV patches showed better characteristics Fig. 11 shows the 10kV I-V characteristics, as well as for comparison the characteristic of the bare GaAs surface being contacted by the probe. Somewhat encouraged by these results we also deposited submicrometer gate electrodes between existing source and drain contacts to form MESFETs. Unfortunately, in this case the desired diode characteristics were not observed, and the deposited contacts (gate to source or gate to drain) were almost ohmic so no transistor action could be observed.

All of the contact work was carried out in collaboration with Chang-Lee Chen and Len Mahoney of Lincoln Laboratory.

Given that these initial experiments did not yield altogether positive results we devoted more of our efforts to the successful projects described above.

The problem with making contacts to III-V's using focused ion beam induced deposition appears to be the unwanted implantation of the substrate as the film begins to grow. Once the film has attained a significant thickness it will, of course, shield the substrate. This is consistent with the fact that our results were better for lower energy ion beams, and with no ion pre-etching of the substrate.

If we were to revisit the contacts to III-V's, two courses of action might be fruitful. Beam voltages below 1000 V have been achieved with special ion columns and might be used to make rectifying (Schottky) contacts. Alternatively if the ion species were chosen to be a desirable dopant of the substrate, then good ohmic contacts may be formed, provided that the refractory metal is used and the substrate can be annealed. In fact, pre-implantation is sometimes used in the making of ohmic contacts.

III. CONCLUSIONS

The results of our work in the area of ion induced deposition of gold and platinum have been described. The future applications of this work will be to the repair of x-ray masks, to the restructuring and repair of integrated circuits, and possibly to the making of contacts or submicrometer conductors in-situ. Our main contributions to the state-of-the-art are: the first ion induced deposition of Au and Pt, TEM observation of the microstructure and discovery of how it could be improved, 0.1 μm wide features deposited, deposition of conductors to modify an integrated circuit, and the measurement of yield as a function of angle of incidence. This work is of

interest to the scientific community and has resulted in the principal investigator being invited to give 4 talks at international symposia , 8 seminars at various research laboratories, as well as a half-day course. The various oral conference presentations based on the work are listed in Appendix IX.

Carrying out the work on this contact has clearly been a rewarding experience for the participants and we are most grateful for the support.

References

1. R.A.D. Mackenzie and G.D.W. Smith Nanotechnology 1, 163 (1990).

2. For a review of the ion implantation and lithography see J. Melngailis, J. Vac. Sci. Technol.. B5, 469 (1987) or J. Melngailis "Ion Lithography and Focused Ion Beam Implantation" chapter in "Handbook of VLSI Microlithography" W. Glendinning and J. Helbert editors (Noyce Publishers 1991).

   For a review of the field of focused ion beam microfabrication see J. Melngailis, J. Vac. Sci. Technol. B5, 469 (1987).

3. W. Chu, A. Yen, K. Ismail, M.I. Shepard, H.J. Lezec, C.R. Musil, J. Melngailis, Y.-C. Ku, J. M. Carter, and H.I. Smith, J. Vac. Sci. Technol. B7, 1583 (1989).

4. H.J. Lezec, K. Ismail, L.J. Mahoney, M.I. Shepard, D.A. Antoniadis, and J. Melngailis, IEEE Electron Device Letters Vol. 9, 477 (1988).

5. J.E. Murguia, C.R. Musil, M.I. Shepard, H.J. Lezec, D.A. Antoniadis, and J. Melngailis, presented Electron Ion and Photon Beam Technologies Symposium, San Antonio, TX May 29-June 1, 1990 and J. Vac. Sci. and Technol., B8, 1374 (Nov/Dec 1990).

6. J.E. Murguia, M.I. Shepard, J. Melngailis, A.L. Lattes and S.C. Munroe, J. Vac. Sci. B (submitted)

   A.L. Lattes, S.C. Munroe, M.M. Seaver, J.E. Murguia, M.I. Shepard, and J. Melngailis, IEEE Transactions E.D. (to be submitted)

7. J. Melngailis and P.G. Blauner, Materials Research Proc. Vol, 147, p. 127 (1989) (Spring Meeting San Diego invited paper).

8. J. Melngailis, P.G. Blauner, A.D. Dubner, J.S. Ro, T. Tao, and C.V. Thompson, Invited paper. To be published in the Proceedings of Second International Symposium on Process Physics and Modeling in Semiconductor Technology (held as part of the Electrochemical Society Meeting in Montreal May 6-11, 1990).

9. R.L. Kubena, F.P. Stratton, J.W. Ward, G.M. Atkinson, R.J. Joyce, J. Vac. Sci. Technol. B7, 1798 (1989).

10. P.G. Blauner, J.S. Ro, Y. Butt, and J. Melngailis, J. Vac. Sci. Technol. B7, 609 (1989).

11. H.W.P. Koops, R. Weiel, D.P. Kern, T.H. Baum, J. Vac. Sci. Technol. B6, 477 (1988).

12. W. Brünger, Microcircuit Engineering 9, 171 (1989).

13. K. Gamo, N. Takakura, N. Samoto, R. Shimizu, and S. Namba, Japan J. Appl. Phys. 23, L293 (1984).

14. A. Heuberger, J. Vac. Sci. Technol. B6, 107 (Jan/Feb 1988).

15. K. Gamo, D. Takehara, Y. Hamamura, M. Tomita, and S. Namba, Microcircuit Engineering 5, 163 (1986).

16. G. Stengl, H. Loschner, W. Maurer and P. Wolf, J. Vac. Sci. Technol. B4, 194 (1986)

17. G. Shedd, A.D. Dubner, H. Lezec, and J. Melngailis, Appl. Phys. Lett. 49, 1584 (1986).

18. J.S. Ro, A.D. Dubner, C.V. Thompson, and J. Melngailis, MRS Symp. Proc. (Fall 1987) Vol. 101, p. 255 (MRS 1988).

19. P.G. Blauner, J.S. Ro, Y. Butt, C.V. Thompson, and J. Melngailis, MRS Symp. Proc. (Fall 1988) Vol. 129, p. 483 (MRS 1989).

20. A.D. Dubner and A. Wagner, J. Appl. Phys. 66, 873 (1989).

21. A.D. Dubner, A. Wagner, J. Melngailis, and C.V. Thompson to be submitted to J. Appl. Phys. also presented at the US/Japan Seminar on Focused Ion Beam Technology Portland OR. (Dec. 1990).

22. A.D. Dubner, Ph.D. Thesis MIT (1990).

23. P.G. Blauner, Y. Butt, J.S. Ro, C.V. Thompson, and J. Melngailis, J. Vac. Sci. Technol. B7, 1816 (1989).

24. T. Tao, J. Melngailis, Z. Xue, and H. Kaesz, Presented at Electron Ion and Photon Beam Symposium, San Antonio (May 29-June 1, 1990). J. Vac. Sci. Technol. B8, (Nov/Dec 1990).

25. T. Tao, W. Wilkinson, and J. Melngailis, J. Vac. Science and Techn. B9 (1991) to be published.

26. E. Miyauchi and H. Hashimoto J. Vac. Sci. Technol. A4, 933 (1986).

27. H. Airmoto, A. Kawano, H. Kitada, A. Endoh, and T. Fujii. 2nd Japan/US Seminar on Focused Ion Beams and Applications, Portland, OR Dec. 1990.

28. Y.L. Wang, H. Temkin, L.R. Harriott, R.A. Logan, and T. Tanban-Ek. Appl. Phys. Lett. 57, 1864 (1990).

FOCUSED ION BEAM INDUCED DEPOSITION

JOHN MELNGAILIS AND PATRICIA G. BLAUNER
Research Laboratory of Electronics, M.I.T., 77 Massachusetts Avenue, Cambridge, MA 02139

ABSTRACT

Focused ion beam induced deposition is already in use commercially for the repair of clear defects in photomasks, where missing absorber is added. Research is being carried out to extend this technique to the repair of x-ray lithography masks and to the restructuring and repair of integrated circuits, particularly in the prototype phase. In this technique a local gas ambient is created, for example, by aiming a small nozzle at the surface. The gas molecules are thought to adsorb on the surface and to be broken up by the scanned focused ion beam. A deposit is formed with linewidth equal to the beam diameter which can be below 0.1 μm. At small beam diameters and low currents (50-100 pA) the time to deposit 1 μm^3 is in the vicinity of 10-20 sec. If the gas is a hydrocarbon, the deposit is largely carbon, which is useful for photomask repair. On the other hand, if the gas is a metal halide or a metal organic, the deposit is metallic. The deposits have substantial concentrations of impurities due to the atoms in the organometallic, to the ion species used, or to the ambient in the vacuum chamber. Thus the resistivities of the "metal" films deposited typically range from 150 to 1000 μΩcm which is usable for some repairs. (Pure metals have resistivities in the range 2.5 to 12 μΩcm.) We have deposited gold from dimethyl gold hexafluoro acetyl-acetonate and have achieved linewidths down to 0.1 μm, patches of 1 μm thickness with steep side walls and in some cases, resistivities approaching the bulk value. Other workers have reported deposits of Al, W, Ta, and Cr. We will review previous work in the field and present some of our own current results.

INTRODUCTION

The patterning of thin films is a key step in the fabrication of almost all microelectronic devices. In conventional processing, conductors, for example, are created by (1) depositing a thin film of metal using evaporation or sputtering, (2) covering the surface with radiation sensitive polymer, (3) patterning the polymer using incident radiation (lithography), and then (4) removing the metal from the areas not covered by the polymer. This multistep process treats the entire sample the same, i.e. the remaining film is the same thickness everywhere but patterned into, perhaps, millions of features.

In some cases, such as pattern repair, device customization, or in-situ fabrication, a beam writing process may be desired. Such a process combines deposition and patterning into a single step but is necessarily slower since the writing is done serially, point-by-point. Photon beams (usually lasers),

To be published Mat. Res. Soc. Symp. Proc. Vol. 147 (1989) (Proceedings of Spring Meeting San Diego Apr. 1989 Symposium on Ion Beam Proc. of Adv. Elec. Mat.)

electron beams, and ion beams have been used. An appropriate gas ambient, often a metal organic or a metal halide, is created over the sample and a chemical reaction is produced at the point where the beam is incident. By far the most widely studied of these processes is laser deposition,[1] which has been demonstrated for local wiring of integrated circuits.[2] Ablation is used in conjunction with the deposition to cut conductors or to make via holes in insulating layers.[2] These processes are generally limited to dimensions well above 1 μm.

Electron beams and ion beams, on the other hand, can operate in the submicrometer regime and thus are of interest for repair processes as dimensions of microelectronic devices shrink. With electron beams a number of materials have been deposited with submicrometer dimensions including: Cr[3][4], W[4][5], Au[5], and Fe[6]. Tungsten deposition by e-beams has been proposed for x-ray mask repair.[7] The removal of material by e-beam in a controlled fashion is more difficult although stimulated etching of Si with XeF_2 at 0.5 μm dimensions has been reported.[8]

This paper will focus on ion induced deposition. This is of particular interest because focused ion beam systems have recently been developed. (For a review of the subject see Ref. 36.) These ion beams operate with a bright liquid metal (usually Ga) ion source and usually produce beams focused to a spot below 0.1 μm at energies in the 20-70 keV range. Ion beams can be used to induce deposition at submicrometer dimensions. In addition, when no gas ambient is present, the same beams can remove material by sputtering with control of dimensions down to 0.1 μm. The focused ion beam can also be used for imaging when secondary electrons (sometimes also ions) are collected. This works very much like a scanning electron microscope, except that the surface is eroded. By frame storage techniques this erosion can be kept to about a monolayer.

The combination of deposition, milling and imaging has been exploited commercially in focused ion beam repair of photomasks.[9-15] See Fig. 1. This is likely to be the preferred technique over laser repair as dimensions shrink below 1 μm (Ref. 16). Similarly focused ion beams are also expected to play a role in microelectronic circuit repair or restructuring as dimensions shrink. Cutting of conductors has already been used, as well as voltage contrast imaging (see Ref. 17 and 18 for a review of this field and references to the literature). Recently two metal lines have been joined by milling through the passivation layers and depositing a tungsten connection from one line to another. [22] $W(CO)_6$ gas was used, and the deposited

material had a resistivity of 30 to 50 times higher than pure bulk W. The resistance of the connection was nevertheless acceptably low.

Another application which is motivating research on focused ion beam induced deposition is x-ray lithography mask repair. For X-ray lithography, the masks used have the same dimensions as the final samples. Demagnification which is sometimes used in optical lithography is not available. Thus x-ray masks for the next generation of devices will have minimum features in the range of 0.25 to 0.3 μm and metal absorber thickness of 0.3 to 0.7 μm, depending on the x-ray wavelength used. The repair of such high-aspect ratio features of small dimensions presents special challenges. In milling off unwanted features redeposition effects have to be considered[19] and in the deposition of absorber, sidewall steepness and material density are important issues. [20]

In this paper we will discuss ion induced deposition, review the results obtained so far, speculate on the mechanism of the process, and consider the applications.

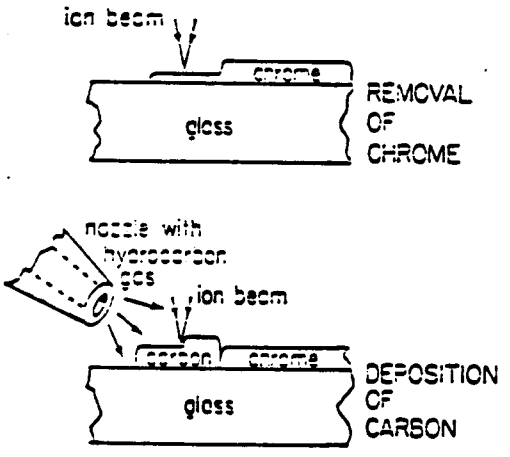

Fig. 1: Schematic of the photomask repair process. The absorbing film deposited is shown to be carbon, but a metal could equally well be used.

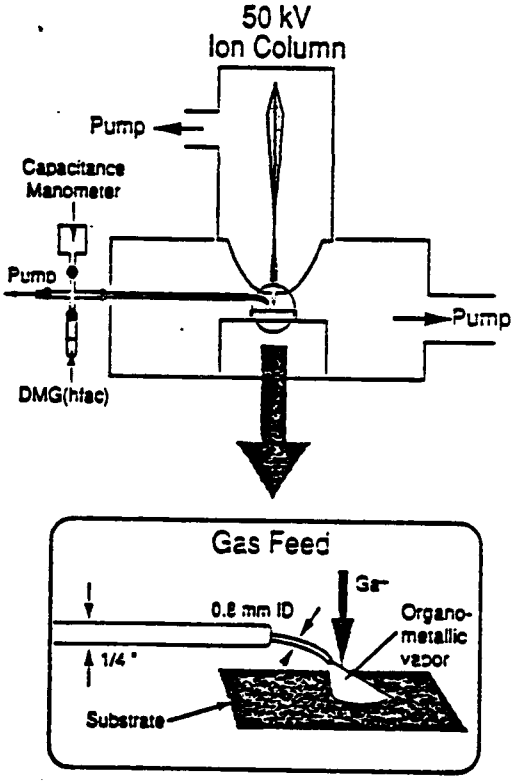

Fig. 2: Schematic of the focused ion-beam-induced-deposition apparatus. The inset shows the details of the gas feed. The ion beam is scanned over the area of the surface where the flux of gas is incident.

ION INDUCED DEPOSITION

a) Apparatus

As discussed above, what is of current technological interest is focused ion beam induced deposition. The apparatus used commercially usually consists of a focused ion beam column which is differentially pumped and a gas feed system which points a fine nozzle at the sample surface where the ion beam is incident.[10-15] In some cases the "gas" is a solid at room temperature e.g. $Cr(CO)_6$ (Ref. 21), or $W(CO)_6$ (Ref. 22). Then all of the gas feed system has to be heated. The apparatus used at MIT which does not include a heated feed system is shown schematically in Fig. 2 (Refs. 23 & 24). The gas pressure on the sample is a function of nozzle height above the sample. The pressure on the substrate at the point where the ion beam writing is carried out was measured as a function of nozzle height by replacing the sample with a "stagnation tube" as shown in Fig. 3. Using these results as calibration one can perform deposition experiments at various gas pressures by simply varying the tube height above the sample.

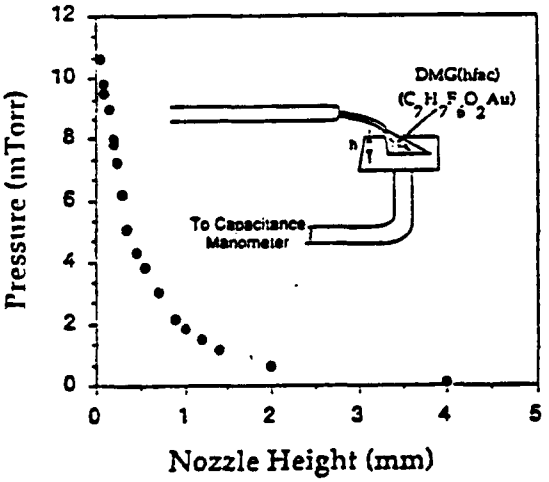

Fig. 3: The pressure as a function of nozzle height above the sample (measured for dimethyl gold hexafluoro acetylacetonate (DMG (hfac)). A 1 mm diameter hole is in the sample and is connected to a capacitance manometer which reads the pressure. From Ref. 24.

Another scheme for creating a local gas ambient consists of enclosing the sample in a box (as shown in Fig. 4) which has a hole in it through which the ion beam enters. Except in cases where the sample is close to the hole, this arrangement provides a measurable, uniform pressure on the sample. This scheme was used in the earliest experiments.[25,26]

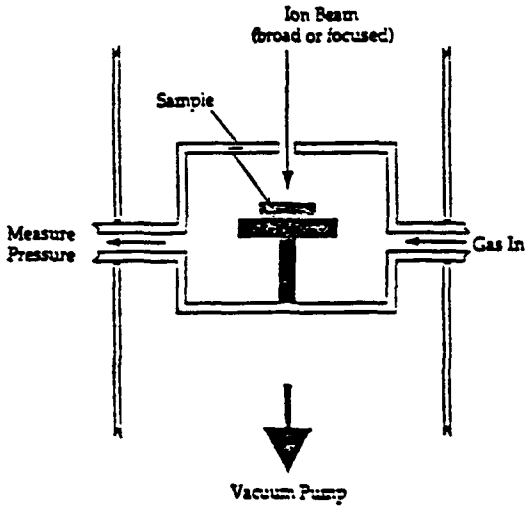

Fig. 4: For some studies of ion induced deposition the sample is enclosed in a cavity where a uniform gas pressure is maintained and into which the gas enters through a small hole.

In order to study the fundamental process by which an ion beam causes adsorbed gas molecules to break apart, a broad ion beam such as from an implanter can be more convenient than a focused beam. Large area deposits can be formed, noble gas ions can be used, and the mass and energy can be varied easily.[25,27,28,30] The results should be directly comparable to focused ion beam induced deposition in those cases where the focused beam is scanned rapidly enough so that the deposition rate is independent of scan rate.[29] This is generally the region in which one would wish to operate with a focused ion beam since at slow scan speeds the deposition rate drops because the supply of adsorbed molecules is depleted.[24,29]

The ion induced deposition process can be affected by the temperature of the sample. Accordingly, heated and cooled stages have been used.[28,30] In addition, in-situ measurement of adsorption rates and deposition rates can be readily obtained by using a quartz crystal microbalance as the "sample" (Ref. 31,32).

b) Films deposited

Ion induced deposition has been demonstrated with a number of metal halides and metal organic gases, as well as with hydrocarbons. In many instances, high concentrations of impurities are observed in the film in addition to the desired metal. There are three main sources of impurities: the parent molecule, e.g. films made from metal organics usually contain carbon; the incident ion, if Ga is used it will, of necessity, be implanted in the film; and the ambient, if the vacuum level is 10^{-6} torr then a monolayer can form in about 1 sec, partly oxidizing a reactive metal film during growth.

Under ideal conditions, namely, a metal halide gas, an ultrahigh vacuum chamber, and the incident ion of the same species as the metal to be deposited or perhaps a noble gas ion, high purity metal films should be achievable. Depositions under such conditions have as yet not been reported. The results reported so far have been summarized in Tables 1 and 2.

Most films are seen to contain high concentrations of impurities and to have resistivities much higher than bulk metal values. The exceptions are the gold depositions carried out on samples at elevated temperatures (100-160° C) using dimethyl gold hexafluoro acetylacetonate, ($C_7H_7O_2F_6Au$), abbreviated as DMG(hfac), and the tungsten deposits formed in well pumped vacuum systems. For the gold films, the higher temperature presumably permits the hydrocarbon products of the dissociated DMG(hfac) to desorb before they are in turn broken up by the incident ions.[30,33]

The gold films deposited at room temperature using an Ar ion beam have carbon concentrations of 30-50%. Transmission electron microscope studies of these films indicate that initially the gold grows in unconnected islands of about 40-60 nm size.[30] Since the electron diffraction pattern of this film is that of pure gold, the carbon must be between the islands. Cross-sectional TEM indicates that, as these films thicken, a columnar structure results.[30] The film deposited at elevated temperatures on the other hand shows the continuous polycrystalline structure expected for e-beam evaporated films (see Fig. 5). Films deposited at room temperature with a Ga focused ion beam have similar island structure when examined by TEM.[24]

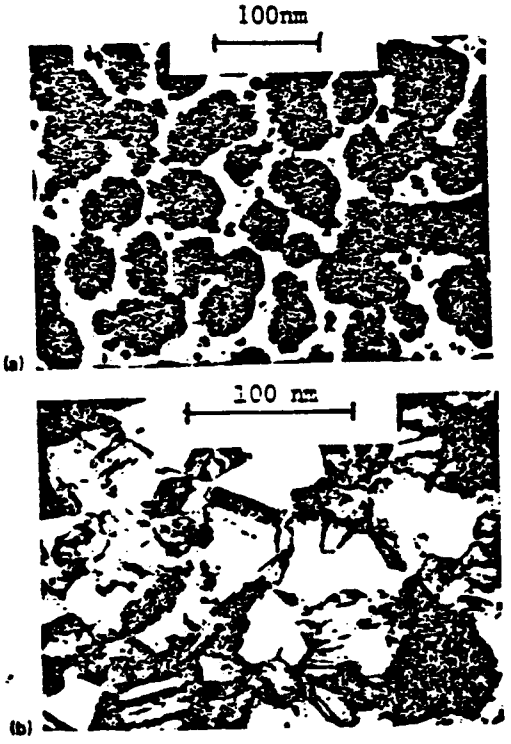

Fig. 5: Transmission electron micrographs of gold films grown by ion-induced deposition at two substrate temperatures: (a) Room temperature, nominal thickness 60 nm, 70 keV Ar^+ ions at 0.7 $\mu A/cm^2$, total dose $1X10^{16}$/cm2. The film is seen to be made up of unconnected gold islands. This discontinuous columnar structure was observed by cross sectional TEM to persist even to 250 nm thicknesses. (b) 160°C, otherwise same conditions, thickness 100 nm. The film is seen to be continuous and has the microstructure typical of conventionally evaporated films (from Ref. 30).

Table 1. Ion Induced Deposition

Gas (Reference)	Ion, Energy	Current Density (A/cm^2)	"Yield" (atoms/ ion)	Deposit Composition	Resistivity ($\mu\Omega cm$)
$Al(CH_3)_3$ (1)	Ar^+ 50 keV		13	Al:O:C 14:70:16 59:39:2	
$Ta(OC_2H_5)_5$ (2)	Ar^+ 50 keV		27	Ta:O:C 56:27:17	
WF_6(RT) (2)	Ar^+ 50 keV		31	W:O 75:25	
WF_6 (80K) (2)	Ar^+ 50 keV		3800	high oxygen content	
WF_6 (3)	Ar^+ 750 eV	4×10^{-4}	5	W:O:C 90:5:5	350 (Bulk = 4.6)
WF_6 (7)	Ar^+ 500 eV	1×10^{-6}		W:F:C 93.3:4.4:2.3	10 (Bulk = 4.6)
$W(CO)_6$ (4)	Ga^+ 25 keV		2	W:C:Ga:O 75:10:10:5	150 - 225
$W(CO)_6$ (8) (40° C)	Ga/In/Sn 16 keV			W:C:O 50:40:10	100
$Cr(CO)_6$ (5)	Au^+ 50 keV	0.7		Cr:C:Au:O 40:40:16:4	
Styrene (6)	Ga^+ 20 keV	0.5	3.6	C:O 65:30	

(1) K. Gamo et al., Japan J. Appl. Phys. 23 (1984) L293.
(2) K. Gamo et al., Microelectronic Engineering 5, 163 (1986).
(3) H. Lezec, MIT (unpublished).
(4) D.K. Stewart, L.A. Stern, and J.C. Morgan, SPIE (1989).
(5) W.P. Robinson, SPIE (1989).
(6) L.R. Harriott and J. Vasile, JVST B6, 1037 (1988).
(7) Z. Xu, K. Gamo and S.Namba, Riken Conf., Mar. 1989.
(8) Y. Madokoro, T. Ohnishi, and T. Ishitani, Riken Conf., Mar. 1989.

Table 2. Ion Beam Induced Au Deposition Using DMG (hfac)

System	Ion			Substrate Temp.	Deposit Characteristics			Ref.
	Energy	Species	Current Density		Yield (Au Atoms/ion)	Composition (Atomic %)	Resistivity (μΩ-cm)	
Focused Beam	40 keV	Ga+	4-1000 $\mu A/cm^2$ *	Room Temp.	~3†	50% Au 35% C 15% Ga	500 - 1,500	1
	40 keV	Ga+	200 $\mu A/cm^2$*	100-125 °C	~3†	80% Au 10% C 10% Ga	3 - 20	2
	20 keV	Ga+	--	--	25-100	--	--	3
Broad Beam	70 keV	Ar+	0.7-7 $\mu A/cm^2$	Room Temp.	15-25†	50-65% Au 50-35 % C	10,000	4
	70 keV	Ar+	0.7$\mu A/cm^2$	100-160 °C	50-60†	> 90% Au	3-10	4
	5 keV	Ar+	5$\mu A/cm^2$	0-15 °C	3-12	50-65% Au 50-35% C	--	5

† Measured assuming a film density is equal to that of Au.

*Average current density of a rastered beam. The instantaneous current density was 0.3-3 A/cm .

1. P.G. Blauner, J.S. Ro, Y. Butt, and J. Melngailis, to be published J. Vac. Sci. Technol. B (1989).
2. P.G. Blauner, J.S. Ro, Y. Butt, and J. Melngailis, submitted for publication.
3. A. Wagner and J.P. Levin, Ion Implantation Conference, Kyoto, Japan, 1988.
4. J.S. Ro, A.D. Dubner, C.V. Thompson, and J. Melngailis, Mat. Res. Soc. Proc. 101, 255 (1988).
5. A.D. Dubner and A. Wagner, to be published, J. Appl. Phys. (July 15, 1989).

c) Mechanism

A model for the deposition process has been formulated in terms of the adsorbate coverage and the ion and gas fluxes[24,31,34] which is similar to the model proposed for electron beam induced deposition.[5] Such a model would be useful for predicting how a given deposition system could be optimized. However, as yet the fit with experimental data is uncertain and optimum conditions can best be determined by measurement. For example, in gold deposition consider the case where the focused ion beam is scanned fast enough to avoid any transient, local adsorbate depletion effects. Then the rate of film growth will increase with average current density until the average adsorbate density becomes depleted. At that point the deposition rate falls rapidly and in fact would become negative as milling takes over (Fig. 6). These results indicate that, for a given focused ion beam current and gas flux, there is a minimum area which can be continuously scanned to achieve maximum growth rate and scanning a smaller area will lead to a reduced rate and, eventually, milling. Thus for a 100 pA beam a 7 μm x 7 μm area can be scanned, but for smaller areas the beam would need to be blanked off for part of the time.

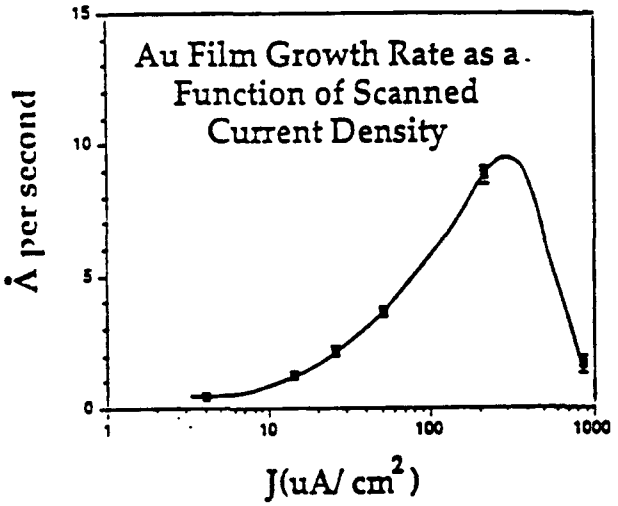

Fig. 6: The deposition rate as a function of average current density (Ref. 24). The pressure of the DMG (hfac) gas is constant at 10 mtorr.

As more data becomes available the type of models discussed up to now[24,31,34] can no doubt be refined to describe ion induced deposition. However, the underlying mechanism responsible for coupling the energy of the scanning ion to the molecules adsorbed on the surface remains unexplained. The quartz crystal microbalance experiments permit the density

of adsorbed molecules to be measured and at the same time also the deposition yield (number of atoms deposited per incident ion). The cross section is then estimated to be 2×10^{-3} cm^2 for 5 keV Ar ions. [31] This means that on the average all molecules are decomposed within a 2.5 nm radius of the point of impact. At 5 keV the yield at pressures of ~5 mtorr is about 4 atoms/ion while for 70 keV Ar ions[30] the yield is 60. The density of adsorbed molecules was not measured in the 70 keV experiment, but since the dependence of density on pressure is very slow in the range of 1-20 mtorr, the coverage is likely to be similar. Thus the cross section is about a factor of 15 higher, and we can say that the incoming ion decomposes the molecules within a 10 nm radius.

How does a molecule sitting on the surface 10 nm from the point of ion impact receive enough energy to break apart? Three mechanisms can be imagined: electromagnetic radiation, electronic excitation, and atomic motion e.g. collision cascades or lattice vibrations. The fact that heavier ions under the same conditions have a significantly higher yield tends to favor the atomic motion, since lighter ions would be expected to produce more electronic or electromagnetic excitation. The limited data available[28] for the deposition from WF_6 is summarized in Table 3, and compared to the energy loss mechanisms for the incident ion. Clearly neither electronic energy loss rate of the incident ion nor the loss rate to substrate nuclei correlates perfectly with the yield. For what it is worth, we note that the square root of the total loss rate correlates reasonably well with the yield. More data is very much needed for yield as a function of ion mass and ion energy to shed light on the mechanism.

The scanning tunneling microscope may be a useful tool for observing the size and shape of deposited material due to individual ions. In fact, the reverse process, craters created by incident ion sputtering, has been observed by scanning tunneling microscopy.[37] For 8 keV Kr ions incident on a PbS (001) surface the area surrounding the point of incidence over which atoms are displaced from equilibrium is seen to be 3 to 5 nm in diameter.[37]

Applications

a) Photomask repair.

In the case of photomask repair most of the systems designed use carbon deposition to replace missing absorber material,[9-15] although Cr is also used.[21] One preferred carbon source that has been reported is styrene[35] (Table I). The deposition time can be estimated from Table 4.

Clearly to deposit large areas with high resolution will take considerable time, but then most repairs are not expected to exceed a few square micrometers.

b) X-ray lithography mask repair.

The repair of clear defects (missing absorber) in x-ray masks will require high aspect ratio structures to be deposited. If the x-ray wavelength is in the range of 0.9 to 1.4 nm, then the absorber, say gold or tungsten, has to be about 0.3 to 0.5 μm thick. Thus minimum circuit features of 0.3 μm will lead to aspect ratios in excess of 1:1. In addition, the features will need to have nearly vertical side walls. Fig. 7 shows a photo of a 3.4 x 3.4 μm patch of gold 1 μm thick with almost vertical side walls. Since the gold contains a substantial percentage of carbon, the x-ray transmission is no doubt increased. In practice, this can be compensated for by increasing film thickness. Such patches are now being evaluated on x-ray masks at the Fraunhofer Institute in Berlin. Tungsten patches produced by ion induced deposition have also shown x-ray opacity.(20)

Fig. 7: SEM of a 3.4 x 3.4 m deposit shown in perspective (top) and in profile (bottom). This feature was written at a deposition rate of 11 Å/s. The height (~1 μm) and high aspect ratio of the edges of this deposit are of particular interest for application in x-ray lithographic mask repair. Ref. 23.

c) Circuit repair.

For restructuring or repair of the conductors on integrated circuits the deposited film must be conducting. In many cases short distances are covered and the deposited film can be thick so that resistivities up to 100 times higher than the bulk metal value may still be acceptable. In addition the contact resistance between the existing metal and the deposited metal must be low. Low resistance "jumpers" of W deposited using $W(CO)_6$ have been used to

Table 3. Mechanisms of Ion Induced Deposition

(Film deposited from WF_6 at 20 mtorr, Ions 50 keV 1 $\mu A/cm^2$ by Gamo et al. ref. 28)

Deposition Ion Yield (a)	Rate of Energy Loss to Electrons (b) keV/μm	Rate of Energy Loss to Nuclei (b) keV/μm	Ion Range in W R_p (μm)	Range Straggle R_p (μm)
He 5.9	225	15	.110	.090
Ar 14.1	770	690	.015	.014
Xe 27.9	830	2900	.008	.005

Notes on table:

a) Calculated from data of K. Gamo et al. Microcircuit Engineering 5, 163 (1986) assuming pure tungsten is deposited.

b) Calculated using the TRIM program, original developed by J.P. Biersack and J.F. Ziegler, see for example, Ion Implantation Techniques, Eds. H. Ryssel and H. Glawischnig, Springer-Verlag, (1982), p. 122.

Table 4. Time to deposit 1 μm^3

(or 5×10^{10} atoms)

Beam Current (nA)	Beam diameter (assuming $4A/cm^2$) (μm)	Yield (atoms/ion)	Time (sec)
0.1	0.06	3	28
0.1	0.06	10	8.3
1.0	0.18	3	2.8
1.0	0.18	10	0.83

connect adjacent metal lines.[22] No evidence of contact resistance was reported.

We have deposited gold films with linewidths down to 0.1 μm (see Fig. 8). In some experiments thin lines were deposited across 4 fingers of Al, nichrome, or Au. By comparing 4 point and 2 point measurements we found that the contact resistance was negliable [24,33] As shown in Table 2, we have succeeded in depositing gold films with resistivity nearly equal to the bulk metal value. This should make repair of integrated circuits more convenient in that thinner films can be used.

Fig 8: SEM of deposited line. This line was written by repeatedly and continuously scanning of 50 pA ion beam over 25 μm at 300 cm/s for 30 s.

In any repair process the ability of the focused ion beam to image the area to be altered is critical as well as the ability to mill out via holes through the passivation layer and to cut conductors where needed.

In-situ deposition of contacts on III-V's, for example, is another potential area of application, particularly if lower energy ions can be used.

CONCLUSIONS:

Focused ion beam induced deposition is a novel process which is as yet not understood in detail. A number of metals have been deposited with submicrometer control of dimensions and some of the deposition parameters have been studied. The field is motivated by applications in photomask repair, x-ray mask repair and by circuit restructuring and repair.

ACKNOWLEDGEMENTS:

The authors wish to acknowledge the contributions of their colleagues at MIT to this work, in particular Jae Sang Ro, Andy D. Dubner, Yousaf Butt, Carl V. Thompson, and Henry I. Smith. Ion induced deposition at MIT is funded by the Army Research Office contract no. DAAL03087-K-0126 and by Draper Laboratory.

REFERENCES:

(1) For reviews of laser-microchemical processing see, for example, D.J. Ehrlich and J.Y. Tsao, J. Vac. Sci. Technol. B4, 299 (1986) or D. Bauerle, Chemical Processing with Lasers (Springer, Berlin 1986).
(2) J.G. Black, S.P. Doran, M. Rothschild and D.J. Ehrlich, Appl. Phys. Lett. 50, 1016 (1987).
(3) S. Matsui and K. Mori, Jpn. J. Appl. Phys. 23, L706 (1984).
(4) S. Matsui and K. Mori, J. Vac. Sci. Technol. B4, 299 (1986).
(5) H.W.P. Koops, R. Weiel, D.P. Kern and T.H. Baum, J. Vac. Sci. Technol. B6, 477 (1988).
(6) R.R. Kunz and T.M. Mayer, Appl. Phys. Lett. 50, 962 (1987).
(7) W. Brünger, Microcircuit Engineering to be published (proceedings of Microcircuit Engineering Conference, Vienna, 1988).
(8) S. Matsui and K. Mori, Appl. Phys. Lett. 51, 1498 (1987).
(9) A. Wagner, Nucl. Instr. and Methods in Physics Research 218, 355 (1983).
(10) J.R.A. Cleaver, H. Ahmed, P.J. Heard, P.D. Prewett, G.J. Dunn, H. Kaufman, Microelectronic Engineering 3, 253 (1985).
(11) M. Yamamoto, M. Sato, H. Kyogoku, K. Aita, Y. Nakagawa, A. Yasaka, R. Takasawa, O. Hattori, SPIE vol. 632, 97 (1986).
(12) H.C. Kaufman, W.B. Thompson, and G.J. Dunn, SPIE vol. 632 (1986).
(13) B.W. Ward, D.C. Shaver, M.L. Ward, SPIE 537, 110 (1985).
(14) N.P. Economou, D.C. Shaver, B. Ward, SPIE 773, 201 (1987).
(15) W.P. Robinson and N.W. Parker, SPIE vol. 773, 216 (1987).
(16) P.J. Heard, P.D. Prewett, and R.A. Lawes, Microelectronic Engineering 6, 597 (1987).
(17) P. Sudraud, G. Benassayag and M. Bon, Microelectronic Engineering 6, 583 (1987).
(18) L.R. Harriott, Applied Surface Science 36, 432 (1989).
(19) K.P. Müller, U. Weigmann, and H. Burghause, Microelectronic Engineering 5, 481 (1986).
(20) H.C. Petzold, H. Burghause, R. Putzar, U. Weigmann, N.P. Economou, and L.H. Stern, to be published SPIE Proceedings "Electron Beam, X-Ray and Ion Beam Technologies: Submicrometer Lithographies VIII (San Jose, Calif., Mar, 1989).
(21) W.P. Robinson, to be published SPIE Proceedings "Electron Beam, X-Ray and Ion Beam Technologies: Submicrometer Lithographies VIII" (presented San Jose March 1989).
(22) D.K. Stewart, L.A. Stern and J.C. Morgan, to be published SPIE Proceedings "Electron Beam, X-Ray and Ion Beam Technologies: Submicrometer Lithographies VIII" (presented San Jose March 1989).

(23) P.G. Blauner, J.S. Ro, Y. Butt, C.V. Thompson and J. Melngailis, Materials Research Society Proceedings, vol. 129 (1989) to be published.
(24) P.G. Blauner, J.S. Ro, Y. Butt, C.V. Thompson and J. Melngailis, J. Vac Sci. Technol. B, to be published (July/Aug 1989).
(25) K. Gamo, N. Takakura, N. Samoto, R. Shimizu, and S. Namba, Jpn. J. Appl. Phys. 23, L293 (1984).
(26) K. Gamo, N. Takakura, D. Takehara, and S. Namba, Extended Abstract 16th International Conference on Solid State Devices and Materials (Kobe, Japan, 1984), p. 31.
(27) K. Gamo and S. Namba, in Proceedings of Symposium on Reduced Temperature Processing for VLSI (Electrochemical Society, Pennington, NJ, 1986), vol. 86-5.
(28) K. Gamo, D. Takehara, Y. Hamamura, M. Tomita and S. Namba, Microelectronic Engineering 5, 163 (1986).
(29) G.M. Shedd, A.D. Dubner, H. Lezec and J. Melngailis, Appl. Phys. Lett. 49, 1584 (1986).
(30) J.S. Ro, A.D. Dubner, C.V. Thompson, J. Melngailis, Mat. Res. Soc. Symp. Proc. vol. 101, p. 255 (Mat. Res. Soc. 1988).
(31) A.D. Dubner and A. Wagner, J. Appl. Phys. to be published, July 15, 1989.
(32) A.D. Dubner and A. Wagner, J. Appl. Phys. to be published, May 1, 1989.
(33) P.G. Blauner, Y.Butt, J.S. Ro, C.V. Thompson, J. Melngailis, submitted for publication.
(34) F.G. Rudenauer, W. Steiger, and D. Schrottmayer, J. Vac. Sci. Technol. B6, 1542 (1988).
(35) L.R. Harriott and M.J. Vasile, J. Vac. Sci. Technol. B6, 1035 (1988).
(36) J. Melngailis, J. Vac. Sci. Technol. B5, 469 (1987).
(37) I.H. Wilson, N.J. Zheng, V. Knipping, and I.S.T. Tsong, Appl. Phys. Lett. 53, 2039 (1988).

FOCUSED ION BEAM INDUCED DEPOSITION

J. Melngailis, P.G. Blauner*

A.D. Dubner,* J.S. Ro, T. Tao,**

and C.V. Thompson

Research Laboratory of Electronics

Massachusetts Institute of Technology
Cambridge, MA 02139

Abstract

Ion induced deposition is a process of film growth where incident ions cause absorbed gas molecules to break up, leaving some constituents on the substrate. For example, gold can be deposited from a local mTorr ambient of the organometallic $C_7H_7O_2F_6Au$. Using focused ion beams, patterned deposits down to 0.1 μm dimensions can be grown. This technique is used commerically in microfabrication for local repair of photomasks and circuits It is being developed also for x-ray lithography mask repair. In these repair processes ion induced deposition complements material removal by ion milling. Models of the ion induced deposition are being developed both to describe the deposition rate as a function of the controlled parameters and to describe the microscopic mechanism of energy transfer from the incident ion to the adsorbed molecule. In the latter case a collision cascade model is found to fit the measured data.

INTRODUCTION

Patterned thin films are the building blocks of microelectronic devices. Whether the film is an oxide or a metal, the patterning is usually achieved using a resist. This radiation sensitive polymer is spun on a wafer exposed in a fine pattern, most often by ultraviolet light, and the exposed (or unexposed) resist is removed leaving the surface partly covered and partly uncovered. The film is removed in the uncovered part by either plasma or wet chemical etching. The result is that the film on the entire wafer is patterned in one step. This is a very efficient process and is universally used in integrated circuit fabrication.

*Now at IBM Research Center Yorktown Heights, NY.
**Now at Teknor Apex

To be published in the Proceedings of Second International Symposium on Process Physics and Modeling in Semiconductor Technology (held as part of the Electrochemical Society Meeting in Montreal May 6-11, 1990)

In some circumstances a more flexible process may be desirable. One may, for example, wish to modify locally some part of a circuit to repair a defect or to alter the operation during a prototyping phase. A beam induced process fulfills that need. Lasers, electron beams and ion beams[1] have been used to locally break down gases and leave a deposit on the surface patterned according to a programmed beam scan. This is a simple flexible process since the deposition and patterning are combined in one step. Of course, it is also a slow, point-by-point deposition process.

Considerable work has been done on laser deposition[2] and this technique has been applied to circuit modification and repair. (See for example Ref. 3). Control of this process however, is not in the submicrometer range. Electron beam induced patterning[4-8] is capable of submicrometer control, but material removal with the e-beam is not straightforward. An etching gas needs to be used[9] and the process is likely to be selective.

In this review paper we will confine ourselves to focused ion beam induced deposition. (See Fig. 1) It appears to have some promising applications. Submicrometer patterns have been written down to 0.1 μm, (Ref. 10) and material removal at 0.1 μm dimensions also appears to be feasible.[10] The material removal is accomplished simply by turning off the gas ambient and sputtering the film with the focused ion beam. This flexibility of focused ion beams is being exploited commercially for photomask repair. (See Ref. 1 for citations of literature). Circuit restructuring and repair have also been reported, including deposition[11] [12] [23] [25] of conductors. (See Fig. 2) X-ray lithography mask repair is another very current application. The challenge here is the deposition and removal of material with a high aspect ratio. (See Fig. 3)

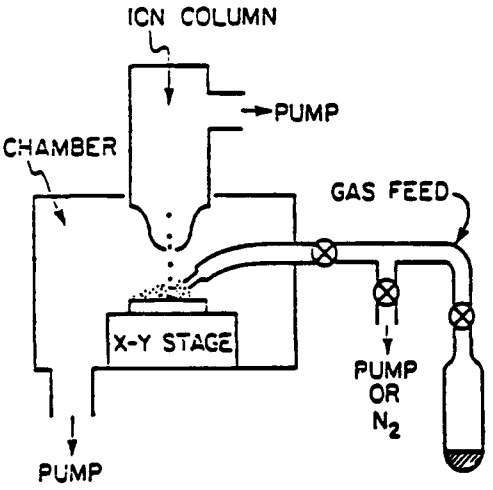

Fig. 1 Schematic of focused ion beam induced deposition apparatus showing a differentially pumped ion column. A gas feed creates a local gas ambient in the area scanned by the focused ion beam. When low vapor pressure materials are used as the gas source, such as $W(CO)_6$, the entire gas feed system may need to be heated.

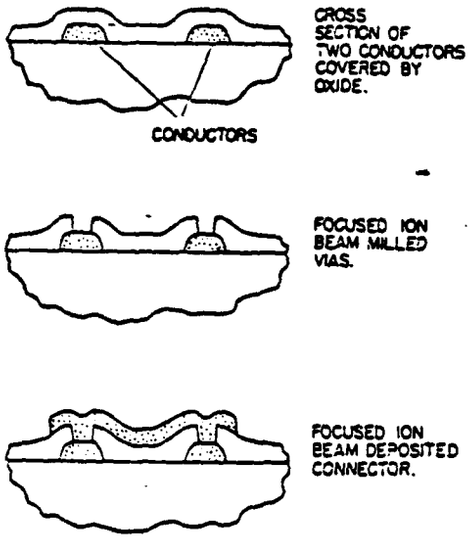

Fig. 2 Schematic of circuit repair or restructuring. Two parallel conductors shown in top sketch in cross section need to be connected electrically. Vias are first milled with the focused ion beam by scanning small rectangles over the passivation until the metal is exposed. (Middle). Imaging in the scanning ion microscope mode can be used for end point detection since thesecondary electron yield of the metal is usually higher than that of the passivating oxide. Finally (bottom) a metal connector is made by focused ion beam induced deposition.

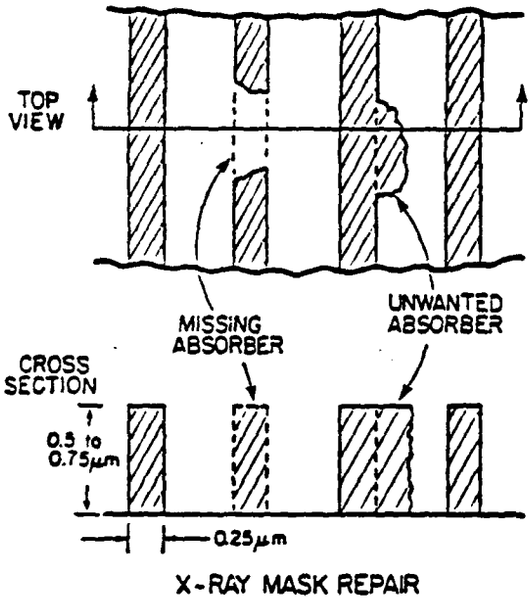

Fig. 3 Schematic of a small portion of an x-ray mask showing 4 parallel metal lines with two defects. The missing absorber with a high aspect ratio needs to be replaced by the focused ion beam deposition, and the unwanted absorber needs to be milled off.

In this review we will briefly discuss results obtained in ion induced deposition. More detail can be found in an earlier review (ref. 1) and in the literature. Modelling of the process will be examined both from a macroscopic point of view, namely, prediction of deposition rates, and from a microscopic point of view, namely, the mechanism of adsorbed molecule breakup by the incident ion.

RESULTS REPORTED

Numerous precursor gases have been used in ion induced deposition including $Al(CH_3)_3$ (ref. 13), $Ta(OC_2H_5)_5$ (ref. 14), $Cr(CO)_6$ (ref. 15), and various hydrocarbons.[16] In the case of the metal containing precursors the deposited films in the earlier experiments generally contained large concentrations of impurities such as carbon and oxygen and no resistivity values were reported. In the case of the gold deposition from dimethyl gold hexafluroacelylacetonate ($C_7H_7F_6O_2Au$), resistivity values 500 μΩcm and higher were observed.[17] Since then a number of the films have been grown and resistivity values reported as summarized in Table I.

Table 1. Ion Induced Deposition of Conducting Films

Gas (Reference)	Ion, Energy	"Yield" (atoms/ion)	Deposit Composition	Resistivity (μΩcm)
WF_6	Ar^+ 750 eV	5	W:O:C	350
(1)			90:5:5	(Bulk W = 4.6)
WF_6	Ar^+ 500 eV		W:F:C	15
(2)			93.3:4.4:2.3	
$W(CO)_6$	Ga^+ 25 keV	2	W:C:Ga:O	150 - 225
(3)			75:10:10:5	
$W(CO)_6$	Ga/In/Sn 16 keV	W:C:O	100	
(4)			50:40:10	
(40°C)				
$C_7H_7F_6O_2Au$	Ga^+ 40 KeV	3-8	Au:C:Ga	500-1500
(5)	(room T)	50:35:15		(Bulk Au = 2.44)
$C_7H_7F_6O_2Au$	Ga^+ 40 KeV	3	Au:C:Ga	3-10
(6)	at 120°C		80:10:10	
$C_9H_{17}Pt$	Ga^+ 35 KeV	0.2-30	Pt:C:Ga:O	70-700
(7)			45:24:28:3	(Bulk Pt = 10.4)
			24:55:19:2	

(1) H.Lezec, MIT (unpublished).
(2) Z. Xu T. Kosugi, K. Gamo, and S. Namba, J. Vac. Sci. Technol. B7, 1959 (1989).
(3) D.K. Stewart, L.A. Stern, and J.C. Morgan, SPIE (1989).
(4) Y. Madokoro, T. Ohnishi, and T. Ishitani, Riken Conf., Mar. 1989.
(5) P.G. Blauner, J.S. Ro, Y. Butt, and J. Melngailis, J. Vac. Sci. Technol.B7, 609 (1989).
(6) P.G. Blauner, Y. Butt, J.S. Ro, C.V. Thompson, and J. Melngailis, J. Vac. Sci. Technol. B7, 1816 (1989).
(7) T. Tao, J. Melngailis, Z. Xue, and H.D. Kaesz, EIPB 1990 and to be published J. Vac. Sci. Technol. (1990).

Generally the films that are grown from organometallic gas or hydrocarbons contain carbon. The decomposition of the molecules is not selective, and the incident ion not only dissociates the metal atom from the molecule but also may decompose the hydrocarbon reaction products. Thus, as seen in Table I, many of the films contain large percentages of carbon. In addition, the incident ions are imbedded in the growing film. Thus films grown using Ga ions will contain Ga. If the yield (number of atoms deposited per incident ion) is high, then the percentage of Ga will be low.

One may, therefore, imagine that the lowest resistivity films should be grown from metal halides since they contain no carbon. This has indeed been observed in deposition of tungsten from WF_6 using low energy Ar ions in an ultrahigh vacuum environment.[18] However, attempts to repeat this with a Ga ion focused ion beam have so far proven to be unsuccessful.[19]

On the other hand the deposition of gold from dimethylgold hexafluoro acetylacetonate onto a substrate at elevated temperatures (e.g. 120°C) yielded films which had resistivities about two orders of magnitude lower than those deposited at room temperature;[20] [21] which typically contained 50% carbon. When examined by TEM these films showed a polycrystaline gold structure typical of evaporated films while the films deposited at room temperature had a columnar, discontinuous structure consisting of gold islands in a matrix of carbon.[20]

The carbon content of the focused ion beam deposited films is important in applications to circuit repair where low resistivity films are desired. However, even at a few hundred μΩcm, films are still usable in most cases since the resistivity is comparable to polysilicon. The carbon content is also undesirable for x-ray lithography mask repair. For example, "gold" films containing 50% carbon need to be twice as thick as pure gold films to have the same x-ray opacity.[22]

The problems of purity notwithstanding some remarkable and useful structures have been fabricated by focused ion beam induced deposition: 0.1μm wide gold lines,[10] ultrahigh aspect ratio gold walls, 0.15 μm wide 5 μm high,[22] see (Fig. 4), high aspect ratio tungsten structures,[11] integrated circuit repair jumpers (as shown schematically in Fig. 2 and on an IC in Fig. 5) in tungsten[12] and in platinum.[23]

For practical applications the deposition rate is a key parameter. The yields for most materials are in the 1 to 10 atoms/ion range although values of up to 100 have been reported.[22] The time needed to deposit one μm^3 of material, taken to be 5×10^{10} atoms, is shown in Table II for various conditions. To lowest order, the beam current density is constant. Thus if higher resolution (small beam diameter) is desired then the beam current has to be reduced. The beam current is proportional to the square of the beam diameter. These circumstances are reflected in Table II. To achieve the optimum deposition rate the ion beam generally has to be scanned rapidly over reasonable areas so as not to deplete the precursor gas.[10] [17] [24]

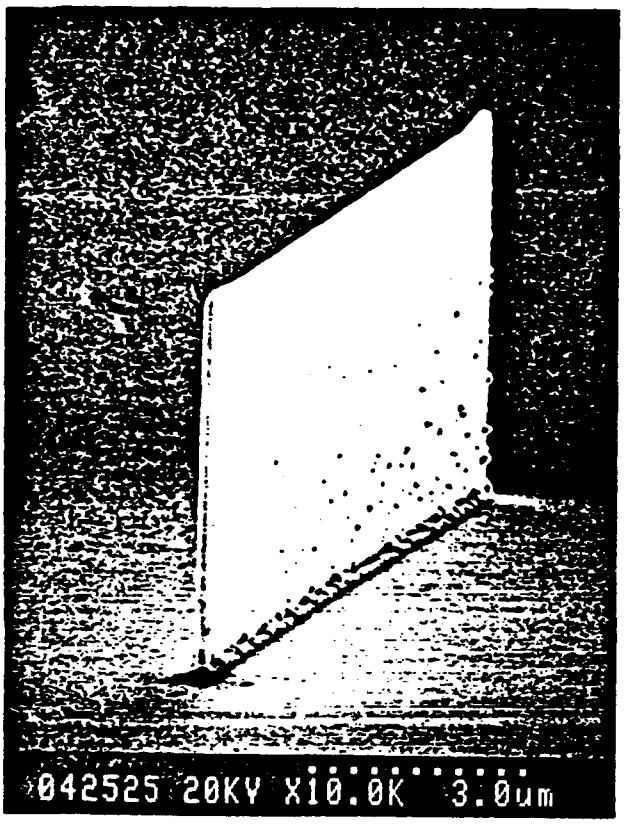

Fig. 4 From Ref. 22. Scanning electron micrographs of a high aspect ratio gold deposit consisting of a wall 0.15 μm thick 5 μm high and 14 μm long. A 100 keV Ga^+ ion beam of 0.1 μm diameter was used withdimethyl gold hexafluoro acetylacetonate as the precursor gas.

Fig. 5 (Below) From Ref. 12. A tungsten jumper deposited to short together several conductors on an integrated circuit.

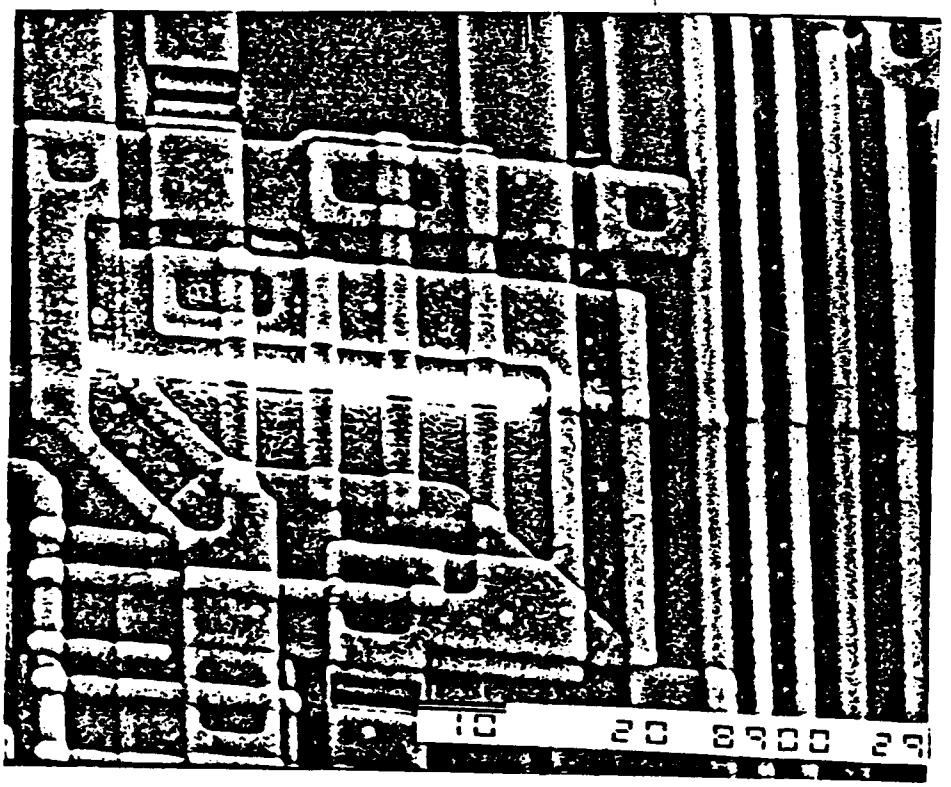

Table II Time to deposit 1 μm^3
(or 5×10^{10} atoms)

Beam Current (nA)	Beam Diameter (assuming 4A/cm^2) (μm)	Yield (atoms/ion)	Time (sec)
0.1	0.06	3	28
0.1	0.06	10	8.3
0.1	0.06	100	0.83
1.0	0.18	3	2.8
1.0	0.18	10	0.83
1.0	0.18	100	0.083

In both the repair of x-ray masks and integrated circuits focused ion beam induced deposition may not always take place on a planar surface. Just as ion milling (sputtering) is known to increase as the angle of incidence departs from normal, the ion induced deposition yield is also found to increase as the angle of incidence moves from normal toward grazing incidence. This has been demonstrated by depositing on a small glass fiber[23] and by noting that the deposition yield increases inside of a previously ion milled trench.[19] See Fig. 6.

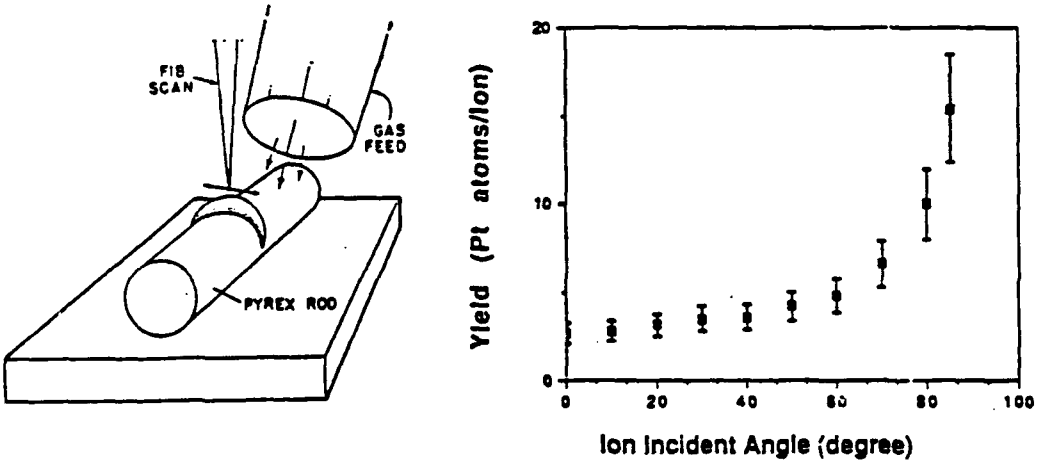

Fig. 6 From Ref. 23. Measurement of focused ion beam deposition yield as a function of incidence angle. The results were obtained by depositing over a pyrex fiber 3 μm in diameter as shown schematically (on the left). The yield is found to increase as the angle of incidence approaches 90°. Incidentally the sputtering yield similarly increases as grazing incidence is approached.

The body of experience in ion induced deposition is extensive enough to permit some practical repair processes to be carried out, and, in addition, to permit both macroscopic and microscopic models to be considered.

MACROSCOPIC MODELS

The growth of a film by ion induced deposition results from a competition between material addition resulting from the dissociation of adsorbed molecules and material removal by sputtering. Numerous observations support the view that the reaction occurs on the surface and not in the gas phase above the surface. The net deposition yield (net number of atoms added to the surface per ion) is the difference between the total deposition yield (expressed as $N\sigma$ where N is molecular coverage of the surface, molecules/cm^2, and σ is the cross section for dissociation (cm^2)) and the sputter yield (atoms removed from the surface per ion).[10] [27]

$$Y_D = N\sigma - Y_S \qquad (1)$$

If the deposited film is made up of several constituents, for example gold and carbon, the situation can be more complex.[10] However, the general description of the deposition process (Eq. 1) has been verified in detail[27] as shown in Fig. 7 for 5 kV Ar ions and for 40 keV Ga^+ ions[10].

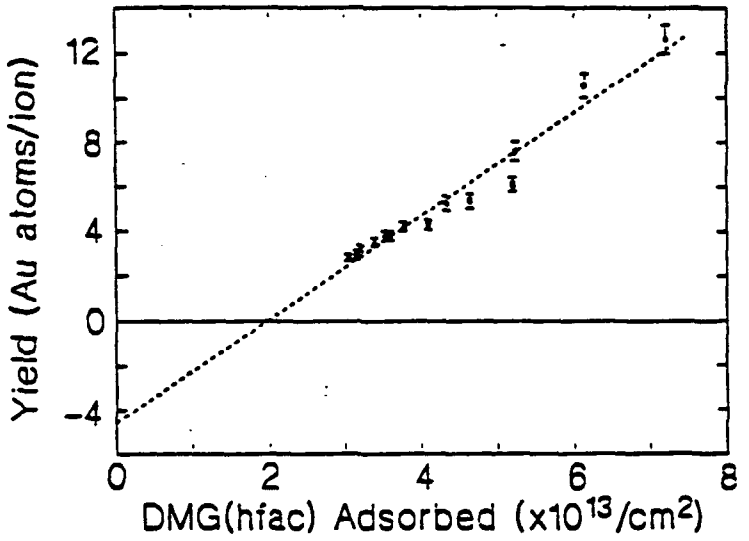

Fig. 7 From Ref. 27. A plot of the yield vs. surface coverage by the precursor gas, dimethyl gold hexafluoro acetylacetonate, abbreviated DMG (hfac). These results were obtained using 5 keV Ar^+ ions (broad beam) by depositing on a quartz crystal microbalance. The microbalance was also used to measure the surface coverage by the precursor. The linear relationship verifies Eq. 1. The slope is the cross section $\sigma = 2 \times 10^{-13}$ cm for this case, and the negative intercept is the sputter yield $Y \sim 4$.

An expression relating the rate of change of the molecular coverage N to the gas flux on the surface Φ, the sticking coefficient g and the average particle current flux <J> has been used to model electron beam induced deposition[6] [26]

$$\frac{dN}{dt} = g\Phi\left(1 - \frac{N}{N_0}\right) - \frac{N}{t} - \Phi N\langle J\rangle. \tag{2}$$

where N_0 is the molecular density on the surface for monolayer coverage τ is the mean lifetime of a molecule on the surface, and σ is the dissociation cross section. Eq. 2 implies that monolayer coverage is the maximum possible coverage. This has been found to be the case for dimethyl gold hexafluro acetylacetonate at room temperature.[27] This treatment was extended to ion induced deposition by including the effects of sputtering. (ref. 10) If we calculate the steady state coverage by solving for N when $\frac{dN}{dt} = 0$, and insert the result in Eq. 1, we get.[10]

$$Y_D = \frac{N_0\sigma}{1 + \frac{N_0}{\tau g\Phi} + \frac{\sigma N_0\langle J\rangle}{g\Phi}} - Y_s. \tag{3}$$

To simplify the expression one can assume that $g \approx 1$ and $\tau\Phi >> N_0$ then

$$Y_D = \frac{N_0\sigma}{1 + \frac{\sigma N_0\langle J\rangle}{\Phi}} - Y_s \tag{4}$$

The milling yield Y_s is evaluated by measuring the removal rate of the deposited material with no gas present, $\Phi = 0$. This expression, Eq. 4, was fitted to measurements of Y_D vs. pressure (in effect Φ) and Y_D vs. <J> by treating $N_0\sigma$ as an adjustable parameter. With $N_0\sigma = 15.6$ the fit was good (within $\pm$ 20% in Y_D except at pressure below 2 mTorr). Except for the case of Al deposition[28] where somewhat different assumptions were made, no other attempts to quantitatively model the macroscopic features of ion induced deposition have been published.

Equation 4 accounts for some of the qualitative observations. For example, in focused ion beam induced deposition the average current density <J> can be quite high ~ $1A/cm^2$ if the beam is kept stationary. (<J> is defined as the average current density and is usually low due to the fact that the beam is scanned rapidly over a given area). Thus in Eq. 4 if <J> is high the first term can be smaller than Y_s and Y_D is negative, i.e. material is removed. This has been observed by a number of workers.[17] [24] A sample result is shown in Fig. 8 where a stationary focused ion beam is defocused by various amounts to vary <J>. Since <J> is highest at the center, cratered structures are produced with milling in the center, and deposition at larger radii where the current density is lower.[24]

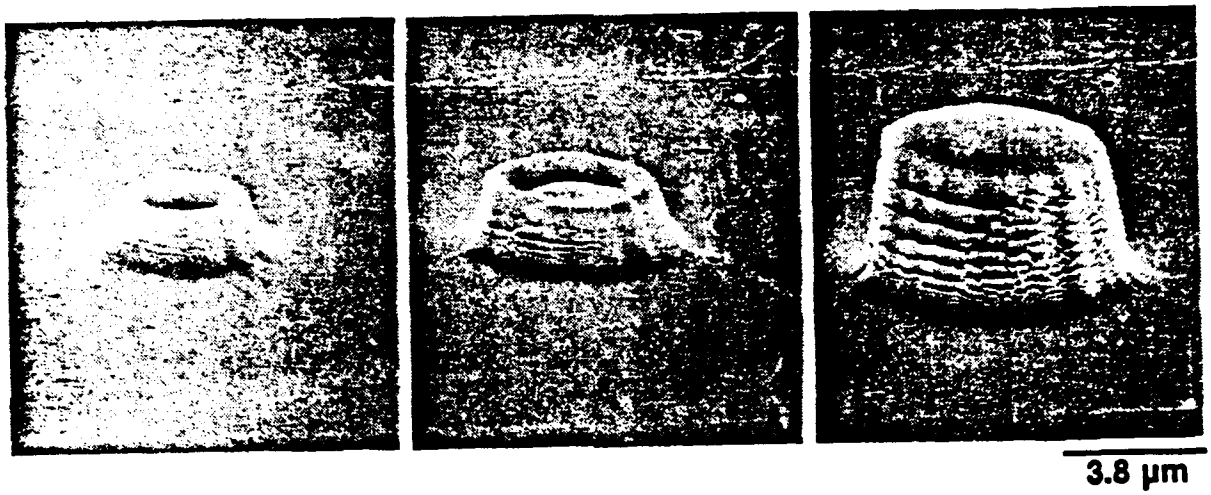

Fig. 8 From Ref. 24. SEM of gold deposits made with a stationary beam which is *defocused to give different peak current densities. The current densities are from left to* right 0.014, 0.077, and 0.001A/cm^2. At the higher current density the precursor gas is depleted and sputtering rather than deposition takes place (see Fig. 7) in the center of the beam and deposition takes place only at the periphery of the beam where the current density is lower.

Overall, even though attempts to describe ion-induced deposition yields as a function of the external control parameters with detailed mathematical models have had only partial success in a few cases, qualitative understanding has been developed from the numerous studies and in many instances the desired practical results can be achieved.

MICROSCOPIC MODELS

A better understanding of the microscopic mechanism by which an incident ion decomposes molecules adsorbed on the surface is likely to be helpful in the development of the macroscopic model. From the measurements of dissociation yield, $N\sigma$, mentioned above and from the measurements of surface coverage, (ref. 27), we can deduce that the cross section $\sigma = 5.2 \times 10^{-13}$ cm^2, i.e. that molecules are dissociated in an area of 80Å diameter for 40 keV Ga ions.[10] Thus direct impact between the incident ion and the

One early model for ion-solid interaction is the thermal spike.[29] The energy which the incident ion deposits in the substrate is represented by means of a delta function in temperature at the point of entry. In time this delta function spreads. (Fig. 9 top left) Thus an area surrounding the point of entry sees a decaying temperature distribution. Sputtering has been modelled as evaporation produced by this high temperature but the results are not entirely satisfactory.[35] This concept may be applied to ion induced deposition by calculating the number of adsorbate molecules dissociated.[30] [31] [32] Without actually calculating the heat flow we can judge whether the order of magnitude of the thermal spike is reasonable. If we assume that all of the energy of the ion is dissipated in a cyclinder of 100Å diameter and a length equal to the ion range, then the temperature rise of such a volume is expected to be 360°C for He ions and 5000°C for Xe ions for an incident energy of 50 keV. Extensive data has been obtained for the deposition and sputter yields of gold with noble gas ions (He to Xe) in the energy range of 2-10keV [31] and in the range of 50-100keV (ref. 20 and 34). The total decomposition yield was found to increase with increasing ion mass and increasing ion energy and to be approximately proportional to the nuclear stopping power. In the lower energy range, analysis of the data has already been carried out. By calculating the heat flow around the point of ion incidence (see Fig. 9) and taking a dissociation energy of 0.95 eV[31] for the dimethylgold hexafluoro acetylacetonate molecule values for the total decomposition yield were obtained. The agreemnt with the measurements is qualitatively reasonable for the heavier ions (Ar, Kr, Xe) but the calculations predict too low a yield for the light ions. (Ne, He) Ref. 31 and 32.

An alternate model based on a Monte Carlo calculation of the ion and scattered substrate atom collision cascades was found to give a considerably better fit to the data[31]. The simulation program used is called TRIM-TC (Ref. 33). This model treats the ion-solid, interaction more realistically. The incident ion is scattered and displaces lattice atoms, some with sufficient energy to in turn displace other atoms producing so called, collision cascades. Some of the collision cascades "double back" and result in surface atoms acquiring excess energy. See Fig. 9. If this energy is high enough to remove the atom (the surface binding energy is 3.8 eV in the case of gold) sputtering occurs. If this energy is above 0.95 eV, then dissociation of the adsorbate is assumed to occur. This TRIM-TC, Monte Carlo based model of sputtering is quite successful in fitting sputter yield data[31] The fit to the deposition yield for gold is very good[31] [32] which lends support to this microscopic model of the ion induced deposition over the simple thermal spike model.

The thermal spike model can be thought of as "averaging" over all of the collision cascade events to describe them as a rise in temperature. Since the decomposition is an activated process, it is very non-linear in energy and temperature. (of the form exp (-E/kT)). Thus "averaging" over the collision cascades may not be valid particularly for the lower mass and energy. This may explain why the thermal spike calculations predict much lower yields for He and Ne than are observed.

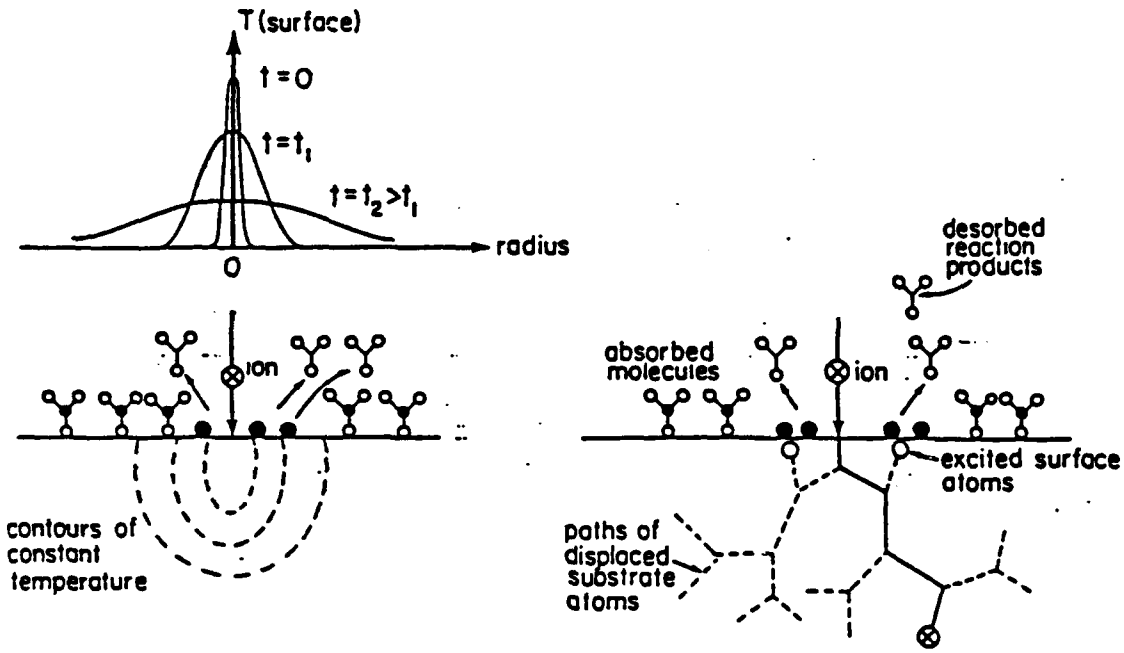

Fig. 9 (On the left) A schematic of the thermal spike model. The incident ion creates a momentary region of high temperature surrounding the point of entry causing adsorbed molecules to dissociate. The surface temperature around the point of incidence is modelled as a decaying Gaussian as shown at the top. (On the right) A schematic of the collision cascade model. The incident ion (path represented by solid line) collides with host lattice atoms displacing them through the lattice (dotted paths). These displaced atoms collide in-turn with other lattice atoms. Some of these collision cascades reach the surface causing sputtering, if enough energy is transfered, or causing dissociation of adsorbed molecules, if the energy is above a lower threshold value.

SUMMARY

Focused ion beam induced deposition is proving to be a useful complement to ion milling. It permits material addition in patterns of 0.1 μm minimum dimension and is being used in circuit restructuring and in mask repair. The dependence of the deposition rate on various parameters of the process has been measured and appears to follow qualitatively the available models. The microscopic mechanism of energy transfer from the ion to the adsorbate appears to require participation by the substrate. A model which integrates over the surface excitations produced by the collision cascades fits the observed dependence of deposition yield on ion mass and energy.

There are a number of unanswered questions about the chemistry of the reactions: What are the reaction products? Why under some circumstances is the deposited film purity higher, such as gold deposition at low pressure for 2-10keV ions and at elevated temperatures for 40-60keV ions? Could the surface chemistry be favorably influenced by addition of other gases besides the metal bearing precursor? Answers to these questions may have important practical consequences.

ACKNOWLEDGEMENTS

The authors wish to thank Diane Stewart of Micrion and Peter Levin of IBM for providing copies of figures. Although the writing of this review paper has not been directly sponsored, the authors' work on ion induced deposition at MIT is supported by the Army Research Office, Contact No. DAAL-03-87-K-0126, by the Naval Research Laboratory contract No. N00014-89-2238 under a subcontract from Micrion Corp. and by the IBM Corp.

REFERENCES

(1) For a recent review of ion induced deposition and for more complete references to the literature see J. Melngailis and P.G. Blauner, Mat. Res. Symp. Proceedings Vol. 147, p. 137 (1989).

(2) For reviews of laser-microchemical processing see, for example, D.J. Ehrlich and J.Y. Tsao, J. Vac. Sci. Technol. B4, 299 (1986) or D. Bauerle, Chemical Processing with Lasers (Springer, Berlin 1986).

(3) J.G. Black, S.P. Doran, M. Rothschild and D.J. Ehrlich, Appl. Phys. Lett. 50, 1016 (1987).

(4) S. Matsui and K. Mori, Japan. J. Appl. Phys. 23, L706 (1986).

(5) S. Matsui and K. Mori, J. Vac. Sci. Technol. B4, 299 (1986).

(6) H.W.P. Koops, R. Weiel, D.P. Kern and T.H. Baum, J. Vac. Sci. Technol. B6, 477 (1988).

(7) R.R. Kunz and T.M. Mayer, Appl. Phys. Lett. 50, 962 (1987).

(8) W. Brünger, Microcircuit Engineering 9, 171 (1989).

(9) S. Matsui and K. Mori, Appl. Phys. Lett. 51, 1498 (1987).

(10) P.G. Blauner, J.S. Ro, Y. Butt, and J. Melngailis, J. Vac. Sci. Technol. B7, 609 (1989).

(11) D.K. Stewart, Micrion (Private communication).

(12) D.K. Stewart, L.A. Stern, and J. C. Morgan S.P.I.E. Symp. Proc. "Electron Beam X-Ray and Ion Beam Technologies: Submicrometer Lithographies VIII" (Mar. 1989) Vol. 1089. p. 18

(13) K. Gamo, N. Takakura, N. Samoto, R. Shiminzu and S. Namura, Japan Journal of Physics. 23 L293 (1984).

(14) K. Gamo, Takehara, Y. Hamamura, M. Torita, and S. Namura, Microcircuit Engineering 5, 163 (1986).

(15) W.P. Robinson, S.P.I.E. Symp. Proceedings "Electron Beam X-Ray and Ion Beam Technologies: Submicrometer Lithographies VIII" Vol.1089 (1989). p. 228

(16) L. Harriot and M.J. Vasile, J. Vac. Sci. Technol. B6, 1035 (1988).

(17) G. N. Shedd, A.D. Dubner, H. Lezec, and J. Melngailis Appl. Phys. Lett. 49, 1584 (1986).

(18) Z. Xu, T. Kosugi, K. Gamo, and S. Namba, J. Vac. Sci. Technol. B7, 1959 (1989).

(19) T. Tao, J.S. Ro, J. Melngailis, Z. Xue, and H. Kaesz, 34th Intrn. Symp. of Electron, Ion, and Photon Beams, San Antonio, TX (May 29-June 1, 1990). To be published J. Vac. Sci. Technol. B (Nov/Dec 1990). Also T. Tao private communication.

(20) J.S. Ro, A.D. Dubner, C.V. Thompson, J. Melngailis, Mat. Research Soc. Symp. Proc. Vol. 101 p. 255 (MRS 1988).

(21) P.G. Blauner, Y. Butt, J.S. Ro, C.V. Thompson, and J. Melngailis, J. Vac. Sci. Technol. B7, 1816 (1989).

(22) A. Wagner, J.P. Levin, J.L. Mauer, P.G. Blauner, S.J. Kirch, and P. Longo J. Vac. Sci. Technol. B (Nov/Dec 1990). To be published.

(23) T.Tao, W. Wilkinson, and J. Melngailis, J. Vac. Sci. Technol. B (to be published).

(24) P. Levin, P.G. Blauner, and A. Wagner SPIE Symp. Proc. "Electron Beam, X-ray, and Ion Beam Technologies: Submicrometer Lithographies IX", Vol. 1263 p. 2 (1990.

(25) Y. Mashiko, H. Morimoto, H. Koyama, S. Kawazu, T. Kaito, and T. Adachi, 5th Annual Proceedings Reliability Phys. Symp. San Diego Apr. 9-7, 1987 p. 111.

(26) V. Scheuer, H. Koops and T. Tschudi Microelectronic Engineering 5, 423 (1986).

(27) A.D. Dubner, and A. Wagner J. Appl. Phys. 66, 870 (1989).

(28) F.G. Rüdenauer, W. Steiger, and D. Schrottmayer, J. Vac. Sci. Technol. B6, 1542 (1988).

(29) F. Seitz, and J.S. Koehler, Solid State Physics Vol. 2 p. 251 (Academic Press 1956).

(30) J. Melngailis, A.D. Dubner, J.S. Ro, G.M. Shedd, H. Lezec, and C.V. Thompson, Emerging Technologies for In-Situ Processing, D.J. Ehrlick & V.T. Nguyen Eds. p. 153-161 (M. Nijhoff 1988).

(31) A.D. Dubner, Mechanism of Ion Induced Deposition Ph.D. Thesis MIT (Sept. 1990).

(32) A.D. Dubner, et al. (to be published)

(33) J.P. Biersack and L.G. Hagmark Nucl. Instr. and Methods 174, 257 (1980).

(34) J.S. Ro et al. to be published.

(35) D.A. Thompson, Radiation Effects 56, 105 (1981).

MICROSTRUCTURE OF GOLD FILMS GROWN BY ION INDUCED DEPOSITION

J.S. RO,* A.D. DUBNER,* C.V. THOMPSON,* J. MELNGAILIS**
*Materials Science & Engineering, M.I.T., 77 Massachusetts Avenue, Cambridge, MA 02139
**Research Laboratory of Electronics, M.I.T., Cambridge, MA 02139

ABSTRACT

A beam of ions incident on a substrate can cause adsorbed gas molecules to break up, resulting in material deposition. We have previously demonstrated deposition of gold from a gas of dimethyl gold hexafluoro acetylacetonate ($C_7H_7F_6O_2Au$) using both focused and broad ion beams. Here we investigate growth at various substrate temperatures and examine microstructure using transmission electron microscopy. Films grown at room temperature were discontinuous even up to the thickness of 250μm while films grown at higher substrate temperatures were continuous even at lower thicknesses. Deposition carried out on substrates at 100°C and 160°C using 70 kev Ar^+ ions resulted in resistivities approaching the bulk value and a deposition yield of 60 to 75 atoms/ion. The relationship between growth conditions, micro-structure and resistivity will be discussed.

INTRODUCTION

Beam induced surface modification is of interest in fabrication of microelectronic devices because lithography steps can be avoided. Usually an appropriate local gas ambient is created over the sample. A chemical reaction occurs where the beam is incident on the surface leading to deposition via decomposition of the gas. Lasers have been used to deposit metals and other materials [1]. Recently electron beam induced deposition [2-7] and ion beam induced deposition [8-14] have also been demonstrated. These charged particle beams are of particular interest because they can be focused to smaller spot diameters than lasers, e.g. below 100 nm. In addition ion beams can be used to remove material by ion milling if the gas ambient is turned off. This has led to the development of special machines for photomask repair where opaque defects (unwanted chrome) are repaired by milling and clear defects (absence of chrome) are repaired by ion induced deposition of carbon or metals [15-17]. Other potentially important applications of ion beam induced deposition are integrated circuit restructuring or repair, x-ray lithography mask repair, and in-situ processing [18,19].

Ion beam induced deposition from gases such as $Al(CH_3)_3$, WF_6 and $Ta(OC_2H_5)_2$ has resulted in films with high (approaching 50%) concentration of impurities, such as carbon and/or oxygen [8-11] with no conductivity reported. We have previously reported deposition of gold from dimethyl gold hexafluoro acteylacetonate ($C_7H_7F_6O_2Au$) with low concentration of impurities (less than 5%) but still with resistivities at least 200 times higher than the bulk value [12]. This was true for focused ion beam induced deposition or deposition from broad (implanter or ion miller) beams.

In the study reported here we used a broad ion beam to investigate the mechanism of ion induced deposition and to reduce the impurity concentration of the gold film and the resistivity.

EXPERIMENTAL

For the purposes of this work we have constructed a differentially pumped chamber, 15 cm diameter and 25 cm long, shown in Fig. 1 which fits into the end station of an ion implanter. The ion beam enters the chamber through a 3 mm diameter aperture and is incident on a sample. A capillary

MRS Symp. Proceedings (Fall 1987) Vol. 101. p.255 (MRS 1988)

gas feed tube with 1.4 mm inside diameter located about 1 mm above the sample produces a local ambient of the deposition gas. By scaling previous results [12] we estimate the pressure on the surface at the area of deposition to be 1-4 mtorr. A small 2 cm diameter glass bottle was sealed to stainless tubing 6 mm dia and held the liquid deposition gas which was degassed by several pumping and freezing cycles.

The gas used is dimethyl gold hexafluoro acetyl acetonate ($C_7H_7F_6O_2Au$), abbreviated as DMG (hfac) which melts at 5°C [21] and has a vapor pressure 0.4 Torr (at room temperature). (It was purchased from American Cyanamid Corp.)

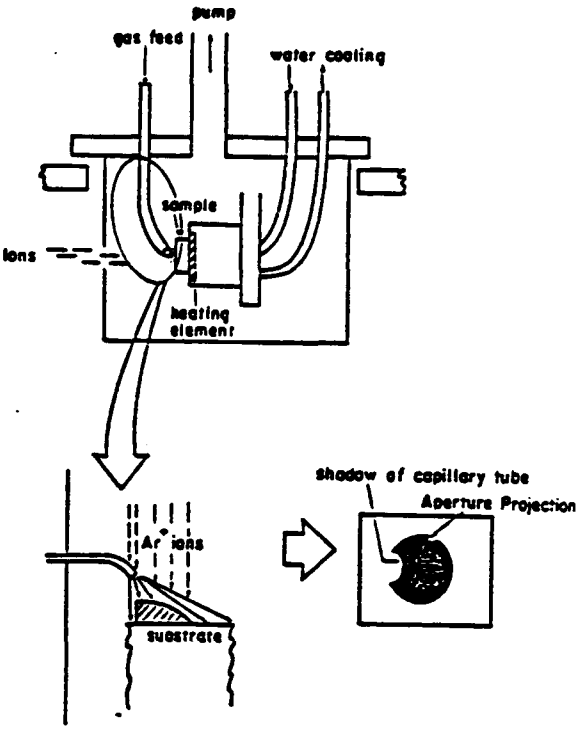

Fig. 1 Schematic of apparatus for ion beam induced deposition using implanter.

The sample stage consisted of a resistively heated element under a copper plate 2.5 mm thick. The sample was held on the copper plate using silver paint and vacuum grease. The temperature of the copper plate was monitored using a thermocouple. Films were deposited on Si wafers with 100 nm of thermally grown SiO_2. Substrate temperatures were varied between 25° C and 160° C. 70 keV Ar^+ ions were used, and the current density on the sample was varied from 0.7 to 7 $\mu A/cm^2$. The current was monitored by positioning a Faraday cup under the beam in place of the sample.

The thicknesses of the deposited films were measured with a profilometer; no smearing of the gold could be observed except for very thin films. The resistivity was measured with a 4 point probe, and the chemical composition was analyzed by Auger Electron Spectroscopy.

The film structure was analyzed using transmission electron microscopy (TEM) both at normal incidence and in cross section. The samples were back etched with HF/HNO_3 solution for the plane view, and dimpled and ion milled for the cross-sectional view.

RESULTS AND DISCUSSION

As is shown in Fig. 2, we observed that the film thickness depends linearly on the total ion does in agreement with our previous results [14]. If we assume the bulk density of gold, this dependence implies a yield of 30-40 gold atoms per ion at room temperature. Since DMG(hfac) can thermally decompose, the role of the ion beam heating of the sample must be addressed. The thermal decomposition of DMG (hfac) has been demonstrated in both CVD and laser CVD processes [22]. At a current density of 0.7 $\mu A/cm^2$ (Fig. 2) a temperature rise of less than 1°C was observed. However, when we increased the current density to 7 $\mu A/cm^2$, we observed a temperature rise of the copper plate of approximately 10°C in 30 min.

The effect of beam heating on yield was investigated by changing the current density over one order of magnitude while keeping the total dose

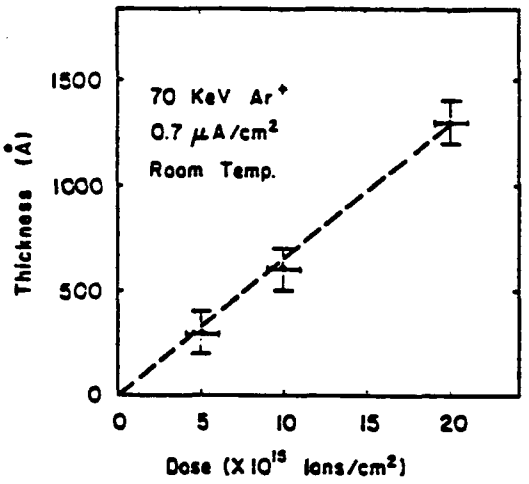

Fig. 2 Film thickness vs ion dose.

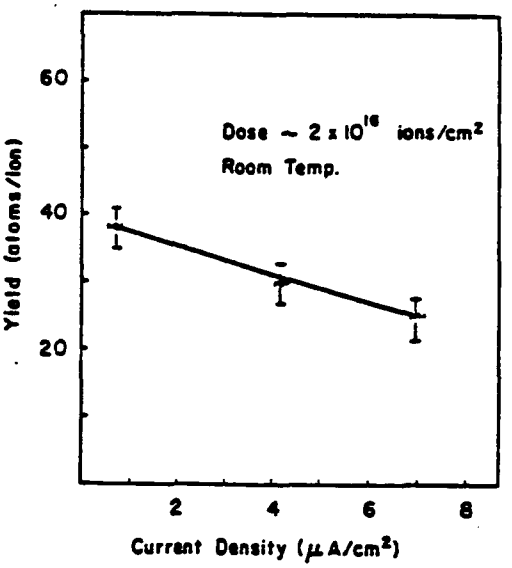

Fig. 3 Yield as a function of current density under the same total ion dose.

constant. The results in Figs. 3 & 4 suggest that beam heating is not the decomposition mechanism since the yield does not rise with current density. As noted below, we observe limited, spontaneous thermal deposition only above 100° C. (Laser induced deposition is known to be pyrolytic but the power density is 5 orders of magnitude higher than our maximum power density.[20,21])

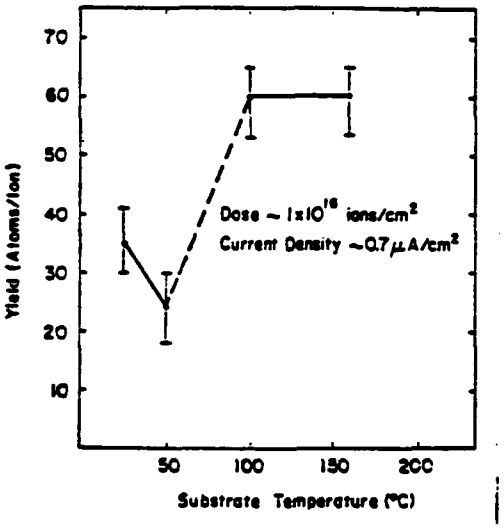

Fig. 4 Yield as a function of substrate temperature.

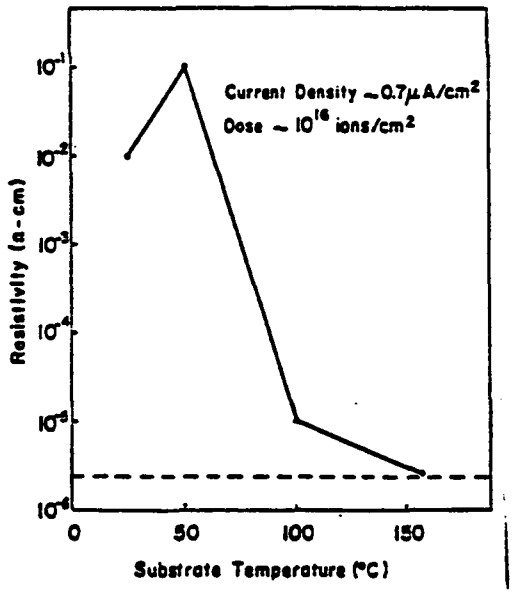

Fig. 5 Resistivity as a function of substrate temperature. The dotted line represents the bulk value for gold. The high value of resistivity at the lower temperatures is observed even at thicknesses of 1μm (grown at 7μA/cm²) while the low values at the higher temperatures are observed for thicknesses of 0.1μm.

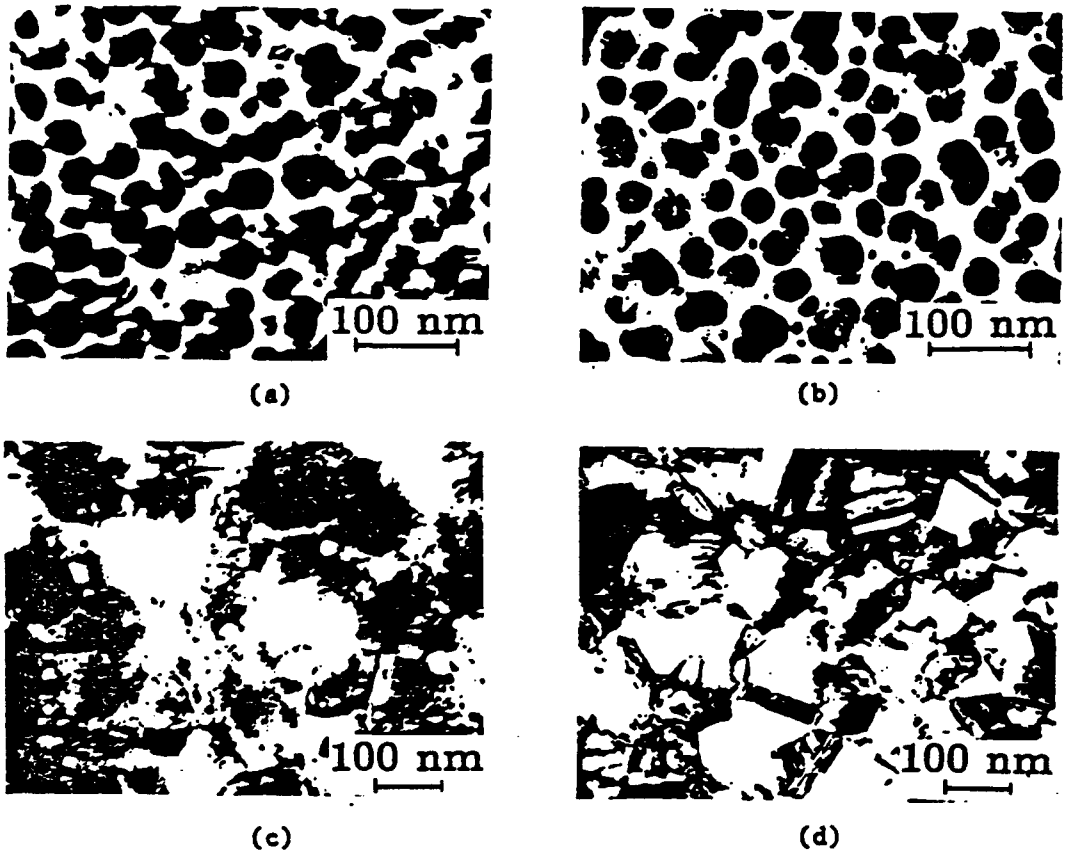

Fig. 6 Transmission electron micrographs of gold films deposited at various substrate temperatures:
a) room temperature b) 50° C
c) 100° C d) 160° C

Films deposited previously at room temperature have shown high resistivity, and poor purity [13,14]. The measured resistivity was about 10,000 μΩcm, and, according to Auger Electron Spectroscopy, the films have the following range of atomic compositions: 50-65% Au and 50-35% C. In addition to confirming these past results, in the current study we observed the microstructure of the films using transmission electron microscopy.

We investigated the effect of substrate temperature on the yield, resisitivity, and the microstructure of the films between 25° C and 160° C. All other conditions were held constant (e.g., a current density of 0.7 uA/cm^2, and a total dose of 1x10^{16} ions/cm^2). When the substrate temperature was raised from room temperature to 50°C, the yield decreased slightly as shown in Fig. 4. The yield however, increased when the substrate temperature was above 100°C. The measured resistivity of samples deposited at 100° C shows a sharp drop by about 4 orders of magnitude as shown in Fig. 5. In fact, the films deposited at 160° C show resistivities approaching those of bulk gold.

Microstructure of the films as observed by TEM for the above deposition temperatures are shown in Fig. 6 for several substrate temperatures. Below 50°C, the microstructure of the films was discontinuous, however discrete islands are beginning to coalesce. At 100° C, the microstructure of the films was almost fully continuous. At 160° C, the films were fully continuous and had the well defined polycrystalline structure similar to those of evaporated films [23]. These microstructural changes can account for the observed drop in resistivity when the substrate temperature was

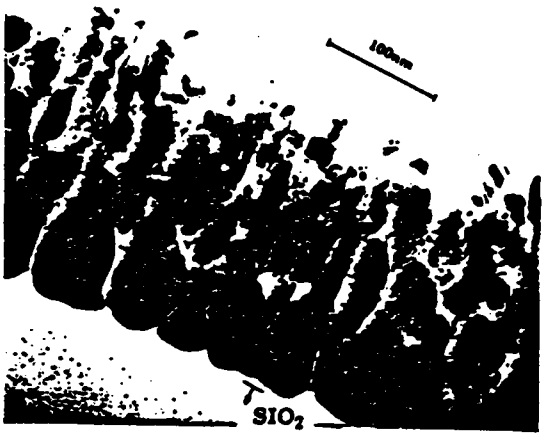

Fig. 7 Transmission electron micrograph of 0.24 μm thick gold film in cross section. This film was deposited with 50 keV Si^+ ions from the implanter. Films deposited by Ar^+ ions should be qualitatively similar.

raised above 100°C. The films deposited at room temperature were still discontinuous even at a thickness as high as 0.25μm as shown in Fig. 7. In this micrograph it can be seen that while the film is dense, and at best partially columnar, most gold islands are not in actual contact but are separated by less dense material. We believe that carbon incorporation into the films deposited at lower temperatures inhibits the coalescence of the gold islands.

Some spontaneous decomposition of the DMG (hfac) was observed at the higher substrate temperature in the form of deposits outside of the region bombarded by the ion beam. However, a sharp boundary was always observed, and the thickness of gold deposited at 160°C in the unbombarded region was always less than 10% of the thickness in the bombarded region.

Another simple observation is that the thickness of the deposit in the ion bombarded moon shaped region, schematically illustrated in the inset in Fig. 1, varied as a function of position. The thickness was greatest near the center directly below the mouth of the tube, and decreased gradually to 50% at the edge of the deposit. (For the results discussed above we always used the thickness at the center). Since the flux of the reactants is expected to decrease as a function of distance from the mouth of the tube, this implies that the yield in our experiments is a function of the local pressure of the DMG (hfac) molecules.

The detailed atomic mechanism of ion induced deposition is not well understood at the present time. Possible rate limiting steps in this process are adsorption of molecules, decomposition of molecules, and desorption of reaction products. Adsorption, decomposition, and desorption can all be affected by the substate temperature. Both enhanced decomposition and desorption may be responsible for our observation of higher purity in films deposited at the higher temperatures. Decreasing adsorption of DMG (hfac) should result in decreasing yield with increasing temperature as observed between room temperature and 50°C (Fig. 4). However, the jump in yield at the higher temperatures leads us to suspect a change in the adsorption mechanism.

In summary, gold films deposited at elevated substrate temperatures (≥ 100° C) have resistivities approaching bulk values and can be grown with a fully continuous microstructure.

ACKNOWLEDGEMENT

This work was supported by the Draper Laboratory, the Army Research Office (Contract no. DAAL03-87-K-0126), Nippon Telegraph and Telephone, and Hitachi. The authors are grateful to R.R. Perilli for ion implantations, to E.L. Shaw for Auger Analysis, and to P.G. Blauner for useful discussions.

REFERENCES

1. See, for example, most of the articles in this volume or for a review D.J. Ehrlich and J.Y. Tsao J. Vac. Sci. Technol. B1, 969 (1983).
2. S. Matsui and K. Mori J. Vac. Sci. Technol. B4, 299. (1986)
3. S. Matsui and K. Mori, Appl. Phys. Lett. 51, 647 (1987).
4. R.B. Jackman and J.S. Foord Appl. Phys. Lett. 49, 196 (1986)
5. H.W. P. Koops, R. Weiel, D.P. Kern, and T.H. Baum to be published J. Vac. Science and Technol. (Proceedings of 31st Conf. on Electron Ion and Photon Beam, Woodland Hills, CA May 1987).
6. R. R. Kunz and Mayer, Appl. Phys. Lett. 50, 962 (1987).
7. T.M. Mayer, R. R. Kunz, and T.E. Allen (this volume).
8. K. Gamo, N. Takakura, N. Samoto, R. Shimizu, and S. Namba Japan J. Appl. Phys. 23 L293 (1984).
9. K. Gamo, N. Takakura, D. Takehara, and S. Namba Extended Abstracts. 16th International Conference on Solid State Devices and Materials (Kobe, Japan 1984) p. 31.
10. K. Gamo and S. Namba in Proceedings of Symp. on Reduced Temperature Processing for VLSI (Electrochem. Soc. Pennington, NJ 1986) Vol. 86-5.
11. K. Gamo, D. Takehara, Y. Hamamura, M. Tomita and S. Namba, Microelectronic Engineering 5, 163 (1986).
12. G.M. Shedd, A.D. Dubner, H. Lezec and J. Melngailis, Appl. Phys. Lett. 49, 1584 (1986).
13. J.M. Melngailis, A.D. Dubner, J.S. Ro, G.M. Shedd, H. Lezec and C.V. Thompson, "Proceedings of the NATO Symposium on Emerging Technologies for In Situ Processing," held in Cargese May 1987, V.T. Nguyen and D.J. Ehrlich editors (to be published by Martinus Nijhoff).
14. A.D. Dubner, G.M. Shedd, H. Lezec and J. Melngailis, J. Vac. Sci. Technol. B5, 1434 (1987).
15. J.R.A. Cleaver, H. Ahmed, P. J. Heard, P.D. Prewett, G.J. Dunn, H. Kaufman, Microelectronic Engineering 3, 253 (1985)
16. N. Economou, D. Shaver, B. Ward, SPIE March 1987 Santa Clara (to be published).
17. M. Yamamoto, M. Sato, H. Kyogoko, K. Aita, Y. Nakagawa, A. Yasaka, R. Takasawa, O. Hattori, SPIE Vol. 632 (1986).
18. E. Miyauchi, and H. Hashimoto, J. Vac. Sci. Technol. A4, 933 (1986), E. Miyauchi and H. Hashimoto, Nuclear Instr. and Methods in Physics Research B21, 104 (1987).
19. For a recent view of focused ion beam applications and references, see J. Melngailis, J. Vac. Sci. Technol. B5, 469 (1987).
20. T.H. Baum, J. Electrochem. Soc. 134, 2616 (1987).
21. T.H. Baum and C.R. Jones, J. Vac. Sci. Technol. B4, 1187 (1986).
22. D.W. Pashley, M.J. Stowell, M.H. Jacobs, and T.J. Law, Phil. Mag. 10, 127 (1964).

THE MICROSTRUCTURE OF GOLD FILMS WRITTEN BY FOCUSED ION BEAM INDUCED DEPOSITION

Patricia G. Blauner, Jae Sang Ro, Yousaf Butt, Carl V. Thompson, and John Melngailis,
Research Laboratory of Electronics
Massachusetts Institute of Technology, Cambridge, MA 02139 USA

ABSTRACT

Focused ion beam induced deposition of gold microfeatures is accomplished by 40 keV Ga^+ bombardment of a substrate on which dimethyl gold hexafluoro acetylacetonate is continuously adsorbed. Under optimum conditions, deposition rates exceeding 11 Å/s have been achieved as well as high aspect ratio features, linewidths of approximately 0.1 μm, and resistivities of 500–1500 μΩ·cm. The microstructure, composition, and yield of the deposits have been examined as a function of various process parameters. Improved film growth and purity are observed in deposits made with lower organometallic pressures or higher current densities.

INTRODUCTION

Ion beam induced deposition uses ion bombardment to induce the growth of a film from a precursor gas adsorbed on a substrate. Typically, a local high pressure region of the appropriate gas is created using either a small pressure cell or nozzle. The ion beam then dissociates adsorbed molecules, the undesired by-products ideally desorb from the surface and the film grows. In contrast to processes involving beam assisted deposition [1], no film growth occurs in the unbombarded region. By using a highly focused beam of ions, this process may be used for deposition of submicron features. As such, it holds promise as a microelectronics repair or prototyping tool where it can be combined with the focused beam's ability to mill material with submicron resolution.

Focused ion beam induced deposition was first demonstrated by Gamo *et al.* [2] and followed earlier work on localized deposition using lasers [3]. Highly localized deposition using electron [4–7], ion [2,8–11], and photon bombardment have now been demonstrated using a large variety of precursor gases to produce films of W, Ta, Fe, Al, Au, Cr and carbon, to name a few. The latter two materials have already found commercial application in the field of photolithographic mask repair [12–15]. Future applications now being explored for focused ion beam induced deposition include x-ray lithographic mask repair and integrated circuit restructuring [16]. Both of these would exploit the focused ion beam's potential both to deposit and mill with sub-tenth micron resolution.

With these applications in mind, we have concentrated our work on the deposition of Au, since it is both a good x-ray absorber and a good conductor. The experimental results discussed below concentrate on the parameterization of the deposition process, and in particular, the characterization of the deposited films as a function of ion and organometallic molecular flux. These issues are of particular relevance to focused ion beam work, where the balance between these two fluxes can be quite close. In extending the deposition process from one employing broad ion beams with current densities of a few microamperes per square centimeter to one employing fo-

Preprint: Presented at Materials Research Society Meeting, Symp. B, Fall 1988 (Boston).

cused beams with current densities of amperes per square centimeter, challenging problems arise. By systematically parameterizing the process, our aim has been to develop a more complete understanding of the basic mechanisms involved in ion beam induced deposition.

EXPERIMENTAL

Thin film and microfeature deposition were accomplished using 40 keV Ga^+ bombardment of SiO_2 substrates (100 nm thermally grown oxide on Si wafers) over which dimethyl gold hexafluoro acetylacetonate vapor was introduced (hereafter referred to as DMG(hfac). Details of the ultra high vacuum focused ion beam apparatus and the gas delivery system are described elsewhere [17]. Summarizing, referring to figure 1, a gas delivery tube creates a local pressure ambient of DMG(hfac) over the substrate and the focused ion beam (diameter 70 – 100 nm and current 25 – 100 pA) is rapidly scanned in this area. The pressure of the organometallic at the surface was measured using a stagnation tube [17] and could be varied from <0.1 mTorr to 10 mTorr by adjusting the height of the delivery tube over the surface. The scanned or averaged beam current density (beam current divided by scanned area) could be varied from 4 $\mu A/cm^2$ to >1 A/cm^2 (stationary beam) by adjusting the size of the scanned area. In all cases scan speeds in excess of 30 cm/s were used to avoid instantaneous depletion of the adsorbed gas coverage [9, 17].

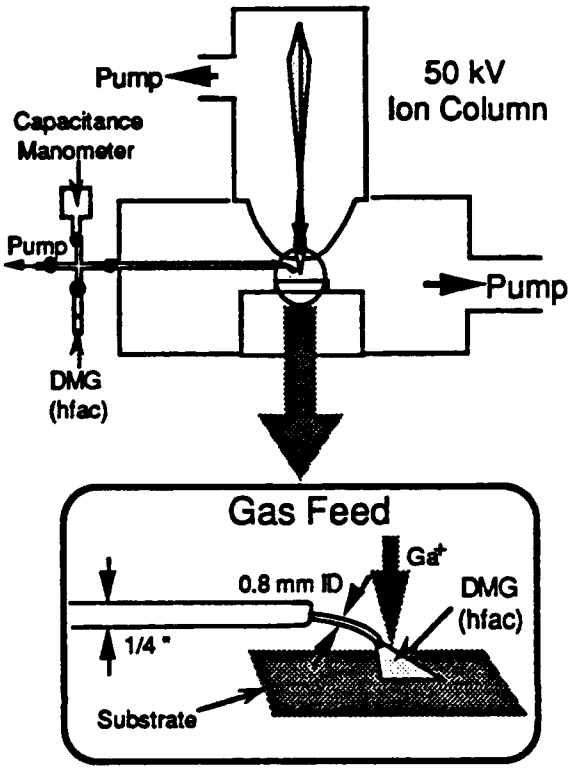

1. Schematic of the apparatus: Focused beams from a differentially pumped ion column were incident on targets in the work chamber (base pressure $5x10^{-8}$ Torr). During deposition, DMG(hfac) vapor was delivered through a small tube suspended over the substrate. This delivery apparatus was mounted on an XYZ manipulator so that the molecular flux could be controlled by varying the height of the tube over the substrate.

The compositions of deposits were analyzed by Auger electron spectroscopy. Film thicknesses were measured either by stylus profilometry or high angle scanning electron microscopy. Resistivity was measured by depositing a line across a pre-evaporated metal pattern (4 point contact). Film microstructure was evaluated using both high resolution scanning electron microscopy and transmission electron microscopy. For TEM analysis, deposits were made directly onto 1000 Å thick silicon nitride membranes.

RESULTS AND DISCUSSION

An example of a 1 μm high Au deposit is shown in figure 2. This 3.4 x 3.4 μm patch took 15 minutes to write using a 25 pA beam and a DMG(hfac) pressure of 10 mTorr, indicating a deposition yield† of 5.8 ± 0.6 atoms per incident ion and a deposition rate of 11 Å/s. Its thickness and high aspect ratio suggest the utility of this technique for x-ray mask repair. Auger analysis of this film indicates a composition of approximately 50% Au, 35% C and 15% Ga, with no F or O detectable. Figure 3 shows 2 examples of lines written with submicron widths. They were written with 50 pA, 70 nm diameter beams under conditions of various scanned current densities and hence deposition efficiencies, as will be discussed below. The measured resistivity of lines such as these, 500 – 1500 μΩ·cm, is comparable to that of polysilicon, indicating that they would be of use in many circuit restructuring applications.

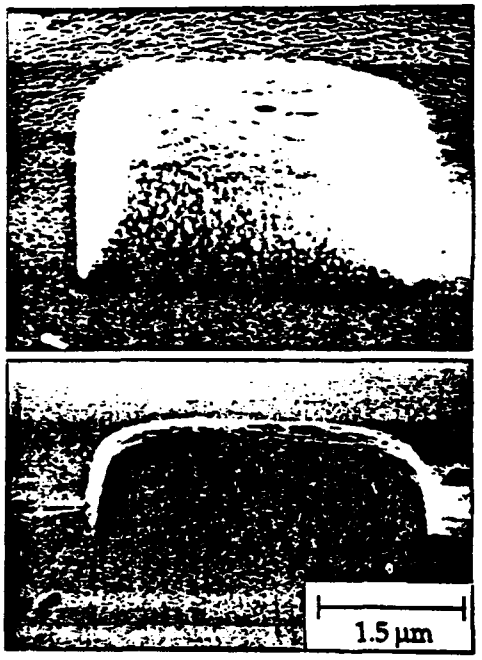

Fig. 2 SEM of a 3.4 x 3.4 μm deposit shown in perspective (top) and in profile (bottom). This feature was written at a deposition rate of 11 Å/s. The height (~1 μm) and high aspect ratio of the edges of this deposit are of particular interest for application in x-ray lithographic mask repair.

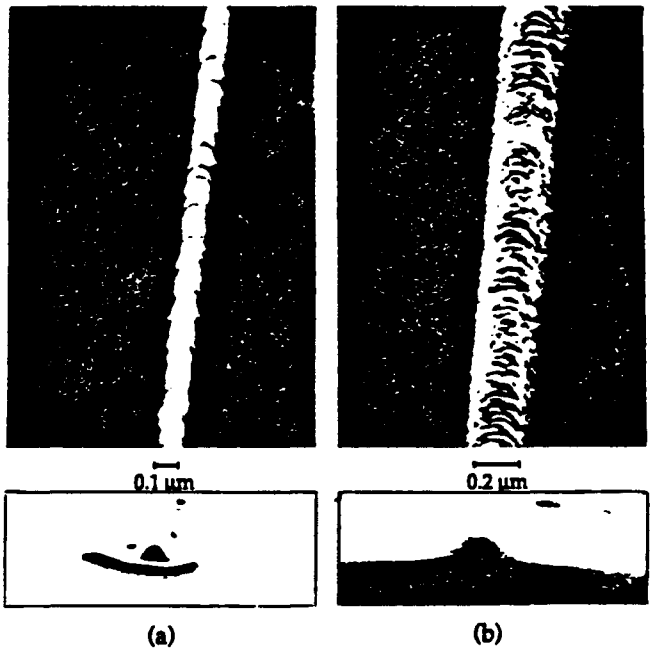

Fig. 3 SEM of deposited lines shown in perspective (top) and in cross section (bottom). These lines were written by repeatedly and continuously scanning a 50 pA ion beam over (a) 25 μm at 300 cm/s for 30 s (deposition yield† < 1 atoms/ion) and (b) 90 μm at 180 cm/s for 2 min. (deposition yield† ~2.5). The resistivity of lines such as (b) was measured to be 500 – 1500 μΩ·cm. The larger width of the line in (b) is believed to be due to drift in the ion beam perpendicular to the scan direction. The feature in the foreground of the cross section in (a) is an artifact of the beam not being blanked at the end of the line.

A critical sensitivity of the deposition efficiency to various process parameters was evident in these experiments and led to a study of the process as a function of both ion and DMG(hfac) flux [17]. We found that the deposition efficiency or yield (atoms/ion) increased to a limiting value both with increasing DMG(hfac) flux and decreasing ion flux [see ref. 17 for details of these measurements]. This is the expected behavior since under ion bombardment the steady-state coverage

of the adsorbate will increase with increasing molecular flux and decrease with increasing ion flux and the data have been fit qualitatively to models of the deposition mechanism which account for adsorption, beam induced adsorbate dissociation and sputtering of the growing film [17]. The latter phenomenon is of particular importance in this work since 40 keV Ga^+ sputters with high efficiency and, if adsorbate coverage is sufficiently depleted, milling rather than the desired deposition will result. Our measurements in the absence of the organometallic vapor indicate sputtering yields of 15.7 ± 1.3 and 12.6 ±1.3 atoms/ion from evaporated Au and the deposited Au/C/Ga films, respectively.

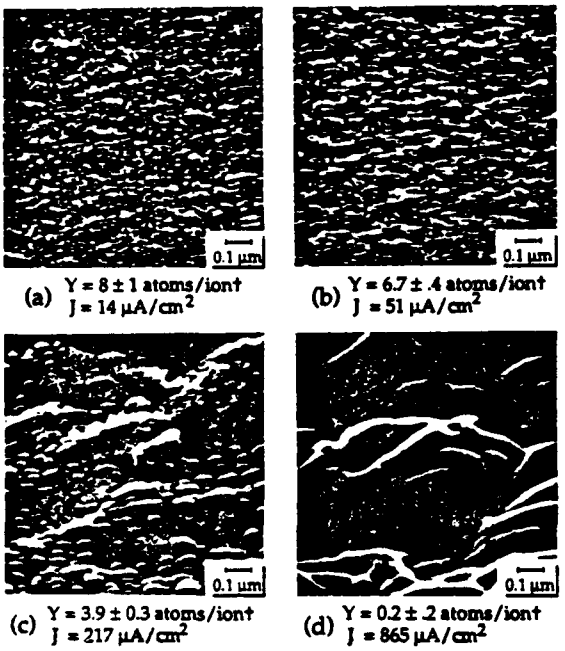

Fig. 4 SEM of films (> 500 Å thick) deposited at various scanned current densities. All other parameters were kept fixed (a DMG(hfac) pressure of 10 mTorr, 100 pA, 0.1 μm diameter beam, scanned at 35 cm/s, and a 0.05 μm spacing between raster lines). Y is the deposition yield†.

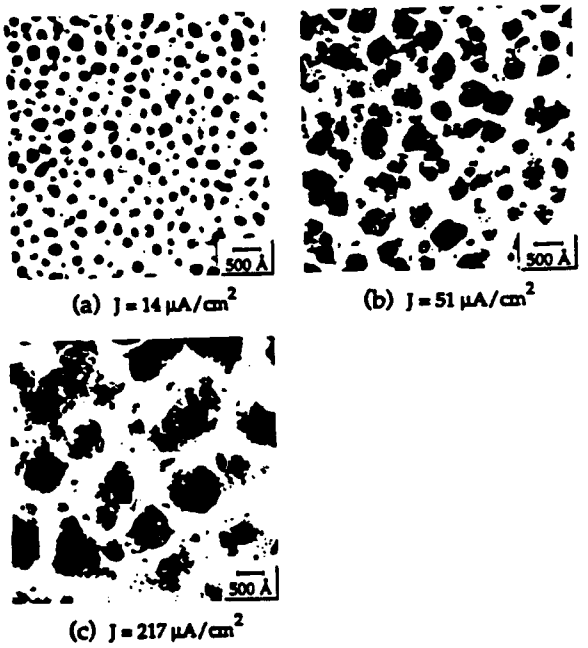

Fig. 5 Plan view TEM of ~1000 Å thick films deposited with different current densities. All other parameters were kept fixed as in fig. 4.

In varying ion and DMG(hfac) fluxes we observed important changes in the film composition and microstructure which can be correlated with the deposition yield itself. Figure 4 shows SEM's of films deposited with scanned current densities of 14–865 μA/cm². These films were all deposited using 100 pA beam currents and 10 mTorr (10^{18} molecules/cm²) of DMG(hfac) pressure. As can be surmised from these micrographs and the composition data shown in table 1, increased ion flux and the associated decreased deposition yield correlate with lesser carbon content and increased coarsening of the crystalline islands which compose the film. As shown in figure 5, TEM analysis of films deposited onto thin membranes under identical conditions confirm that this coarsening is associated with the film microstructure and not just the surface topography.

Figure 6 shows SEM's of films deposited with DMG(hfac) pressures varying from 0.1 – 10 mTorr (10^{16} – 10^{18} molecules/cm²) and a scanned current density of 25.7 μA/cm² (all other

conditions were identical to those of the films shown in figure 4). In comparing the microstructure of these films with the composition data given in table 1, we find that, again, the decreased deposition yield, this time associated with decreased DMG(hfac) flux, correlates with both a lesser carbon content and improved film growth. We note, however, that the film deposited with a yield† of 5.5 atoms/ion at a pressure of 0.1 mTorr is significantly purer than that deposited with a yield† of 3.9 atoms/ion at 10 mTorr, suggesting a more complicated relationship between carbon content and the various deposition parameters than a simple dependence on the deposition yield.

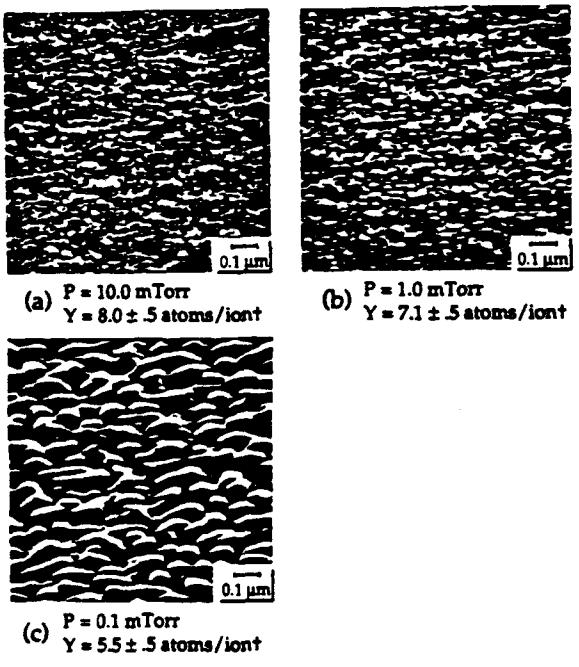

Fig. 6 SEM of films (> 1000 Å thick) deposited with various DMG(hfac) pressures. All other parameters were kept fixed (a scanned current density of 26 μA/cm^2, 100 pA, 0.1 μm diameter beam, scanned at 125 cm/s, and a 0.05 μm spacing between raster lines). Y is the deposition yield†.

P (mTorr)	J (μA/cm^2)	Y (atoms/ion)	%Au	%C	SEM
10	14	8 ± 1	34	58	Fig. 4a
10	51	6.7 ± 0.4	38	54	Fig. 4b
10	217	3.9 ± 0.3	52	40	Fig. 4c
10	26	8.0 ± 0.5	38	55	Fig. 6a
1.0	26	7.1 ± 0.5	53	40	Fig. 6b
0.1	26	5.5 ± 0.5	64	30	Fig. 6c

Table 1 The composition of the deposited films at various scanned current densities and DMG(hfac) pressures. Composition is given in atomic % of Au and C, the remainder being Ga from the implanted beam and is based on results from Auger analysis performed after sputter removal of the first ~100 Å of material (no carbon contamination was observed outside of the deposit after this sputter cleaning). SEM micrographs of the microstructure of the corresponding films are shown in the indicated figures.

These results suggest that at high adsorbate coverage, where deposition is more efficient and more adsorbate molecules are dissociated per incident ion, the by-products of the dissociation are less efficiently desorbed from the growing film, leading to a high carbon content in these films. This carbon then impedes island growth, leading to nucleation of new islands. The resulting discontinuous microstructure explains the relatively high resistivities we have measured for deposited lines.

This interpretation agrees with the results obtained by Ro *et al.* [18] for 70 keV broad beam Ar^+ induced Au deposition. These authors examined the microstructure, carbon content and resistivity of films deposited at constant current density (0.7μA/cm^2) and DMG(hfac) pressure but at substrate temperatures from 21°C to 160 °C (the thermal decomposition temperature of

DMG(hfac). They found that at higher temperatures carbon content and resistivity drops dramatically and film microstructure becomes continuous. From this, they concluded that at higher temperatures, where by-product desorption is aided by the additional thermal energy, the film growth is not impeded by the presence of excessive carbon and, as a result, film resistivity approaches that of bulk Au. Furthermore, the microstructure of films deposited at room temperature with Ar^+ and Ga^+ show similar characteristics. This suggests that the presence of implanted Ga in focused ion beam deposited films does not grossly affect the film growth.

CONCLUSION

We have demonstrated the utility of focused ion beam induced deposition of Au in the fabrication of submicron Au features. The microstructure, composition, and yield of the deposits have been examined for various ion current densities and various gas pressures. We suggest that the resistivity of deposited lines could be reduced below the observed value of 500 – 1500 μΩ-cm by modest substrate heating, as reported for broad beam induced deposition [18].

ACKNOWLEGEMENTS

The authors thank J. Martin and E.L. Shaw for their assistance with the Auger analysis, Y.C. Lin for generously supplying thin membranes for TEM work, and J. Carter and the staff of the Submicron Structures Laboratory for their constant support. This work has been supported by U.S. Army Research Office Contract No. DAAL 03087-K-0126 and Draper Laboratory.

REFERENCES

† The deposition yield was calculated assuming the deposit has an atomic density equal to that of bulk Au.

1. See, for example: J.M.E. Harper, J.J. Cuomo, and H.R. Kaufman, J. Vac. Sci Technol. 21, 737 (1982).
2. K. Gamo, N. Takakura, N. Samoto, R. Shimizu, and S. Namba, Japan. J. Appl. Phys. 23, L293 (1984).
3. For review of the subject: D.J. Ehrlich and J.Y. Tsao, J. Vac. Sci. Technol. B1, 969 (1983).
4. S. Matsui and K. Mori, J. Vac. Sci. Technol. B4, 299 (1986).
5. R.B. Jackman and J.S. Foord, Appl. Phys. Lett. 49, 196 (1986).
6. H.W.P. Koops, R. Weiel, and D.P. Kern, J. Vac. Sci. Technol. B6, 477 (1988).
7. R.R. Kunz and T.M. Mayer, Appl. Phys. Lett. 50, 962 (1987).
8. K. Gamo, D. Takehara, Y. Hamamura, M. Tomita, and S. Namba, Microel. Eng. 5, 163 (1986).
9. G.M. Shedd, H. Lezec, A.D. Dubner, and J. Melngailis, Appl. Phys. Lett. 49, 1584 (1986).
10. F.G. Rüdenauer, W. Steiger, and D. Schrottmayer, J. Vac. Sci. Technol. B6, 1542 (1988).
11. L.A. Stern, D.K. Stewart, Presented at 35th Meeting of Amer. Vac. Soc.(1988).
12. J.R.A. Cleaver, H. Ahmed, P. Heard, P. Prewett, G. Dunn, H. Kaufman, Microel. Eng. 3, 253 (1985).
13. N.P. Economou, D.C. Shaver, and B. Ward, SPIE 773, 201 (1987).
14. M. Yamamoto, M. Sato, H. Kyogoko, K. Aita, Y. Nakagawa, A. Yasaka, R. Takasawa, O. Hattori, SPIE 632, 97 (1986).
15. W.P. Robinson and D.W. Williams, Presented at 35th Meeting of Amer. Vac. Soc. (1988).
16. For review of applications of focused ion beams: J. Melngailis, J. Vac. Sci. Technol B5 469 (1987).
17. P.G. Blauner, J.S. Ro, Y. Butt, C.V. Thompson, and J. Melngailis, to be published.
18. J.S. Ro, A.D. Dubner, C.V. Thompson, and J. Melngailis, Mat. Res. Soc. Symp. 101, 255 (1988).

Focused ion beam fabrication of submicron gold structures

Patricia G. Blauner, Jae Sang Ro, Yousaf Butt, and John Melngailis
Research Laboratory of Electronics, Massachusetts Institute of Technology, Cambridge, Massachusetts 02139

(Received 6 February 1989; accepted 8 April 1989)

Because of their ability to both mill and deposit material with submicron resolution, focused ion beams are now used to repair photolithography masks and are of increasing technological interest in the repair of x-ray lithography masks and in integrated circuit restructuring. With the latter two applications in mind, we have fabricated milled and deposited Au features with linewidths of <0.1 μm using a 40 keV Ga focused ion beam. In addition, we present the results of a study parameterizing focused ion beam induced Au deposition under conditions of practical interest. Milling is accomplished by simple physical sputtering. Examples of milled microfeatures include a grating with a 210 nm period milled through a 5000 Å thick evaporated Au film. Deposition is accomplished by ion bombarding a SiO_2 substrate on which a precursor gas, dimethyl gold hexafluoro acetylacetonate, is continuously being adsorbed. Examples of deposited Au features include a 3×3 μm patch 1-μm-thick with steep sidewalls. The deposition rate was measured at room temperature as a function of ion and precursor flux, and a simple model of the process is fitted to the data. Ion beam induced deposition efficiency is shown to depend critically on the time averaged beam current density and only weakly on the precursor flux. The maximum achievable growth rate is shown to be ~10 Å/s. Deposited Au films contain 30–60 at. % carbon and have conductivities 200–600 times less than that of bulk Au. Those films formed using lower organometallic pressures or higher ion beam current densities are characterized by greater purity with more continuous microstructure.

I. INTRODUCTION

Since the invention of the liquid metal ion source over 10 years ago,[1,2] uses of focused ion beams (FIB) in various aspects of the *semiconductor* industry have been explored, including direct write implantation, lithographic resist exposure, micromachining of optical structures, circuit restructuring, and repair of photolithography masks.[3] The last two applications are of special interest, since they take full advantage of the ability of the focused ion beam to image, mill, and deposit material with submicron resolution without the use of masks or resists. Material is removed by scanning the ion beam over a selected region, thus sputtering away the unwanted feature. Alternatively, material is deposited by introducing a vapor containing the desired element and using the ion beam to locally dissociate molecules adsorbed on the surface. This dual ability of focused ion beams is now exploited commercially in the repair of photolithography masks[4–7] and is being actively explored for integrated circuit restructuring, where the ion beam can be used to cut or join conductors on prototype or custom devices.[8–12] In addition, because they can be focused to diameters as small as 30 nm, FIB's are being considered for use in repair of x-ray lithography masks. For this application, the deposited material must be an x-ray absorbing heavy metal such as gold or tungsten.

The work presented here addresses several questions regarding submicron focused ion beam induced deposition and milling of gold structures. The deposition technique is similar to that used in our earlier work using dimethyl gold hexafluoro acetylacetonate [hereafter referred to as DMG(hfac)] vapor,[13] but employs a higher energy, smaller diameter beam with a substantially higher current density. Since Au is both a good conductor and x-ray absorber, we have investigated in detail its milling and deposition, concentrating on issues such as achievable linewidths and aspect ratios, deposited film conductivity and purity, and deposition and milling efficiencies. This has necessitated a detailed study of the various process parameters which govern deposition, since little is currently known about the details of the underlying mechanisms.

II. MILLING AND DEPOSITION MECHANISMS

A. Milling

One of the most developed uses of focused ion beams is micromilling. Typically, 0.03–0.25 μm diam Ga^+ beams with energies of 15–50 keV are used, since they can be produced by commercially available machines and sputter virtually all materials of interest with efficiencies exceeding 1 atom per incident ion. Milling is most commonly accomplished by simple physical sputtering of the substrate material, although the efficiency can be enhanced by introducing a chemically reactive species over the substrate.[14,15]

The physical mechanism of focused ion beam sputtering is identical to that of broad ion beam sputtering. However, when milling features with extremely high aspect ratios, effects such as redeposition of sputtered material and self-focusing of incident ions scattered by the steep sidewalls being formed must be carefully accounted for.[16–18] As a result, milling rates are conventionally defined only for situations where these geometric factors are minimized by repeatedly scanning the beam over an area with lateral dimensions much larger than the depth milled. In these cases, the rate may be defined in terms of the sputtering yield:

$$Y_S = \rho d / C, \tag{1}$$

where ρ (atoms/cm^3) is the density of the material being

 0734-211X/89/040609-09$01.00

milled to a depth d (cm), and C (ions/cm^2) is the ion dose. Even so, this definition does not take into account possible swelling of the milled material due to implantation of the incident ion species. Therefore, the yield as defined in Eq. (1) may not correspond exactly to the number of atoms removed per incident ion.

B. Deposition

Work on ion[7,12,13,19–21] and electron[22–25] beam induced metal deposition followed earlier studies on the use of laser beams to dissociate an organometallic or metal halide precursor adsorbed on a surface either indirectly through substrate heating (pyrolytic deposition) or directly through photolytic processes.[26] For ion beam induced deposition, the metal bearing gas must be introduced either into a small pressure cell surrounding the sample or through a small nozzle suspended over the sample in order to minimize ion beam scattering. Thus far, W, Ta, Al, Au, and Cr films have been deposited using various precursor gases with both broad and focused ion beams and a large variety of ion energies and species.[7,12,13,19–21] In all cases, impurities such as O or C were present. To date, all work depositing Au has used DMG(hfac) as a precursor.

Although details of the mechanisms of ion beam induced deposition are not well understood, several important experimental observations have been made which allow us to build a partial working model. The first is that a sharp boundary in the deposit is observed where the substrate is shadowed from the ion beam, indicating that gas phase dissociation of the metal bearing vapor is not significant and that it is only the adsorbed molecules which contribute to deposition.[27] It follows then that the adsorption properties of the system being studied will play an important role. Secondly, deposition has been accomplished using a large variety of ion species and energies, and its efficiency increases with the total stopping power of the ion.[20] Since electron bombardment has also been shown to induce deposition but generally with an efficiency much lower than that of ion bombardment, it can be submitted that the nuclear (elastic) contribution to the stopping power will play a more critical role than the electronic (inelastic) stopping power. However, in ion bombardment the elastic stopping also contributes to sputtering, a process which competes with film growth. Since in most systems of interest to FIB induced deposition the sputtering yield is high, it, too, will play an important role, competing with the deposition process. Thirdly, deposition yields in excess of one deposited atom per incident ion have been reported under conditions where monolayer (or less) adsorbate coverage is assumed. Because direct collision between an energetic ion and several adsorbed molecules is unlikely, these large yields suggest that the ion beam indirectly dissociates adsorbed molecules by exciting the substrate below. Since the average energy of the recoiling substrate atoms in the collision cascade which results from the passing of a single ion is low (a few eV) and the excitation volume (cascade diameter) is large (50–100 Å, the transverse range straggle estimated from Ref. 28), it is likely that this indirect process is an efficient means of dissociating adsorbed molecules.

If the deposition process is characterized in terms of the number of atoms deposited per incident ion or net yield (Y_D), these observations allow us to express this yield in terms of a balance between deposition and sputtering:

$$Y_D = N\sigma - Y_s, \tag{2}$$

where N is the molecular coverage of the adsorbate (molecules/cm^2), σ is the cross section for molecular dissociation (cm^2) associated with the size of the collision cascade, and Y_s is the sputtering yield [Eq. (1)] of the deposited film. Although the linear relationship between Y_D and N has been confirmed for Au deposition using 5 keV Ar^+ broad beam bombardment,[29] this relationship is complicated by the fact that the parameters in Eq. (2) are functions of many variables. N is a function of the flux of metal bearing molecules, Φ, which replenishes the surface coverage, the ion current density, J, which depletes the surface coverage (either through deposition or beam induced desorption), and the substrate temperature, T (through thermal desorption). σ and Y_s are functions of the ion beam energy and mass as well as the substrate composition. Furthermore, experimental measurements of Y_D are frequently made in terms of t (cm), the measured thickness of the deposit:

$$Y_D = t\rho/C, \tag{3}$$

where ρ (atoms/cm^3) is the density of the deposited material and C (ions/cm^2) is the ion dose. This measured value does not take into account implanted ions in the deposit and is commonly calculated assuming the film density is equal to that of the pure material, despite the impurities present. In the results presented below, Y_D is calculated assuming $\rho = 5.9\times10^{22}$ atoms/cm^3, the atomic density of pure Au.

Although data reported by several investigators bear out the qualitative aspects of Eq. (2), there have been few attempts to quantify the relationship (with the exception of Refs. 21 and 29) and little or no systematic variation of the parameters of the process to test any such existing models. In the case of submicron feature fabrication, where current densities are necessarily high, a means of predicting Y_D as a function of these parameters would be especially useful, since, as Eq. (2) indicates, a small variation in $N(\Phi,J,T)$ could result in ion milling rather than the intended deposition.

III. APPARATUS

Au microfeatures were fabricated using a 50 kV focused ion beam column[30] and a custom built UHV work chamber, as shown in Fig. 1. The column is a two lens electrostatic, nonmass separated ion optical system with a movable aperture and octopole astigmatism correction and is operated with a Ga liquid metal ion source.[31] The working distance between the bottom of the column (final einzel lens) and the sample is 2.5 cm. A source emission current of 2 μA and a total accelerating potential of 40 keV were used. This column produces 70–250 nm diam beams with currents of 25 pA–1 nA, respectively. Beam diameters are estimated by scanning the beam across the edge of a cleaved single crystal or across a Ni mesh placed over a Faraday cup and measuring the resulting secondary electron signal as a function of beam displacement with a channel electron multiplier. Val-

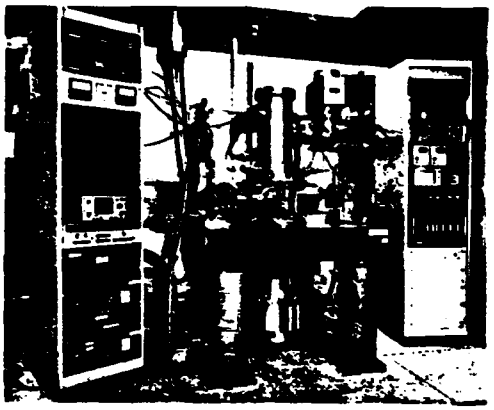

(a)

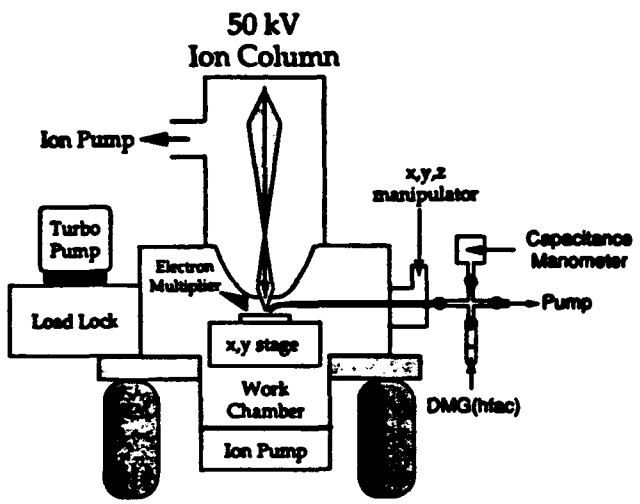

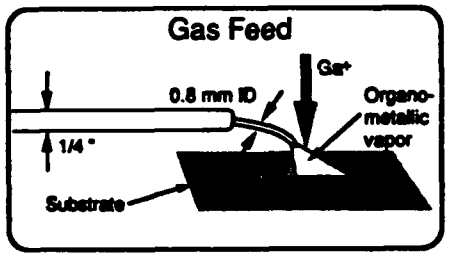

(b)

FIG. 1. Photograph (a) of the SIM50 ion column and differentially pumped UHV work chamber mounted vertically on a vibration isolation table. The load lock, shown on the left-hand side, can introduce up to 4 in. samples and is also used for pumping the large gas load introduced during deposition work. Shown schematically in (b), the DMG(hfac), which is a liquid at room temperature, is contained in a vial attached to a manifold equipped with a capacitance manometer and roughing pump. After degassing by successive freeze, thaw, and pump cycles, DMG(hfac) vapor is delivered through ¼ in. tubing which ends in a 1 in. section of 0.8-mm-i.d. tubing suspended over the substrate (inset). This delivery system was mounted on an X–Y–Z motion feedthru to allow exact positioning by ion beam imaging.

ues quoted are the diameter represented by the 10%–90% amplitude of this signal.

Imaging is accomplished by detecting secondary electrons while synchronously rastering the beam. The deflection system driver is a simple function generator and allows fast rastering (up to 100 kHz), but limited patterning capabilities. In practice this restricts features to simple rectangles or lines. Spacing between the rastered lines of rectangular features is determined by the ratio of the fast (horizontal) and slow (vertical) deflection frequencies and the amplitude of the slow deflection signal. Lines were written simply by grounding one set of the deflection signals. Currently, no beam blanking has been implemented on the system so all writing is done by continuous scanning.

The ion column is connected to the work chamber via a 1 mm differential pumping aperture in the final element of the objective lens. This arrangement provides up to 3 orders of magnitude pressure differential, allowing deposition experiments to proceed without contamination of the liquid metal ion source. For ion milling experiments, the work chamber was pumped using an ion pump (base pressure 5×10^{-10} Torr), while for deposition experiments it was pumped using the load lock turbomolecular pump and liquid nitrogen cold trap (base pressure 5×10^{-8} Torr).

DMG(hfac), a liquid at room temperature with a vapor pressure of 350 mTorr, was introduced through a 0.8-mm-i.d. tube suspended over the substrate (Fig. 1), thus creating a local high pressure in the region scanned by the ion beam while maintaining a work chamber pressure of $<4\times10^{-6}$ Torr (as measured far from the gas delivery nozzle). This arrangement also minimizes ion beam scattering in the gas. The pressure at the substrate was measured as a function of gas delivery tube height by replacing the sample holder with a "stagnation tube" as shown in Fig. 2. These measurements were then used as a calibration to determine the molecular flux of the organometallic under various experimental conditions. Except where noted, the tube was suspended 0.2 mm above the substrate, corresponding to a pressure of ~10 mTorr or a flux of 10^{18} DMG(hfac) molecules/cm^2 s and the substrate was thermally grown SiO_2 (100 nm thick) on a Si wafer.

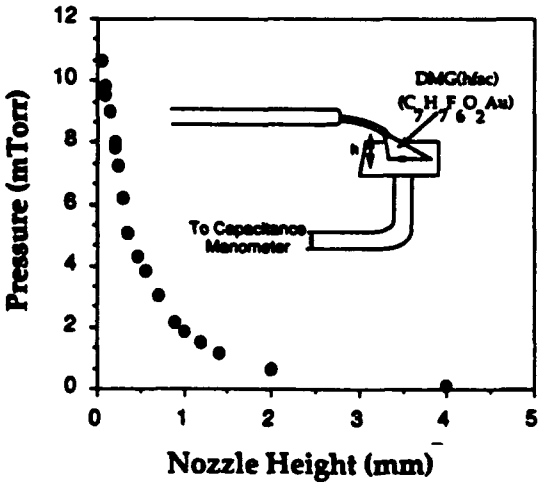

FIG. 2. DMG(hfac) pressure as a function of gas delivery nozzle height as measured by a stagnation tube situated in the place of the sample (inset). The stagnation tube consists of ¼ in. tubing with a 1 mm opening located under the gas nozzle. Since equilibrium gas flow is established at the opening, the pressure measured by the capacitance manometer is equal to the pressure at the sample surface. This curve is used to calibrate the flux of organometallic molecules as a function of nozzle height above the sample surface.

IV. RESULTS

In all the work described in this paper, high scan speeds (> 30 cm/s) were used to minimize effects of the large beam current density of the focused ion beam. When milling at low scan frequencies (high instantaneous beam current), sputtering yields will be affected by the surface topography and redeposition caused by the large amount of material removed in a single pass of the ion beam.[16,17] In the case of deposition, as reported by Shed *et al.*, low scan speeds result in local depletion of the adsorbed organometallic species, leading to a decreased deposition yield and eventually to milling.[13] Our measurements indicated that, with a DMG(hfac) flux of 10^{18} molecules/cm^2 s and beam current densities of ~ 1 A/cm^2, the deposition yield is independent of scan speed at speeds of 10 cm/s or greater. If point-by-point exposure were used, this analog scan speed would correspond to a pixel dwell time of less than 1 μs (for 0.1 μm pixel size and beam diameter).

By employing high scan speeds, we can then define a time averaged beam current density:

$$\langle J \rangle = I/A, \tag{4}$$

where I (ions/s) is the beam current and A (cm^2) is the area of the rastered region. Except where noted, this definition of average beam current density, $\langle J \rangle$, will be used.

A. Milling

The sputtering rate of 40 keV Ga^+ on pure Au was measured by rapidly scanning a 50 pA beam in a 13×14 μm rectangular pattern over a 5000 Å thick evaporated Au film and then measuring the depth of the resulting milled box using a stylus profilometer. This indicated a sputtering yield, as defined in Eq. (1), of 15.7 ± 1.3 atoms per incident ion (Table I). This is consistent with measured and calculated yields for broad beam sputtering of Au (Ref. 32) and confirms our understanding of this process as physical sputtering.

TABLE I. The composition and deposition yield, Y_D of the deposited films at various average current densities, $\langle J \rangle$ and DMG(hfac) pressures, P. Composition is given in at. % of Au and C, the remainder being Ga from the implanted beam and is based on results of Auger analysis performed after sputter removal of the first ~ 100 Å of material (no carbon contamination was observed outside of the deposit after this sputter cleaning). SEM of the microstructure of the corresponding films are shown in the indicated figures. The bottom two rows represent sputtering yields of an evaporated Au film (100% Au) and an ion beam deposited Au film (50% Au) in the absence of the organometallic.

P (mTorr)	$\langle J \rangle$ (μA/cm)	Y (atoms/ion)	% Au	% C	SEM
10	14	8 ± 1	34	58	Fig. 9(a)
10	51	6.7 ± 0.4	38	54	Fig. 9(b)
10	217	3.9 ± 0.3	52	40	Fig. 9(c)
10	26	8.0 ± 0.5	38	55	Fig. 7(a)
1.0	26	7.1 ± 0.5	53	40	Fig. 7(b)
0.1	26	5.5 ± 0.5	64	30	Fig. 7(c)
0	...	-15.7 ± 1.3	100	0	...
0	...	-12.6 ± 1.3	50	35	...

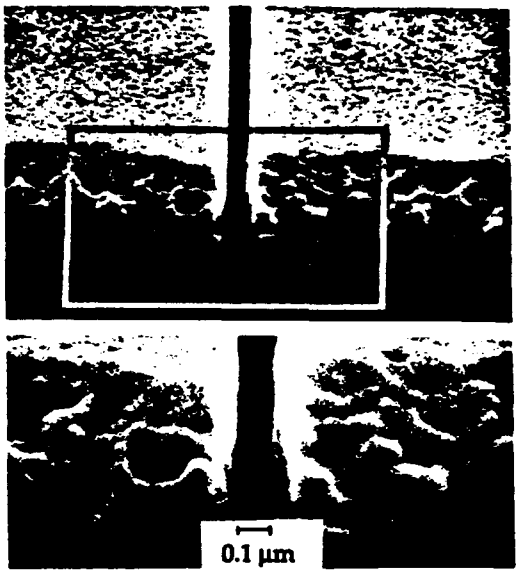

FIG. 3. SEM of 0.1 μm wide line milled through a 2000 Å thick evaporated Au film using 40 keV Ga^+ focused to 70 nm diameter (below: close up).

Figure 3 shows a 0.1 μm wide line milled through a 2000 Å thick evaporated Au film by repeatedly scanning the beam along a single deflection axis. By synchronously scanning along both deflection axes, a grating pattern can be milled whose period is equal to the rastered line spacing. The 210 nm period grating shown in Fig. 4 was milled through 5000 Å of evaporated Au and shows a milled linewidth of ~ 50 nm. It was written over a 13×14 μm area and took 5 min to write. Both side wall redeposition of sputtered material and self-focusing of the ion beam are believed to enhance the aspect ratio of features milled to such depths.

B. Deposition

1. Process parameterization

Using a 1 nA 40 keV Ga^+ beam focused to $\frac{1}{4}$ μm diameter (10%–90%), 99×86 μm deposits were written on a SiO_2 substrate with ion doses of between 1.8×10^{16} and 1.8×10^{17} ions/cm^2. All other conditions were held fixed. The beam was scanned continuously over the substrate at a speed of

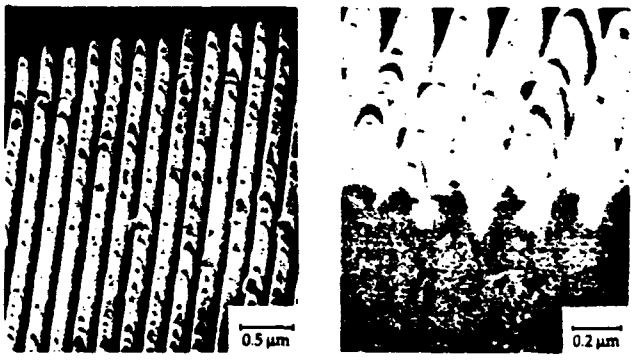

FIG. 4. SEM of a grating milled through a 5000 Å thick evaporated Au film using a 50 pA beam focused to ~ 70 μm diam. It has a periodicity of 210 nm and a spacing between Au lines of ~ 50 nm (right: close up in profile).

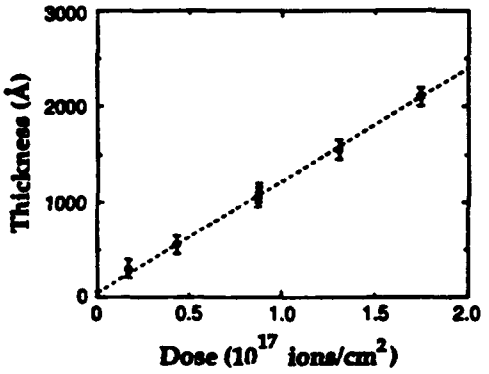

FIG. 5. Thickness of Au deposits as a function of ion dose. The slope of this line corresponds to a deposition of 7 atoms/ion, assuming the films have a density of 5.9×10^{22} atoms/cm^3 (bulk gold).

500 cm/s with a spacing of 0.2 μm between raster lines. The thicknesses of the resulting films were then measured by stylus profilometry and are shown in Fig. 5. Deposition is proportional to ion dose down to a film thickness of 300 Å and has a yield, as defined in Eq. (3), of 7 atoms/ion.

Deposition as a function of DMG(hfac) flux was investigated by varying the height of the gas delivery nozzle, as described in Sec. III. In this case, a 100 pA 40 keV Ga^+ beam focused to <0.1 μm diameter (10%–90%), was used to write 21×18 μm rectangles by scanning continuously over a SiO_2 substrate at a speed of 125 cm/s with a spacing of 0.05 μm. Figure 6 shows the deposition yields [Eq. (3)] inferred from the thickness of films deposited using DMG(hfac) pressures between 0.1 and 10 mTorr (Fig. 2). As the gas flux increases, the deposition yield increases, but changes by only 10% between 1 and 10 mTorr. Auger electron spectroscopy (AES) of these films indicate that films deposited using a higher gas flux contain significantly more carbon and that O and F, both constituents of DMG(hfac), were not detected in any of the films. When the yield measurements are corrected for the fraction of Au in the films, no variation in Au deposition yield as a function of organometallic flux is seen (Fig. 6). However, scanning electron microscopy (Fig. 7) shows that as the gas flux and carbon content decrease, the film microstructure begins to coarsen.

We investigated deposition yield as a function of ion flux ($\langle J \rangle$) by varying the size of the deposits. All other parameters were kept constant, including the beam (100 pA, 0.1 μm diameter), the DMG(hfac) pressure (10 mTorr), scan speed (35 cm/s), and rastered line spacing (0.05 μm). The resulting deposition yield as a function of averaged current density is shown in Fig. 8. As $\langle J \rangle$ increases, the yield falls off rapidly from ~ 10 atoms/ion at an ion flux of 4 μA/cm^2 to approximately zero at 1 mA/cm^2. Although the films deposited at higher $\langle J \rangle$ contain less carbon and more Au (Table I), a significant decrease in the Au deposition yield at higher current densities remains when the data are corrected for the fraction of Au present (2–3 Au atoms/ion for $\langle J \rangle < 100$ μA/cm^2 to less than 0.2 Au atoms/ion for $\langle J \rangle > 900$ μA/cm^2). Scanning electron microscopy (SEM) of the films indicates that decreased carbon content is again associated with coarsening of the film microstructure (Fig. 9). This coarsening has been confirmed by transmission electron microscopy (TEM) analysis and is discussed in more detail in Ref. 33.

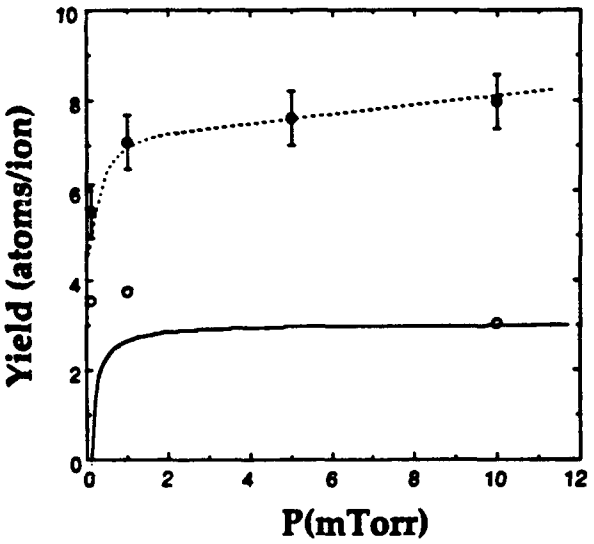

FIG. 6. Deposition yield as a function of the pressure of the organometallic at the substrate. These films were deposited with a time averaged beam current density of 26 μA/cm^2. A pressure of 10 mTorr corresponds to a flux of 10^{16} molecules/cm^2 s. The closed symbols represent yield calculated assuming the films are pure Au, while the open symbols represent the deposition yield corrected for the fraction of Au present. No corrected value is given at 5 mTorr, since AES compositional analysis was not performed on that film. The dashed line is to guide the eye, while the solid curve is the prediction of the theoretical model [Eq. (7)].

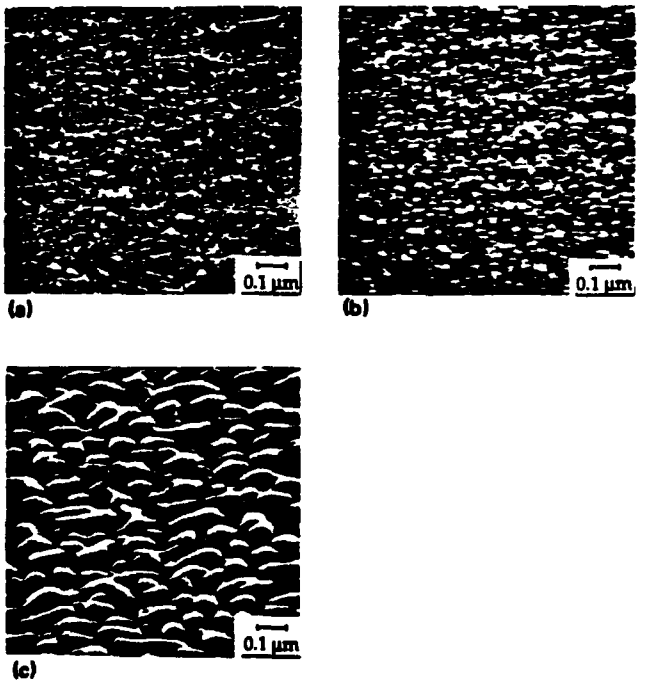

FIG. 7. SEM of films (> 1000 Å thick) deposited at various DMG(hfac) pressures (P), corresponding to data points in Fig. 6. Y is the deposition yield, uncorrected for Au composition. (a) $P = 10.0$ mTorr, $Y = 8.0 \pm 0.5$ atoms/ion[36]; (b) $P = 1.0$ mTorr, $Y = 7.1 \pm 0.5$ atoms/ion[36]; and (c) $P = 0.1$ mTorr, $Y = 5.5 \pm 0.5$ atoms/ion.[36]

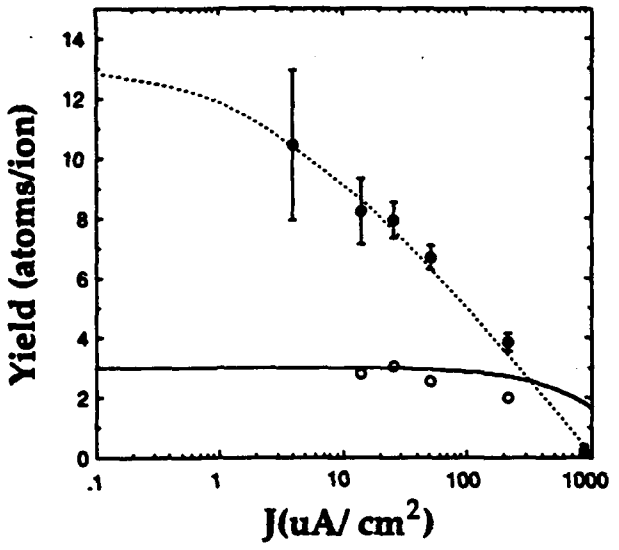

FIG. 8. Deposition yield as a function of $\langle J \rangle$, the time averaged beam current density as defined in the text. These films were deposited with an organometallic pressure of 10 mTorr. The closed symbols represent yield calculated assuming the films were pure Au, while the open symbols represent the deposition yield corrected for the fraction of Au present in those films for which AES compositional analysis was performed. The dashed line is to guide the eye, while the solid curve is the prediction of the theoretical model [Eq. (7)].

We also measured the sputtering yield of the deposited films bombarded by 40 keV Ga^+ in the absence of DMG(hfac) gas. This was done by depositing a thick film (5400 Å thick, ~50 at. % Au), pumping out the organometallic gas and then sputtering away a small region of the deposit. The depth of the sputtered region was then measured by SEM at high incidence angle and used to calculate [Eq. (1) assuming, to first approximation, ρ is that of pure Au] a sputtering yield of 12.6 ± 1.3 atoms/ion, as compared to 15.7 ± 1.3 atoms/ion for an evaporated Au film (Table I).

2. Microfeatures

Examples of Au microfeatures deposited on SiO_2 substrates are shown in Figs. 10 and 11. The 3.4×3.4×1 μm patch in Fig. 10 took 15 min to write with a 25 pA beam, indicating a deposition yield of 5.8 ± 0.6 atoms per incident ion and a growth rate of 11 Å/s. At an average current density of 180 μA/cm², the yield is consistent with the results shown in Fig. 8. The feature was written by synchronously scanning repeatedly over the deposit at a speed of 43 cm/s with a spacing of 0.09 μm between raster lines. Auger analysis of a film deposited under similar conditions indicates that it has a composition of 50% Au, 35% C, and 15% Ga.

The deposited lines shown in Fig. 11 were written with a 50 pA beam scanned repeatedly and continuously over (a) 25 μm at 300 cm/s for 30 s and (b) 90 μm at 180 cm/s for 2 min. Assuming a beam diameter in both cases of ~0.1 μm, these lines were written with $\langle J \rangle = 2$ mA/cm² and $\langle J \rangle = 560\,\mu$A/cm², respectively. The effect of the factor of four difference in the $\langle J \rangle$ can be seen both in their deposition yields ($\ll 1$ and ~2.5, respectively) and in their microstructure.

The conductivity of deposited lines was measured by writing across preevaporated metal (Au, W, Al, and NiCr) contacts patterned by standard photolithography (Fig. 12). Identical lines were written on pre-scribed SiO_2 wafers and

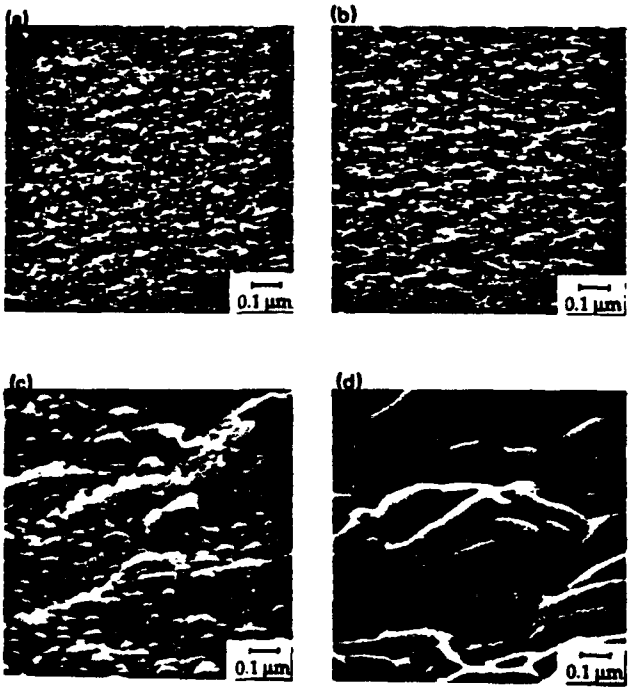

FIG. 9. SEM of films (> 500 Å thick) deposited at various time averaged current densities (J), corresponding to data points in Fig. 8. Y is the deposition yield uncorrected for Au composition. (a) $Y = 8 \pm 1$ atoms/ion,[36] $J = 14$ μA/cm²; (b) $Y = 6.7 \pm 0.4$ atoms/ion,[36] $J = 51$ μA/cm²; (c) $Y = 3.9 \pm 0.3$ atoms/ion,[36] $J = 217$ μA/cm²; and (d) $Y = 0.2 \pm 0.2$ atoms/ion,[36] $J = 865$ μA/cm².

FIG. 10. SEM of a 3.4×3.4 μm Au deposit shown in perspective (top) and in profile (bottom). This feature was written at a deposition rate of 11 Å/s. The height (~1 μm) and high aspect ratio of the edges of this deposit are of particular interest for application in x-ray lithographic mask repair.

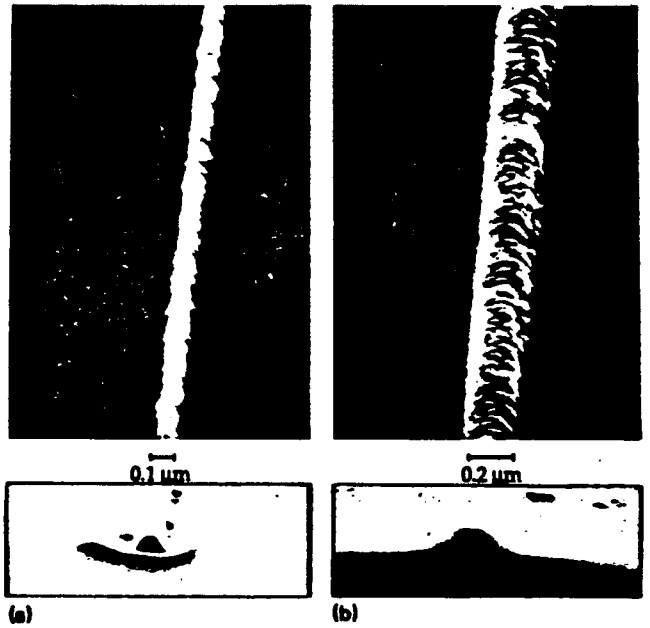

FIG. 11. SEM of deposited Au lines shown in perspective (top) and in cross section (bottom). These lines were written using a 50-pA 40-keV Ga^+ beam focused to <0.1 μm diameter. The line (a) is 25 μm long and was written in 30 s. The line (b) is 90 μm long and was written in 2 min. The larger width of the line in (b) is believed to be a result of drift in the ion beam perpendicular to the scan direction. The feature in the foreground of the cross section in (a) is an artifact of the beam not being blanked at the end of a line.

then cleaved to measure the cross-sectional area of the lines, thus allowing an estimation of the resistivity of the deposited film. These measurements show resistivities in the range of 500 to 1500 μΩ cm (pure Au has a bulk resistivity of 2.44 μΩ cm). As is illustrated in Fig. 13, the lines are easily written over 2000 Å steps and the deposition efficiency is relatively independent of the substrate (~5 atoms/ion). One exception to this was found in the case of Au contacts (Fig. 14). Since the measured sputtering yield of evaporated Au is ~3 atoms/ion greater than that of the deposited Au/C composite and substantially greater than that of any of the other substrates, we would expect, based on Eq. (2), difficulty initializing the deposition process on an Au substrate. Similar substrate dependence in the early stages of deposition has been observed in 5 keV Ar^+ induced Au deposition.[34]

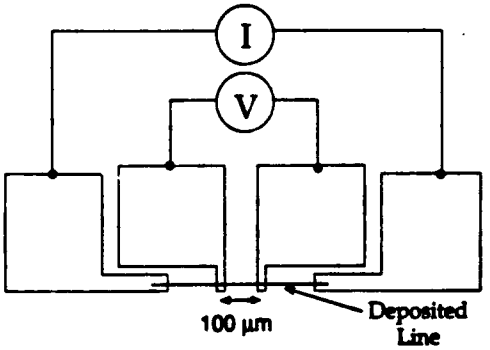

FIG. 12. Schematic of the arrangement used to measure the resistance of ion beam deposited Au lines. The pads were made of evaporated films of Au, W, NiCr, or Al on SiO_2 substrates patterned by standard photolithographic techniques. The spacing between the inner fingers (each 10 μm wide) is 100 μm.

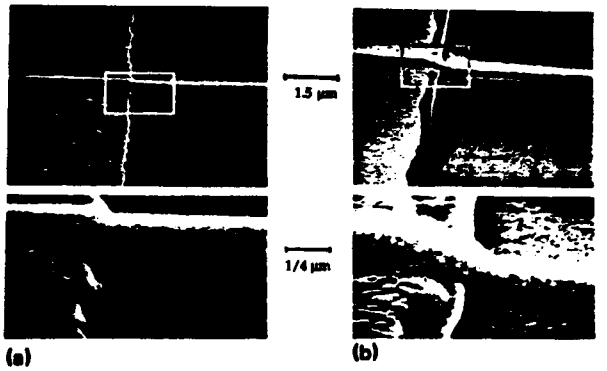

FIG. 13. SEM ion beam deposited line crossing the edge of the evaporated (a) W (600 Å thick) and (b) Al (2000 Å thick) films described in Fig. 12.

V. DISCUSSION

The rather weak dependence of the deposition yield on the DMG(hfac) pressure shown in Fig. 6 indicates that undue effort to increase the DMG(hfac) flux by, for instance, heating the gas delivery system, would not be especially effective. However, the strong dependence on ion flux shown in Fig. 8 is particularly important to microfeature deposition. For example, from the data presented it is clear that a 1×1 μm feature could not be written by *continuous* scanning of a 100 pA beam, whereas a 25×1 μm feature over 0.5 μm thick could be written in less than 10 min. This relationship can be seen more clearly in Fig. 15 where the growth rate, R, is displayed as a function of $\langle J\rangle$:

$$R=\frac{\langle J\rangle Y_D}{\rho}$$

(ρ being the atom density of the deposited film, here taken to be 5.9×10^{22}, that of bulk Au). With an organometallic pressure of 10 mTorr, the maximum measured growth rate of 9

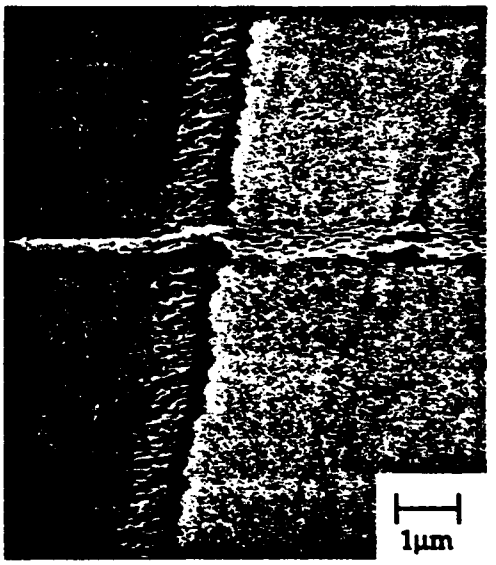

FIG. 14. SEM of ion beam deposited line crossing the edge of the evaporated Au (2000 Å thick) film described in Fig. 12. Whereas substrate independent deposition is observed for W, Al, NiCr, and SiO_2 (Fig. 13), almost no deposition is seen on the Au substrate (right).

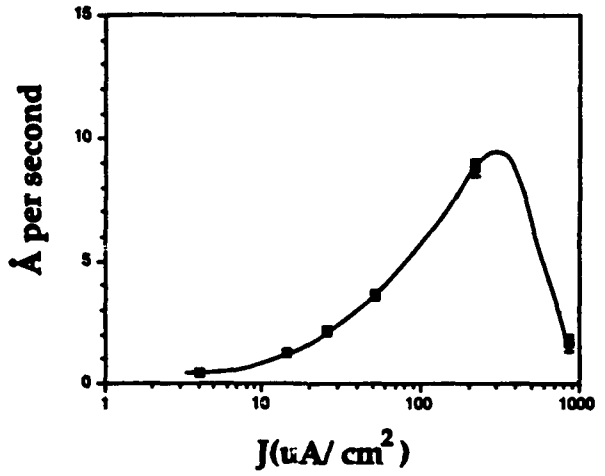

FIG. 15. Deposition rate, as defined in the text, as a function of average current density with a precursor pressure of 10 mTorr. The solid line is to guide the eye.

Å/s was achieved by writing with an average current density, $\langle J \rangle$, of $\sim 220\,\mu A/cm^2$, and is very sensitive to $\langle J \rangle$. If one wished to write arbitrary microfeatures under these optimum conditions, beam blanking could be used to control the scanned current density.

The large variation in film purity as a function of both the ion flux and organometallic flux is also of considerable importance to microfeature fabrication, since it will affect both the electrical resistivity and x-ray opacity of deposited structures. The larger carbon content of the films deposited with low current densities or high organometallic flux suggests that at high adsorbate coverage, where more organometallic molecules are dissociated per ion, the by-products of the dissociation are less efficiently desorbed from the growing film. This trapped carbon then impedes island growth, preventing coarsening and leading to nucleation of new islands as seen in the micrographs in Figs. 7 and 9.

The discontinuous microstructure of the films resulting from the carbon impurities explains the relatively high resistivities measured. Such an interpretation agrees well with previously reported results for 70 keV broad beam Ar^+ induced Au deposition.[27] That study investigated the microstructure, carbon content, and resistivity of films deposited at a constant current density and pressure but at increasing substrate temperature. It was found that at higher temperatures the carbon content and resistivity dropped dramatically and the microstructure became continuous. The authors therefore concluded that at high temperature, where by-product desorption is assisted by thermal energy, the film growth is not impeded by the presence of excessive carbon and as a result, film resistivity approaches that of bulk Au. Furthermore, the microstructure of the films deposited at room temperature with an Ar beam resembles that which we observe in films deposited with a Ga beam. This suggests that the presence of implanted Ga in focused ion beam deposited films does not grossly affect the film growth.

The observed variation of the deposition yield as a function of ion ($\langle J \rangle$) and DMG(hfac) flux (Φ) agrees qualitatively with the simple relationship expressed in Eq. (2), implying, as expected, that increasing $\langle J \rangle$ decreases the adsorbate coverage, N, while increasing Φ increases N. A model for the relationship between N, $\langle J \rangle$, and Φ during electron beam induced deposition using a DMG(hfac) precursor was proposed by Koops *et al.*[24] which was based on their earlier work with tungsten carbonyl.[35] By assuming monolayer type adsorption of the organometallic, they express its molecular coverage, N, as:

$$\frac{dN}{dt} = g\Phi\left(1 - \frac{N}{N_0}\right) - \frac{N}{\tau} - \sigma N \langle J \rangle, \tag{5}$$

where N_0 is the molecular density at a monolayer, g is the sticking coefficient, τ is the mean lifetime of an adsorbed molecule, σ is the cross section for dissociation. [The appropriateness of this monolayer approximation in the pressure and temperature range considered here has recently been born out by measurements of adsorption properties of DMG(hfac).[29]] At steady state ($dN/dt = 0$), the adsorbate coverage may be written:

$$N_E = \frac{g\Phi}{\frac{g\Phi}{N_0} + \frac{1}{\tau} + \sigma\langle J \rangle}. \tag{6}$$

To extend this treatment to the case of ion beam induced deposition, we need only to insert this expression into Eq. (2), in effect, including a term to account for sputtering of the growing film:

$$Y_D = \frac{1}{\frac{1}{\sigma N_0} + \frac{1}{g\Phi\sigma\tau} + \frac{\langle J \rangle}{g\Phi}} - Y_S. \tag{7}$$

If we assume $g = 1$, and the measured value of $Y_s = 12.6 \pm 1.3$ atoms/ion described above for a deposited film which was $\sim 50\%$ Au, we can fit this expression to our data for Y_D (corrected for Au composition) as a function of $\langle J \rangle$ at $\Phi = 10^{18}$ molecules/cm^2 s [10 mTorr DMG(hfac)]. From the fit (solid line in Fig. 8), assuming $\Phi\tau \gg N_0$ we find:

$$\sigma N_0 = 15.6. \tag{8}$$

If N_0 is $\sim 3\times 10^{13}$ molecules/cm^2,[36] this implies $\sigma = 5.2\times 10^{-13}$ cm^2 corresponding to an area of excitation of ~ 80 Å diameter which would be consistent with the diameter of the collision cascade. Unfortunately, Eq. (7) predicts too large a value of Y_D at the higher current densities. However, we have assumed a constant value of Y_s for all values of $\langle J \rangle$. Since the fraction of Au in the film increases as a function of $\langle J \rangle$, Y_s will increase from a measured value of 12.6 atoms/ion for 50% Au films at $\langle J \rangle \sim 200\,\mu A/cm^2$ toward 15.7 atoms/ion (the measured value for 100% Au films) at higher $\langle J \rangle$. Accounting for such composition dependent sputtering will improve the fit to the data, as would including terms to account for beam induced desorption. Increased thermal desorption at high $\langle J \rangle$ due to increased substrate heating can be ruled out since with a 100 pA beam the rise in temperature at the deposition site would be less than 1 °C even with $\langle J \rangle = 1$ mA/cm^2 (see Ref. 3 for the details of this estimation).

We can compare this simple model to the yield data as a function of Φ by assuming $\Phi\tau \gg N_0$ and inserting Eq. (8) into Eq. (7). As shown by the solid line in Fig. 6, it is unable

to fit the low Φ behavior. Accounting for composition dependent sputtering or beam induced desorption does not improve the fit. This suggests that for small Φ either the assumption $g\Phi\tau \gg N_0$ or that the expression for molecular coverage given in Eq. (5) is inappropriate.

Although this modeling is unable to fit the data in detail, it does predict the qualitative trends seen in the data both as a function of $\langle J \rangle$ and Φ. By removing the simplifying assumption that $g\Phi\tau \gg N_0$ and by adding composition dependent sputtering to Y_s in the model, it is believed that a more quantitative fit could be achieved.

The expression in Eq. (7) is similar to that described recently by Rüdenauer *et al.* to model ion beam induced deposition of Al using a trimethyl-aluminum precursor except that these authors allowed for sputtering only from sites which are not occupied by adsorbed organometallic.[21] Accounting for such coverage dependent sputtering in Eq. (7) improves the fit to the data as a function of Φ. However, doing so proves less effective in fitting the data as a function of $\langle J \rangle$, predicting a smaller value for σ and thus an even slower fall off in Y_D as a function of $\langle J \rangle$. In fitting their model to their data covering a limited range of current densities, molecular fluxes and ion energies, Rüdenauer *et al.* found sputtering yields far higher than expected and concluded that this was due to changes in the surface binding energy resulting from the presence of the adsorbate. Since we are depositing Au, a relatively chemically inert species, we have ignored this effect and assumed the value Y_s measured as described in the previous section.

VI. CONCLUSIONS

We have demonstrated focused ion beam induced deposition and milling of submicron Au features with linewidths of 0.1 μm and steep sidewalls. The deposition efficiency has been parameterized as a function of both the incident ion flux and the molecular flux of the precursor gas. Current models of this process account for the qualitative trends of data, but do not fit it in detail. Important variations in film purity have been observed. Discontinuous microstructure and high carbon content have been correlated with ion and precursor fluxes and are believed to be responsible for film resistivities approximately equal to that of polysilicon. These results suggest that film resistivities may be further reduced by modest substrate heating, as reported by Ro *et al.*[27] Such a reduction would make the process more suitable for circuit repair applications.

We have determined that the maximum deposition rate at room temperature is ~ 10 Å/s and that this maximum rate can be achieved by careful control of the time averaged beam current density. This would mean a process time of ~ 5 min to write a microfeature $\frac{1}{2}$ μm high, as might be required for x-ray lithographic mask repair. Increasing the flux of the organometallic gas does not appreciably reduce this time; however, cooling the substrate may help by significantly increasing the adsorbate coverage.

ACKNOWLEDGMENTS

The authors thank J. Martin and E. L. Shaw for their help with the Auger analysis, J. Carter and T. McClure for technical assistance, H. H. Sawin for suggesting the stagnation tube experiments, and C. V. Thompson for many useful discussions. This work has been supported by U.S. Army Research Office Contract No. DAAL 03087-K-0126 and by Draper Laboratory.

[1] R. Clampit, K. L. Aitken, and D. K. Jefferies, J. Vac. Sci. Technol. 12, 1208 (1975).
[2] R. Clampit and D. K. Jefferies, Nucl. Instrum. and Methods 149, 739 (1978).
[3] For review of applications of focused ion beams: J. Melngailis, J. Vac. Sci. Technol. B 5, 469 (1987).
[4] J. R. A. Cleaver, H. Ahmed, P. Heard, P. Prewett, G. Dunn, and H. Kaufman, Microelectron. Eng. 3, 253 (1985).
[5] N. P. Economou, D. C. Shaver, and B. Ward, SPIE 773, 201 (1987).
[6] M. Yamamoto, M. Sato, H. Kyogoko, K. Aita, Y. Nakagawa, A. Yasaka, R. Takasawa, and O. Hattori, SPIE 632, 97 (1986).
[7] W. P. Robinson and D. W. Williams, Presented at 35th Meeting of American Vacuum Society (1988).
[8] J. Melngailis, C. R. Musil, E. H. Stevens, M. Utlaut, E. M. Kellogg, R. T. Post, M. W. Geis, and R. W. Mountain, J. Vac. Sci. Technol. B 4, 176 (1986).
[9] Y. Mashiko, H. Morimoto, H. Koyama, S. Kawazu, T. Kaito, and T. Adachi, 25th Annual Reliability Physics, San Diego (April 1987).
[10] L. R. Harriot, A. Wagner, and F. Fritz, J. Vac. Sci. Technol. B 4, 181 (1986).
[11] D. C. Shaver and B. W. Ward, J. Vac. Sci. Technol. B 4, 185 (1986).
[12] L. A. Stern and D. K. Stewart, Presented at 35th Meeting of American Vacuum Society (1988).
[13] G. M. Shedd, H. Lezec, A. D. Dubner, and J. Melngailis, Appl. Phys. Lett. 49, 1584 (1986).
[14] Y. Ochiai, K. Gamo, and S. Namba, J. Vac. Sci. Technol. B 3, 67 (1985).
[15] Y. Ochiai, K. Shihoyama, T. Schiokawa, K. Toyoda, A. Masuyama, K. Gamo, and S. Namba, J. Vac. Sci. Technol. B 4, 333 (1986).
[16] R. L. Kubena, R. L. Seliger, and E. H. Stevens, Thin Solid Films 92, 165 (1982).
[17] H. Yamaguchi, A. Shimase, S. Haraichi, and T. Miyauchi, J. Vac. Sci. Technol. B 3, 71 (1985). See also: H. Morimoto, Y. Sasaki, Y. Watakabe, and T. Kato, J. Appl. Phys. 57, 159 (1985).
[18] T. Ishitani and T. Ohnishi, Jpn. J. Appl. Phys. 28, L320 (1989).
[19] K. Gamo, N. Takakura, N. Samoto, R. Shimizu, and S. Namba, Jpn. J. Appl. Phys. 23, L293 (1984).
[20] K. Gamo, D. Takehara, Y. Hamamura, M. Tomita, and S. Namba, Microelectron. Eng. 5, 163 (1986).
[21] F. G. Rüdenauer, W. Steiger, and D. Schrottmayer, J. Vac. Sci. Technol. B 6, 1542 (1988).
[22] S. Matsui and K. Mori, J. Vac. Sci. Technol. B 4, 299 (1986).
[23] R. B. Jackman and J. S. Foord, Appl. Phys. Lett. 49, 196 (1986).
[24] H. W. P. Koops, R. Weiel, and D. P. Kern, J. Vac. Sci. Technol. B 6, 477 (1988).
[25] R. R. Kunz and T. M. Mayer, Appl. Phys. Lett. 50, 962 (1987).
[26] For review of the subject: D. J. Ehrlich and J. Y. Tsao, J. Vac. Sci. Technol. B 1, 969 (1983).
[27] J. S. Ro, A. D. Dubner, C. V. Thompson, and J. Melngailis, Mater. Res. Soc. Symp. 101, 255 (1988).
[28] K. B. Winterbon, P. Sigmund, and J. B. Sanders, K. Dan Vidensk. Selsk. Mat. Fys. Medd. 37, No. 14 (1970).
[29] A. D. Dubner and A. Wagner, J. Appl. Phys. (in press).
[30] IBT Dubilier LTD., Abingdon, Oxon, U.K.
[31] FEI Co., Beaverton, OR, U.S.A.
[32] N. Matsunami, Y. Yamamura, Y. Itikawa, N. Itoh, Y. Kazumata, S. Miyagawa, K. Morita, R. Shimizu, and H. Tawara, At. Data Nucl. Data Tables 31, 1 (1984).
[33] P. G. Blauner, J. S. Ro, Y. Butt, C. V. Thompson, and John Melngailis, Mater. Res. Soc. Symp. (to be published).
[34] A. D. Dubner and A. Wagner, J. Appl. Phys. 65, 3636 (1989).
[35] V. Scheuer, H. Koops, and T. Tschudi, Microelectron. Eng. 5, 423 (1986).
[36] This number is based on the 20 Å molecular diameter of DMG(hfac). It is consistent with the adsorption data for this molecule reported in Ref. 29.

Focused ion beam induced deposition of low-resistivity gold films

Patricia G. Blauner,[a] Yousaf Butt, Jae Sang Ro, Carl V. Thompson, and John Melngailis
Research Laboratory of Electronics, Massachusetts Institute of Technology, Cambridge, Massachusetts 02139

(Received 30 May 1989; accepted 10 July 1989)

Focused ion beam induced deposition of metals has up to now produced films with resistivities 30–5000 times higher than bulk values for metals because of high concentrations of impurities from the precursor gas incorporated into the films. We have demonstrated for the first time deposition of submicron Au films with resistivities approaching that of the bulk metal and carbon contents of < 10 at. %. These results are particularly relevant to applications in integrated circuit restructuring and x-ray lithography mask repair, where high film conductivity and purity improves interconnect quality and x-ray opacity.

I. INTRODUCTION

Creation of patterned films of materials in a maskless, resistless fashion is of practical interest and has stimulated much work in laser-direct write deposition.[1] More recently, focused ion beams have been substituted for laser beams, thus permitting patterned deposition at dimensions well below 1 μm. Ion beams have the distinct advantage that they can also be used for material removal by ion milling with submicron precision.

In ion induced deposition, a local gas ambient of an appropriate compound is created by a miniature nozzle aimed at the sample surface. The focused ion beam is scanned over the sample to deposit a patterned film by causing adsorbed gas molecules to break up. This technique is already widely used in the repair of photolithography masks where the ability to both mill and deposit using the same beam is especially valuable.[2–6] Focused ion beam based systems are currently being developed for the repair or restructuring of integrated circuits and for the repair of x-ray lithography masks. To meet the requirements of these applications, research efforts have concentrated on attaining low-resistivity deposits and high aspect ratio deposits of high-Z materials.

However, hitherto attempts to deposit conducting films have typically resulted in high concentrations of impurities and resistivities a factor of 30–5000 times higher than bulk values for metals.[7–11,16] The one exception was gold films deposited over a large area on a heated substrate (100–160 °C) using an Ar^+ beam from an implanter. In this case, resistivities near the bulk value of gold were obtained.[12] Extending this work to a focused Ga^+ beam, we report here for the first time patterned submicron gold deposition with resistivities within experimental error of the bulk value and, in addition, high aspect ratio, submicron lines.

II. APPARATUS

The ion beam system and gold deposition technique used in this work will be described in more detail elsewhere.[13] 20–100 pA, 40 keV Ga^+ beams focused to diameters of less than 0.1 μm were scanned rapidly over samples located in a differentially pumped work chamber (base pressure 1×10^{-7} Torr), as shown in Fig. 1. The samples were mounted on a small platform built on the X-Y positioning stage and designed to accommodate an embedded resistive heater and thermocouple. The gold-bearing gas, dimethyl gold hexafluoro acetylacetonate [$C_7H_7F_6O_2Au$, hereafter referred to as DMG(hfac)],[14] was introduced through a 0.8 mm i.d. tube suspended ~0.2 mm above the sample, 100 μm from the ion beam axis. The resulting DMG(hfac) pressure was measured to be 10 mTorr at the sample surface.[13]

III. RESULTS AND DISCUSSION

In order to allow for resistivity measurements and compositional analyses of the same films, 300 μm long, 1.2 μm wide, 1400–2000 Å high lines were deposited across evaporated Au contacts on a SiO_2 substrate at temperatures of 35, 50, 75, and 100 °C. Resistance was measured by a four-point current and voltage measurement. Resistivity was then calculated based on line cross sections estimated from scanning electron microscopy (SEM) and stylus profilometry measurements. Subsequently, the film compositions were analyzed by high-resolution scanning Auger electron spectroscopy (AES), preceded by 3 keV Ar^+ sputter cleaning (~150 Å) to remove any surface contamination. As can be seen from the open points in Fig. 2, resistivity decreases by more than a factor of 10 between 35 and 100 °C and is accompanied by an increase in film purity. The film compositions varied from ~10 at. % Ga, 40 at. % C, and 50 at. % Au at 35 °C to 10 at. % Ga, 10 at. % C, and 80 at. % Au at 100 °C. Because composition was measured using AES and no alloy standards were available, the atomic percent data are intended to show the trend rather than the absolute composition. No F was detected in any of the films and O was present in the lower temperature films at a level of less than 3% [both O and F are constituents of DMG(hfac)]. Based on the

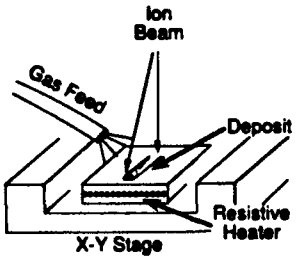

FIG. 1. Schematic of the apparatus showing the resistively heated platform set into the x-y stage and the gas feed used to create a ~10 mTorr atmosphere of the gold-bearing organometallic at the sample surface. Details of the gold deposition technique are given elsewhere (see Ref. 13).

 0734-211X/89/061816-03$01.00

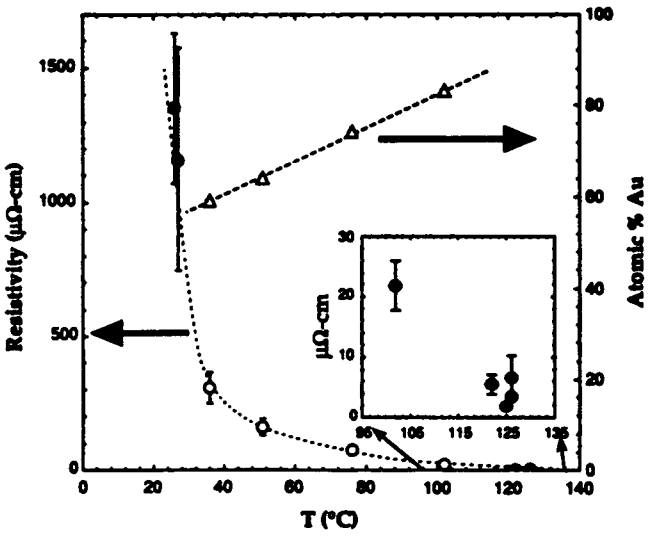

FIG. 2. Resistivity and Au content of lines shown as a function of the temperature of the substrate during deposition. The closed circles represent values associated with deposits under 0.5 μm width, where compositional analysis was not possible. The open circles represent values associated with 1.2 μm wide lines from which both resistance and composition were measured as described in the text. The inset shows the high-temperature region in more detail. The bulk resistivity of Au is 2.44 $\mu\Omega$ cm. The uncertainties in the resistivity data correspond primarily to uncertainties in estimating the cross sections of the lines.

atomic percentages of Au and the estimated cross sections of the lines, the deposition yield, number of Au atoms deposited per Ga ion, was calculated to be ~3 atoms/ion and varied by less than 30% with substrate temperature.

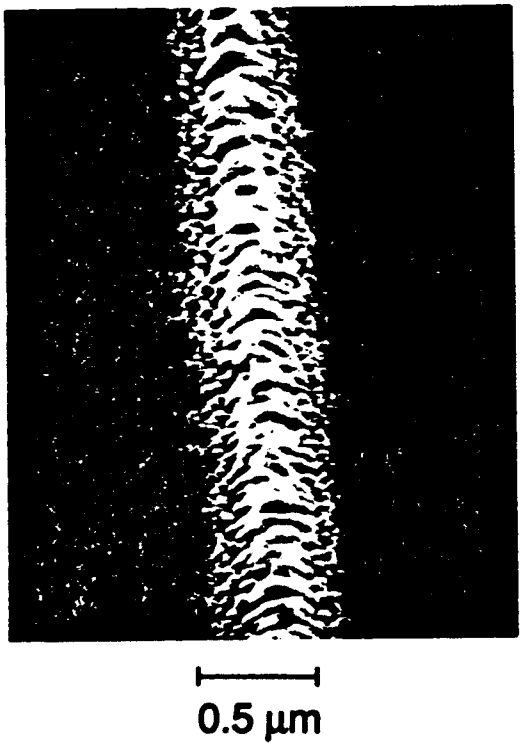

FIG. 3. Scanning electron micrograph of a line deposited at 125 °C. The line is estimated to be 200 Å high and to have a resistivity of 7 ± 4 $\mu\Omega$ cm. It is 120 μm long and was written between two Al contact pads using a rapidly scanned 20 pA, 40 keV Ga^+ focused beam.

The closed points in Fig. 2 correspond to narrower lines 100–300 μm long which were written across Au and Al contacts on substrates held at 25, 120, and 125 °C. The resistivities of these submicron lines were estimated as described above or, in some instances, by a two-point current and voltage measurement (compositional analyses of these lines could not be performed). Note that at 125 °C, resistivity is within experimental error of that of bulk Au (2.44 $\mu\Omega$ cm). Since the deposited gold, of necessity, contains implanted gallium, its resistivity is actually expected to be higher than that of pure gold.[15] Figure 3 shows a SEM of one such line deposited at 125 °C. The resistivity of this 0.3 μm wide line is estimated to be 7 ± 4 $\mu\Omega$ cm. It is 120 μm long and took 2.5 min to write across two Al contacts. Its width, approximately three times that of the ion beam diameter, reflects the mechanical drift in the stage position which has been observed to be large when operating at high sample temperatures. Figure 4 is a SEM of a high aspect ratio line deposited at 25 °C. This 100 μm long, 0.75 μm high line took 30 min to write and, again, its width is limited by the mechanical stability of the system.

IV. CONCLUSIONS

The correlation between resistivity and Au content shown in Fig. 2 is in agreement with results reported for broad Ar ion beam induced Au deposition. The high resistivity of room-temperature ion beam induced Au deposits results from incomplete desorption of by-products and can be eliminated by raising substrate temperatures to the rather moderate value of 120 °C. We have demonstrated that this technique may be extended to focused ion beam induced deposition and therefore can be used for submicron patterning of Au films. Line width and aspect ratio are currently limited not by the ion beam diameter but by the mechanical stability

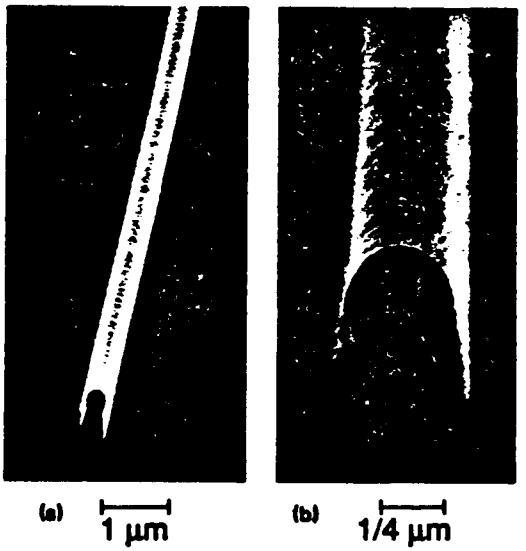

FIG. 4. Scanning electron micrographs of a high aspect ratio deposit shown in (a) perspective and (b) cross section. This line, 100 μm long and 0.75 μm high, was deposited on a SiO_2 substrate at room temperature using a rapidly scanned 20 pA, 40 keV Ga^+ focused beam.

of the heated stage. A local heating technique such as low-power laser irradiation may overcome this limitation.

ACKNOWLEDGMENTS

The authors thank J. Martin and E. L. Shaw for their help with the Auger analysis and J. Carter and T. McClure for their technical assistance. This work has been supported by U. S. Army Research Office Contract No. DAAL 03087-K-0126 and by Draper Laboratory.

[a]Current address: IBM Thomas J. Watson Research Center, Yorktown Heights, NY 10598.

[1]For a review of laser-direct writing, see D. J. Ehrlich and J. Y. Tsao, J. Vac. Sci. Technol. B 1, 969 (1983).
[2]J. R. A. Cleaver, P. D. Prewett, G. J. Dunn, and H. Kaufman, Microelectron. Eng. 3, 253 (1985).
[3]N. Economou, D. Shaver, and B. Ward, Proc. SPIE 737, 201 (1987).
[4]M. Yamomoto, M. Sato, H. Kyogoko, K. Aita, Y. Nakagawa, A. Yasaka, R. Takasawa, and O. Hattori, Proc. SPIE 632, 97 (1986).
[5]W. P. Robinson and N. W. Parker, Proc. SPIE 773, 216 (1987).
[6]L. R. Harriott and M. J. Vasile, J. Vac. Sci. Technol. B 6, 1035 (1988).
[7]K. Gamo, D. Takehara, Y. Hamamura, M. Tomita, and S. Namba, Microcircuit Eng. 5, 163 (1986).
[8]G. M. Shedd, A. D. Dubner, H. Lezec, and J. Melngailis, Appl. Phys. Lett. 49, 1584 (1986).
[9]W. P. Robinson, Proc. SPIE (to be published).
[10]K. K. Stewart, L. A. Stern, and J. C. Morgan, Proc. SPIE (to be published).
[11]P. G. Blauner, J. S. Ro, Y. Butt, C. V. Thompson, and J. Melngailis, Mater. Res. Soc. Proc. (to be published).
[12]J. S. Ro, A. D. Dubner, C. V. Thompson, and J. Melngailis, Mater. Res. Soc. Proc. 101, 255 (1988).
[13]P. G. Blauner, J. S. Ro, Y. Butt, and J. Melngailis, J. Vac. Sci. Technol. B 7, 609 (1989).
[14]Gold acetylacetonate complexes have also been used for laser-direct write deposition [T. H. Baum and C. R. Jones, Appl. Phys. Lett. 47, 538 (1985)] and electron beam induced deposition [H. W. P. Koops, R. Weiel, and D. P. Kern, J. Vac. Sci. Technol. B 6 (1988)].
[15]O. Michikami and Y. Yamaguchi, Jpn. J. Appl. Phys. 10, 660 (1971).
[16]Ion beams have also been shown to selectively enhance nucleation site densities during thermal CVD of high-purity Fe and Al films [R. L. Kubena, F. P. Stratton, and T. M. Mayer, J. Vac. Sci. Technol. B 6, 1865 (1988)]. The resistivities of these films were not reported.

Focused ion beam induced deposition of platinum

Tao Tao, JaeSang Ro, and John Melngailis
Research Lab of Electronics, Massachusetts Institute of Technology, Cambridge, Massachusetts 02139
Ziling Xue and Herbert D. Kaesz
Department of Chemistry and Biochemistry, University of California, Los Angeles, California 90024

(Received 29 May 1990; accepted 1 August 1990)

Focused ion beam induced deposition of platinum from a precursor gas of (methylcyclopentadienyl)trimethyl platinum has been demonstrated. This organometallic compound is solid at room temperature with a vapor pressure of 0.054 Torr. Ga^+ ions at 30–40 keV have been used. The resistivity and composition of the film and the deposition yield have been measured as a function of ion current density, line dose, substrate temperature, geometry, and supplemental hydrogen pressure. Yield varies from 0.2 to 34, and resistivity varies from 70 to 700 $\mu\Omega$ cm depending on the conditions. The resistivity and content of the carbon impurity are reduced as the ion current increases: the lowest resistivity is observed at the highest current density corresponding to 0.222 nA at scan speed 500 cm/s repeated over a 350 μm long line. The minimum linewidth achieved so far is 0.3 μm. Transmission electron microscopy shows the Pt film to be amorphous, and Auger analysis gives the film composition 46% Pt, 24% C, 28% Ga, and 2% O. The addition of hydrogen gas supplied to the same area by a second nozzle is found to have little effect on yield or resistivity. Although the deposition of gold from an organometallic precursor on a substrate at elevated temperature results in low resistivity films, in the case of platinum this is not observed; in fact, deposition yield goes to zero as the substrate temperature is raised. The deposition of platinum at near grazing incidence of ion beam on a cleaved silicon surface has been observed. Such deposition differs from that of normal incidence, tending to form discrete islands at about 0.25 μm dimensions.

I. INTRODUCTION

In the past ten years focused ion beam technology has advanced in a number of areas. The focused ion beam milling and ion induced deposition have found commercial applications in repair of photolithography masks, and recently also in integrated circuit repair. Repair of x-ray lithography masks is a likely important future application. About a half dozen of metal films[1–10] have been successfully made. If deposition is carried out in a poor vacuum, a high concentration of oxygen is often observed. These films usually contain substantial concentrations of unwanted constituents of the precursor gas, mainly carbon. The resistivity of these films is often from 20 to 200 times higher than that of pure metal. Gold deposition at elevated substrate temperature is an exception and shows higher film purity and resistivity nearly equal to that of pure gold.[10]

The lack of volatile metal compound precursors limits new findings of metal deposition induced by focused ion beams. Recently high purity platinum films have been deposited by low temperature[11] and laser-induced[12] organometallic chemical vapor deposition using hydrocarbon platinum compounds as precursors in the presence of hydrogen gas. Platinum film is a promising candidate, not only for repair of x-ray lithography masks, but also for integrated circuit repair. Platinum has a high Z number, and its x-ray absorption is slightly higher than that of gold and tungsten in the range of interest. In addition, platinum is inert and does not degrade due to exposure to air or to elevated temperatures or high current densities. Unlike gold, platinum is not an adverse contaminant of integrated circuits and can even be deposited directly on silicon.

II. EXPERIMENT

A. Preparation of (MeCp)$PtMe_3$

(Methylcyclopentadientyl)trimethyl platinum, (MeCp)$PtMe_3$, is synthesized from trimethylplatinum iodide and sodium methylcyclopentadienide using the method described in the literature.[13] The product is a pale green to while colored solid with a melting point of 29.5–30 °C. The vapor pressure is found to fit the following equations:

$$\ln P(\text{Torr}) = 26.1 - 8600/T, \quad 373 < T < 303 \text{ K},$$

$$\text{heat of sublimination} = 71.5 \text{ kJ/mol};$$

$$\ln P(\text{Torr}) = 15.3 - 5240/T, \quad 303 < T < 333 \text{ K},$$

$$\text{heat of evaporation} = 43.6 \text{ kJ/mol}.$$

The vapor pressure is 0.054 Torr at 23 °C, and 0.40 Torr at 50 °C. This compound will gradually decompose at temperature over 50 °C.

B. Apparatus

Metal films have been deposited by scanning a focused ion beam across the surface of a substrate on which a metal precursor is adsorbed. A differentially pumped focused ion beam column provides Ga ions with energy from 10 to 50 keV, beam diameter possibly less than 100 nm, and ion current up to 1 nA. (See Ref. 14 for a more detailed description.) In a work chamber (base pressure 6×10^{-10} Torr) a main gas jet with opening 0.7 mm delivers the precursor gas onto the substrate surface. A second gas jet with smaller opening of 0.3 mm supplies hydrogen or other gases to the same area. There is no heater on the gas jets, the precursor

 0734-211X/90/061826-04$01.00

gas expands into vacuum at room temperature. The sample is mounted on either a plain stage or a heated stage.

Platinum films are deposited on substrates, such as Si, SiO_2, or Al. The composition of these films is analyzed by Auger electron spectroscopy. The auger results give fairly accurate comparison among different samples. Because of lack of standard sample for concentration calibration, the composition values are accurate to only $\pm 10\%$ to 30%. Film thickness is measured by scanning electron microscopy (SEM) and by stylus profilometry. Resistivity is measured by using a four-point probe, i.e., by depositing a stripe of the film across four metal fingers previously patterned on the sample surface. The microstructure of the films is examined by high resolution scanning electron microscope (SEM) and transmission electron microscope (TEM). For TEM sample preparation, films are directly deposited onto 0.1-μm-thick silicon nitride membranes.

III. RESULTS AND DISCUSSION

A. Deposition on flat surface

Figures 1(a)–1(c) shows platinum deposition on a silicon dioxide substrate. The Pt line is written by a 35-keV Ga ion beam with current of 20 pA over a length of 22 μm. For comparison, a milling line achieved by scanning the ion beam without introduction of Pt precursor is shown (a). The identical line width (0.3 μm) and ripples from oscillation of scan signals suggest that the deposition linewidth is limited by ion beam diameter and a finer structure is possible if the ion beam size is reduced. Transmission electron microscopy, Fig. 1(d), shows Pt films grown by focused ion beam induced deposition are amorphous while gold films have polycrystalline microstructure.[9,15] Figure 2(a) shows the resistivity of platinum films as a function of ion line dose at various ion beam currents. At very low ion doses, the films are so thin and discontinuous that the resistivity is high. The resistivity of Pt films gradually decreases as the total ion dose increases, or, as the film thickness increases. For the same thickness samples, the film resistivity decreases as the ion beam current increases. In fact, the lowest resistivity of 70 $\mu\Omega$ cm is observed at the highest ion beam current of 222 pA. The resistivity of bulk Pt is 10.4 $\mu\Omega$ cm. Figure 2(b) shows the Pt film deposition yield as a function of ion beam current. The yield is defined as a ratio of number of Pt atoms being deposited per ion, assuming that the film consists of only pure platinum. The yield does not vary much as ion beam current increases except when the ion beam density is so large that the adsorbed Pt precursor is depleted, and sputtering begins to dominate. Figure 3 shows Auger electron spectroscopy results of film composition as a function of ion beam current. The Pt films are deposited on an area of 8×8 μm^2 on silicon dioxide. At ion currents larger than 80 pA sputtering instead of deposition occurs. The Auger results are recorded after sputtering away several layers of surface atoms until the carbon concentration stays constant. Figure 3 demonstrates rapid decrease of carbon content and increase of platinum in the film composition as the ion beam current increases. The highest content of platinum in the film is 46 Pt% (Ga 28%, C 24%, O 2%) at an ion beam current 78 pA. These results are consistent with resistivity measurements. A similar trend is also reported for gold films.[10,14]

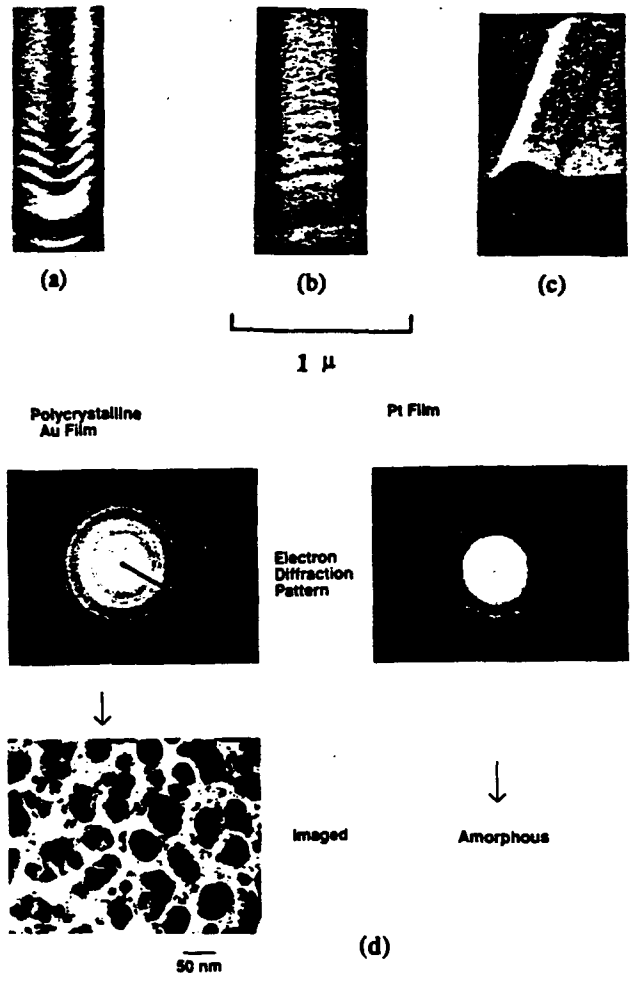

FIG. 1. Platinum deposition induced by focused ion beam on a silicon dioxide 0.1 μm thick on a silicon substrate. (a) A milling only. No Pt precursor gas introduced. Ripples are from oscillations of scan signal; (b) Pt deposition with line width 0.3 μm. Ripples imply that platinum deposition with even finer structure is possible; (c) cross section of Pt deposition; (d) transmission electron microscopy of Pt films grown by focused ion beam induced deposition.

Deposition by higher ion beam currents is of practical importance, because of not only lower resistivity and higher content of platinum, but also a higher growth rate of the film which is achieved at long as the ion current is not so large as to deplete the adsorbed precursor molecules.

B. Deposition in ion milled trench

In packed IC chips, metals leads are usually buried beneath insulating layers. Many ICs in fact have multilayer conductor structures. To repair or reconstruct such multilayers, first a hole or a trench can be milled by a focused ion beam deep into the desired region, and then connections can be made by filling in the hole using ion induced metal deposition. Thus the study of metal deposition in such constrained space is of interest.

Figure 4 shows platinum deposition process in a focused ion milled trench. On a substrate composed of a sandwich of

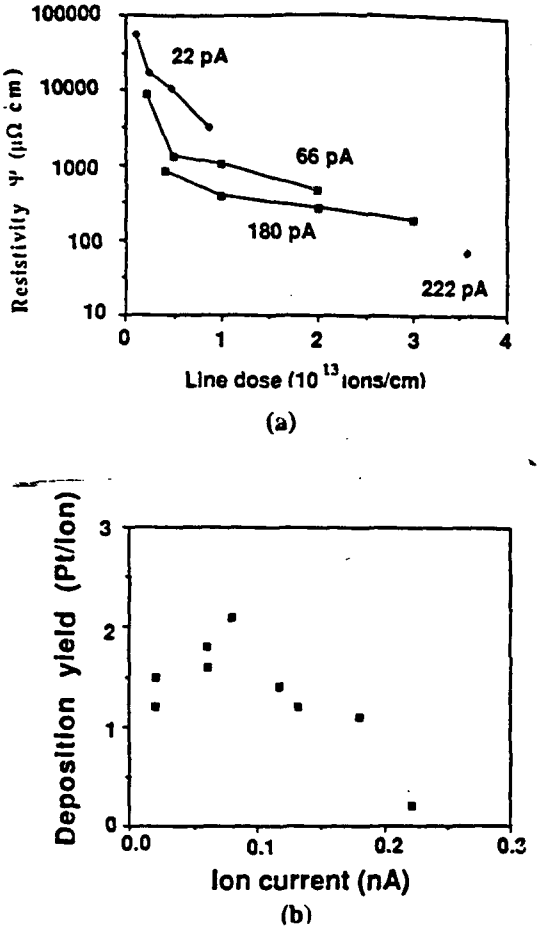

FIG. 2. (a) Resistivity of platinum films as a function of ion line dose at various ion beam current; (b) Platinum deposition yield as a function of ion beam current on silicon oxide. Ga energy 35 keV, scan speed 500 cm/s; line length 350 μm, substrate at room temperature.

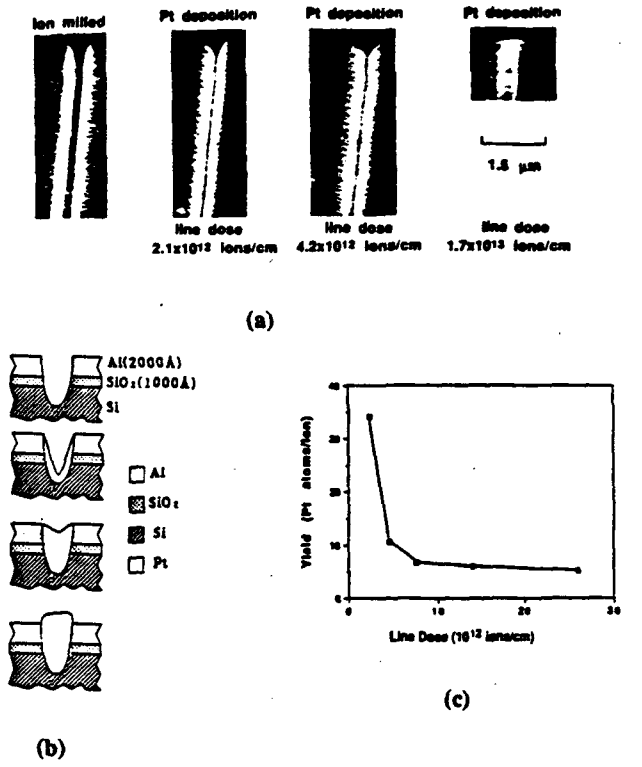

FIG. 4. Platinum deposition in ion milled trench on substrate of aluminum (0.2 μm), silicon oxide (0.1 μm) and silicon at various ion doses. (a) From left to right, Pt deposit fills up the trench as ion dose increases; (b) schematics of Pt filling process; (c) platinum deposition yield variation as trench being filled up. Ga ion energy 40 keV, ion beam current 20 pA, scan speed 50 cm/s.

aluminum (0.2 μm), silicon oxide (0.1 μm) and silicon, a trench 0.7 μm deep is milled by the focused ion beam through the sandwich and into silicon with no precursor gas. With the same ion beam and the Pt precursor turned on, the Pt deposition fills up the trench. A 0.5 μm wide, 1 μm thick, 25 μm long filling connects the first layer of aluminum with underlying silicon substrate. This kind of structure may also be useful in the repair x-ray lithography masks. The yield is found to be 34 at the initial stage of deposition as shown in Fig. 4(c). As the trench is filled up the yield gradually drops to an asymptotic value of about 4, which is about the yield on flat surface. The much larger yield in the constrained space may be due to interaction of adsorbed precursor molecules on side wall surfaces with sputtered particles.

Resistivities of Pt deposited on a flat surface and in an ion milled trench are measured. Ga ion energy is 35 keV and current is 222 pA. The resistivity increases from 70 on the flat surface to 140 $\mu\Omega$ cm in the trench, and the yield increases from 0.2 to 1.3.

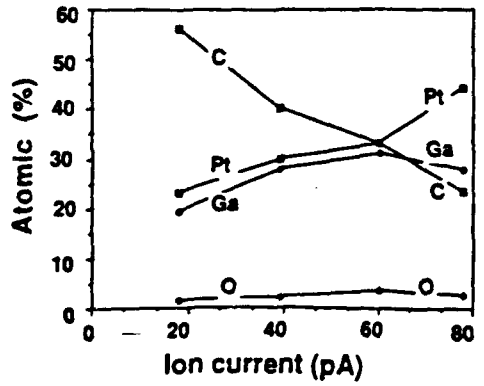

FIG. 3. Auger measurement of Pt film composition as a function of ion beam current on silicon oxide. Ga ion energy 32 keV, deposition area 8 × 8 square micron, ion beam scan frequencies: 80 Hz in x; 4.5 kHz in y.

C. Deposition at near grazing ion incidence

Damage caused by the ion beam can be an issue, for example, if one were to deposit patterned metal films on samples prepared by molecular beam epitaxy. Low energy focused ion beams have been demonstrated,[16,17] but they require floating the samples at high voltage and have larger beam diameters. The angle of ion incidence is known to strongly affect both sputtering and implantation. The sputtering rate generally increases as the angle of incidence departs from the normal while the implantation depth decreases. Little or no damage might be expected at grazing incidence.

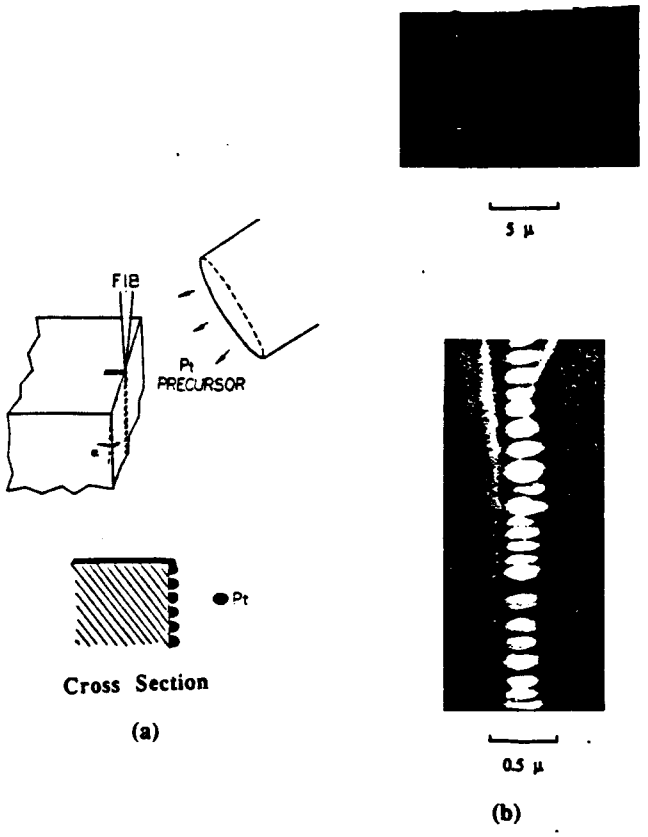

FIG. 5. Platinum deposition at near grazing incidence of ion. (a) Schematics; (b) platinum islands formed. Ga energy 35 keV, ion beam current 20 pA, deposition time 2 min, scan speed 500 cm/s.

Figure 5(a) shows a schematic of platinum deposition at near grazing incidence of the ion beam. Deposition is carried out on the top surface and the cleaved edge of a Si wafer. The cleaved surface is nearly vertical, but the exact angle is hard to determine. Figure 5(b) shows the actual Pt deposition on the nearly vertical face. The deposition appears to occur in discrete ellipsoidal islands each about 0.1 to 0.2 μm thick, 0.2 μm high, and 0.3 μm wide. The width, as expected, corresponds approximately to the beam diameter and the width of the deposit obtained at normal incidence on the top surface. The deposition yield on the nearly vertical face (> 10 atoms/ion) is higher than that observed on the top surface (2–4 atoms/ion). The growth of the discrete islands may be due to a shadowing effect.

D. Effect of hydrogen and elevated substrate temperature

Addition of hydrogen as to the precursor compounds enhances the purity of platinum films in reactions at thermal equilibrium such as chemical vapor deposition[11] and laser induced chemical vapor deposition.[12] We did not observe this effect in the platinum deposition induced by focused ion beam. Within experimental error, resistivity of Pt film does not vary significantly as a function of hydrogen pressure delivered by a second gas jet.

In the case of gold, the resistivity and content of carbon decreases as substrate temperature during deposition increases.[9] At about 120 °C the resistivity is nearly that of pure gold while deposition yield does not drop much. The purity of Pt film does improve as the temperature of the substrate is raised. But the deposition yield drops effectively to zero, the film is so thin that no resistivity and thickness measurement could be made. This may be due to poor adsorption of platinum precursor on the substrate at elevated temperatures.

IV. CONCLUSIONS

Platinum deposition induced by a focused ion beam has been successfully demonstrated. It may find applications in IC chip repair and possible repair of x-ray lithography masks. Deposition in trenches and at near grazing incidence is found to occur with a higher yield.

ACKNOWLEDGMENTS

We are grateful to Libby Shaw of Material Science Center at MIT for the measurement of Auger electron microscopy, and to Patricia G. Blauner now at IBM, Yorktown Heights, for her help in running the focused ion beam machine at an initial stage, and to Diane Stewart and Nick Economou of Micrion Corp., Peabody, MA, for helpful discussions. We also wish to thank James M. Carter for help with scanning electron microscope. This work is supported by ARO contract No. DAAL03-087-K-0126 and by Draper Laboratory.

[1] K. Gamo, N. Takakura, N. Samoto, R. Shimizu, and S. Namba, Jpn. J. Appl. Phys. 23, L293 (1984).
[2] K. Gamo, D. Takehara, Y. Hamamura, M. Tomita, and S. Namba, Microelectron. Eng. 5, 163 (1986).
[3] D. K. Stewart, L. A. Stern, and J. C. Morgan, *Proceedings of Electron Beam, X-Ray and Ion Beam Technologies: Submicrometer Lithographies VIII," March 1989* [SPIE 1089, 18 (1989)].
[4] Z. Xu, T. Kosugi, K. Gamo, and S. Namba, Riken Conference, March 1989; see also J. Vac. Sci. Technol. B 7, 1959 (1989).
[5] Y. Madokoro, T. Ohnishi, and T. Ishitani, Riken Conference, March 1989.
[6] W. P. Robinson, *Proceedings of Electron Beam, X-Ray and Ion Beam Technologies: Submicrometer Lithographies VIII* [SPIE 1089, 228 (1989)].
[7] L. R. Harriott, and M. J. Vasile, J. Vac. Sci. Technol. B 6, 1035 (1988).
[8] G. M. Shedd, A. D. Dubner, C. V. Thompson, and J. Melngailis, Appl. Phys. Lett. 49, 1584 (1986).
[9] P. G. Blauner, J. S. Ro, Y. Butt, C. V. Thompson, and J. Melngailis, J. Vac. Sci. Technol. B 7, 1816 (1989).
[10] P. G. Blauner, J. S. Ro, Y. Butt, C. V. Thompson, and J. Melngailis, *Materials Research Society Proceedings* (MRS, Pittsburgh, 1989), Vol. 129.
[11] H. D. Kaesz, R. S. Williams, R. F. Hicks, Y. A. Chen, Z. Xue, D. Xu, D. K. Shuh, and H. Thridandam, *Materials Research Society Symposium Proceedings* (MRS, Pittsburgh, 1989), Vol. 131, p. 395.
[12] L. V. Koplitz, D. K. Shuh, Y. J. Chen, R. S. Williams, and J. I. Zink, Appl. Phys. Lett. 53, 1705 (1988).
[13] H. P. Fritz and K. Schwarzhans, J. Organomet. Chem. 5, 181 (1966).
[14] P. G. Blauner, J. S. Ro, Y. Butt, and J. Melngailis, J. Vac. Sci. Technol. B 7, 609 (1989).
[15] J. S. Ro, A. D. Dubner, C. V. Thompson, and J. Melngailis, *Materials Research Symposium Proceedings* (MRS, Pittsburgh, 1988), Vol. 101, p. 255.
[16] D. H. Narum and R. F. W. Pease, J. Vac. Sci. Technol. B 6, 966 (1988).
[17] H. Kasahara, H. Sawaragi, R. Aihara, K. Gamo, and S. Namba, J. Vac. Sci. Technol. B 6, 974 (1988).

Focused ion beam induced deposition of platinum for repair processes

Tao Tao*, William Wilkinson**, and John Melngailis

Research Laboratory of Electronics
Massachusetts Institute of Technology
Cambridge, MA 02139

Abstract

Focused ion beam induced deposition of platinum from a gas of (methylcyclopentadientyl) trimethyl platinum has been demonstrated and used for integrated circuit repair. Ga^+ ions in the range of 30-40 keV have been used, and line widths down to 0.3 μm with resistivities as low as 70 μΩcm have been observed. The deposition yield as a function of angle of incidence has been measured by scanning the ion beam across a 2.6 μm diameter pyrex rod. The conductors on an actual integrated circuit have been modified by milling and filling a via to connect two Al lines in a sandwiched configuration as well as by milling two vias through passivation and connecting two adjacent Al lines.

---

*Present Address: Teknor Apex Co. Attleboro, MA 02703
**Also Dept. of Electrical Engineering and Computer Science

To be published J. Vac. Sci. Technol. B.

Introduction:

Focused ion beam induced deposition is a process for growing patterned thin films with submicrometer resolution. A local ambient of an appropriate precursor gas is created on the surface of a substrate where the ion beam is incident. Usually this ambient is created using a capillary tube aimed at the area scanned by the beam. Thus a local pressure can be created up to the 10 mtorr range while a high vacuum (better than ~ 10^{-5} to 10^{-6} torr) exists in other parts of the chamber that houses the ion column. Deposition occurs when the ion beam dissociates adsorbed gas molecules, usually metal halides or organometallics. This process operates equally well with broad ion beams or finely focused ion beams. Numerous gases have been used as precursors such as Al $(CH_3)_3$[1], WF_6[2] [3], $W(CO)_6$[4] or $C_7H_7O_2F_6Au$ [5, 6]. The material deposited often contains a large fraction of impurities such as carbon, oxygen, and the atom species used for deposition, usually Ga. (For a review of the subject and citations of the literature see ref. 7). The only metals which appear to have been deposited with reasonably high purity (~90%) and resistivity approaching the bulk value are Au[8] [9] and tungsten [3]. In most cases, the impurity content is in the 30% to 50% range and the resistivity above 150 μΩcm (ref. 7) compared to the expected values for pure metals which are below 10 μΩcm.

Nevertheless, even at this early state of development focused ion beam induced deposition combined with focused ion beam milling is being used commercially for the repair of photomasks and is being considered for the repair of integrated circuits[4], and for the repair of x-ray lithography masks.[10] Clearly for circuit repair low resistivity deposits are of interest and for x-ray mask repair high Z, high aspect ratio deposits are needed.

Platinum is an attractive metal for focused ion beam induced deposition because, unlike gold, it is not an adverse contaminant of integrated circuits, and its x-ray absorption is slightly higher than that of gold and tungsten in the range of interest. We have previously reported focused ion beam induced deposition of Pt from a precursor gas of (methylcyclopentadientyl) trimethyl platinum[11]. Lines down to 0.3 μm width were obtained, (limited by system operation not by fundamental considerations.) and resistivities of 70 to 700 μΩcm. Higher ion current density on the sample resulted in higher purity, lower resistivity films. Effects of geometry were also reported. For example, the deposition yield inside a trench 0.5 μm wide 0.7 μm deep was found to be a factor of 8 higher than on a flat surface. In both circuit and x-ray mask repair deposition has to be carried out over highly non-planar surfaces so that angles of incidence of the ion beam on the surface other than normal have to be considered.

In this paper we will present results of ion beam induced Pt deposition as a function of incidence angle as well as examples of circuit interconnections made with combined milling and deposition.

Experimental:

The apparatus used has been described previously [6]. It consists of a focused ion beam column differentially pumped by an ion pump, and a UHV, ion pumped chamber with a base pressure of 7×10^{-10} torr. See Fig. 1. During deposition the chamber is pumped by a turbo pump. The two-lens ion column delivers Ga^+ ions of energies between 10 and 50 keV at beam diameters below 0.1 μm. The beam current and minimum diameter can be changed by selecting a beam defining aperture or by moving the beam crossover position relative to the aperture. The precursor gas is delivered to

the surface by a tube with 0.7 mm inside diameter which is connected to a vessel containing the precursor gas. (Methylcyclopentadientyl) trimethyl platinum has a vapor pressure at room temperature of 0.054 torr. To measure resistivity a Pt line is deposited across four lithographically defined conductor fingers (Al in this case). The fingers are connected to contact pads. The resistance of integrated circuit repairs is measured directly with two probes and the series resistance of the Al conductors is subtracted.

Results:

a) Deposition

Figure 2 shows a Pt deposit across an Al conductor on the surface. By measuring the resistance and the cross section of the line the resistivity of this particular film, which was grown at 35 kV and a current of 132 pA, was 300 μΩcm. The time taken to grow this line, 0.3 μm wide and 350 μm long, was 25 min. This implies a yield of 1.2 atoms/ion. Auger analysis of comparable film revealed a composition of 45% Pt, 25% C, 5% O, and 30% Ga. By growing at a higher average current density we were able to obtain 70 μΩcm films.

b) Dependence on incidence angle

In previous ion induced deposition experiments we noticed that the growth rate and yield were dependent on the geometry. In order to quantify this effect we have measured the deposition rate as a function of angle of incidence by depositing over the surface of a cylinder as shown in Fig. 3. The cylinder is a pyrex rod 2.6 μm in diameter. The ion beam is scanned across the cylinder perpendicular to its axis. The precursor gas nozzle is aimed at the

cylinder in the plane defined by the axis of the ion column and the axis of the cylinder. As expected the Pt deposits on half of the circumference which is scanned by the ion beam. Fig. 4 shows the deposit as seen at various viewing angles in an SEM. By measuring the profile of the deposit as a function of angle and calculating the ion current per unit area, which varies from a maximum at normal incidence to zero at grazing incidence, we can calculate the yield as a function of angle of incidence as shown in Fig. 5.

c) Circuit repair

Two types of repairs which use addition of a conductor have been demonstrated, as shown schematically in Fig. 6: a via connecting two intersecting conductors and a "jumper" connecting two parallel conductors. These repairs were carried out on a power supply circuit. For the connecting via a cavity was first milled by scanning the ion beam in a rectangle 4 μm by 5 μm, as shown on the right in Fig. 7. The precursor gas was then introduced, and the cavity was filled with Pt as shown on the left in Fig. 7. The resistance of this connection was 5 Ω and currents up to 100 mA were passed through it with no apparent damage. This suggests also that there is no significant contact resistance between the deposited Pt and the Al.

To connect two parallel conductors which are covered by a passivation layer, Si_3N_4 in this case, two vias are first milled

4 μm by 4 μm, to expose the Al conductors. With the precursor gas flowing the ion beam is scanned in a large rectangle 10 μm by 30 μm which spans the two milled out vias. Using a current of 100 pA a film of about 0.08 μm thickness was deposited in 35 minutes. This is not optimized. Given that high resolution is not required the current can be increased to reduce the writing time per unit area. The resistance of this connection was 290 Ω due to its limited thickness. (~ 0.08 μm) In making this connection the precursor gas nozzle was aimed from the side in Fig. 8. If it is aimed from the top or bottom, the vertical parts of one of the steps will be left uncovered due to shadowing. Note that in Fig. 8 the coverage at the step appears to be thicker than on the flat surface, as expected from our previous results, Fig. 5. We have carried out other repairs where conductors were cut by milling and no degradation of adjacent devices was observed.

Conclusions:

Focused ion beam induced deposition of Pt (with C and Ga as impurities) has been demonstrated down to line widths of 0.3 μm. The yield has been measured as a function of angle of incidence and found to increase rapidly as the grazing angle is approached. Connection of conductors by local deposition of Pt as a circuit repair technique has been demonstrated for crossing metal lines separated by an insulator (SiO_2) or for adjacent lines covered by a passivation layer.

Acknowledgements:

This work was supported in part by the ARO contract No. DAAL03-87-K-0126 and in part by the NRL contract No. N00014-89-2238 under a subcontract from Micrion Corp. to MIT.

References:

1. K. Gamo, N. Takakura, N. Samoto, R. Shimizu, and S. Namba, Japan J. Appl. Phys. 23, L293 (1984).

2. K. Gamo, D. Takehara, Y. Hamamura, M. Tomita and S. Namba, Microelectronic Engineering 5, 163 (1986).

3. Z. Xu, T. Kosugi, K. Gamo, S. Namba, J. Vac. Sci. Technol. B7, 1959 (1989).

4. D. K. Stewart, L.A. Stern and J.C. Morgan, Proceedings "Electron Beam, X-Ray and Ion Beam Technologies: Submicrometer Lithographies VIII", SPIE Vol. 1089, March 1989.

5. G.M. Shedd, A.D. Dubner, C.V. Thompson, and J. Melngailis, Appl. Phys. Lett. 49, 1584 (1986).

6. P.G. Blauner, J.S. Ro, Y. Butt, and J. Melngailis, J. Vac. Sci. Technol. B7, 609 (1989).

7. J. Melngailis and P.G. Blauner, Mat. Res. Soc. Symp. Proc. Vol. 147, p. 127 (MRS 1989).

8. J.S. Ro, A.D. Dubner, C.V. Thompson, and J. Melngailis, Mat. Res. Symp. Proc. Vol. 101 p.255 (MRS 1988).

9. P.G. Blauner, J.S. Ro, Y. Butt, C.V. Thompson, and J. Melngailis, J. Vac. Sci. Technol. B7, 1816 (1989).

10. H.-C. Petzold, H. Burghause, R. Pulzar, V. Weigmann, N.P. Economou, and L.A. Stern, SPIE Vol. 1089, (1989).

11. T. Tao, J.S. Ro, J. Melngailis, Z. Xue, and H. Kaesz, to be published J. Vac. Sci. Technol. B, (Nov/Dec 1990)

Figure Captions:

Fig. 1 Schematic of apparatus for focused ion beam induced deposition.

Fig. 2 A 0.3 μm wide platinum line deposited across an Al conductor.

Fig. 3 Schematic of focused ion beam induced Pt deposition across a pyrex cylinder.

Fig. 4 SEM pictures of the Pt deposition on a 2.6 μm diameter pyrex fiber. The fiber is shown at various angles: 90° is top view where the profile of the depositon is seen in the case of glancing ion beam incidence, 0° shows the profile of the deposit at normal ion beam incidence. Lower figure shows a scale drawing of the measured Pt thickness. The deposition was carried out at 32 keV 25 Pa, with the beam scanned at 5 kHz over a length of 24 μm for 8 minutes.

Fig. 5 Yield of the platinum deposition as a function of angle of incidence, θ, calculated by dividing the relative thickness of the deposit as measured in Fig. 4 by $\cos\theta$.

Fig. 6 On the left is shown a schematic of platinum plug in focused ion beam milled via connecting two intersecting conductors. On the right is a schematic of a Pt connection made between two adjacent conductors.

Fig. 7 On the right is an SEM of a rectangular via milled down to the second conductor. On the left is the same via filled with Pt.

Fig. 8 SEM of a "jumper" of deposited Pt connecting two adjacent conductors. On the right is a closeup of one of the via milled and filled through the passivation.

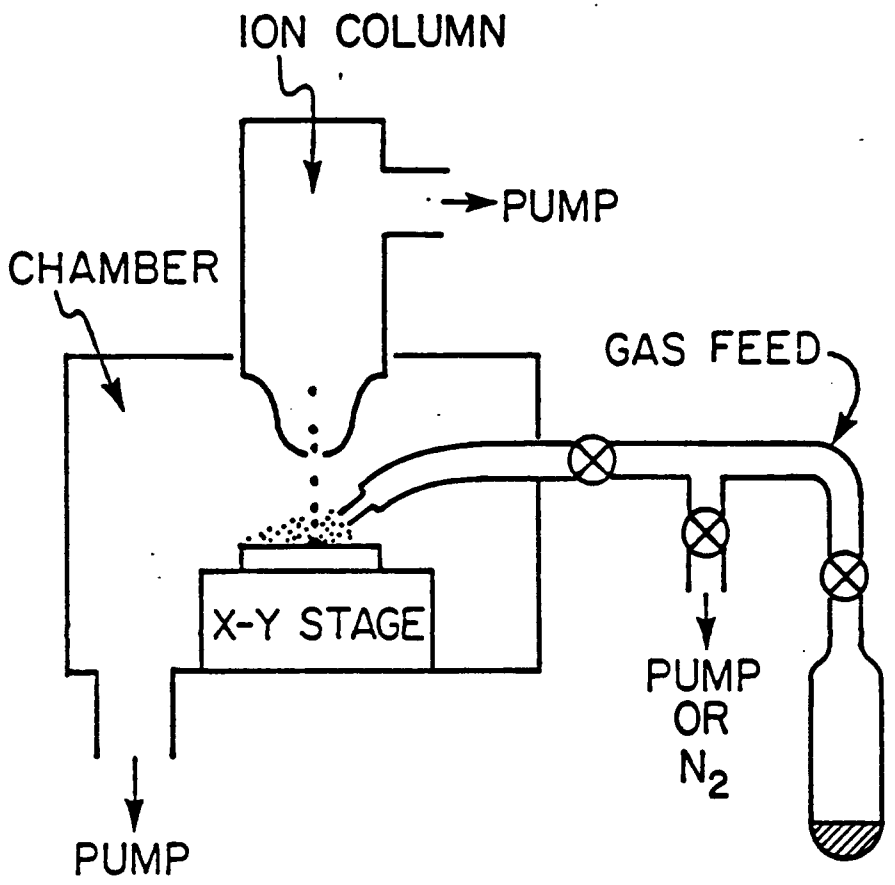

Fig. 1 Schematic of apparatus for focused ion beam induced deposition.

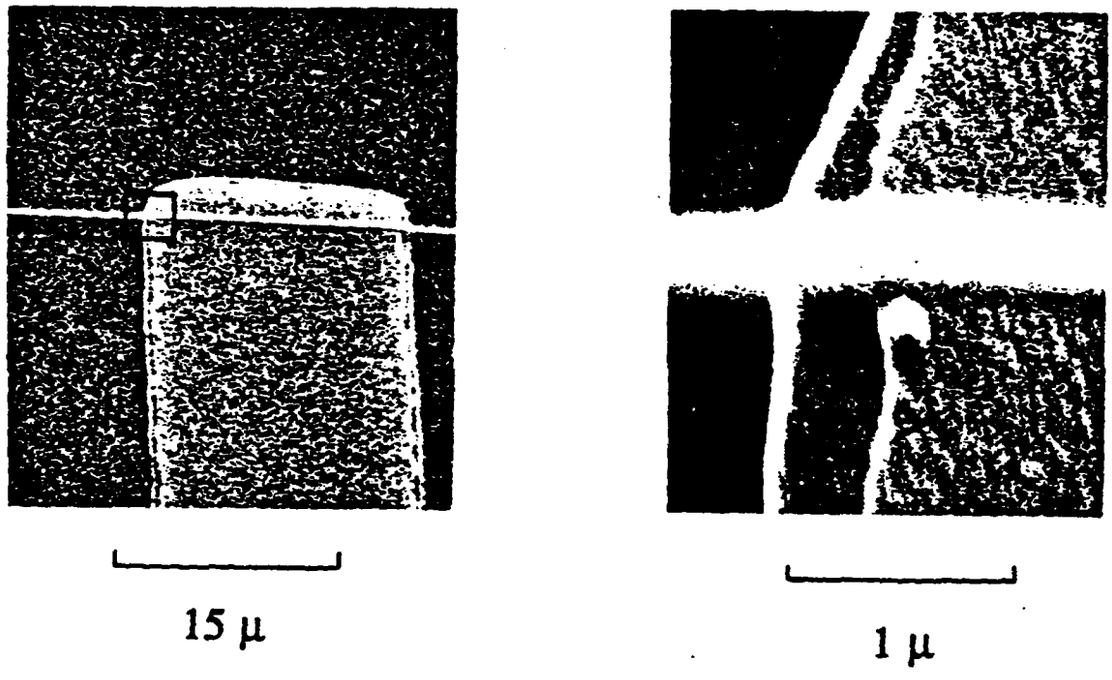

Fig. 2 A 0.3 μm wide platinum line deposited across an Al conductor.

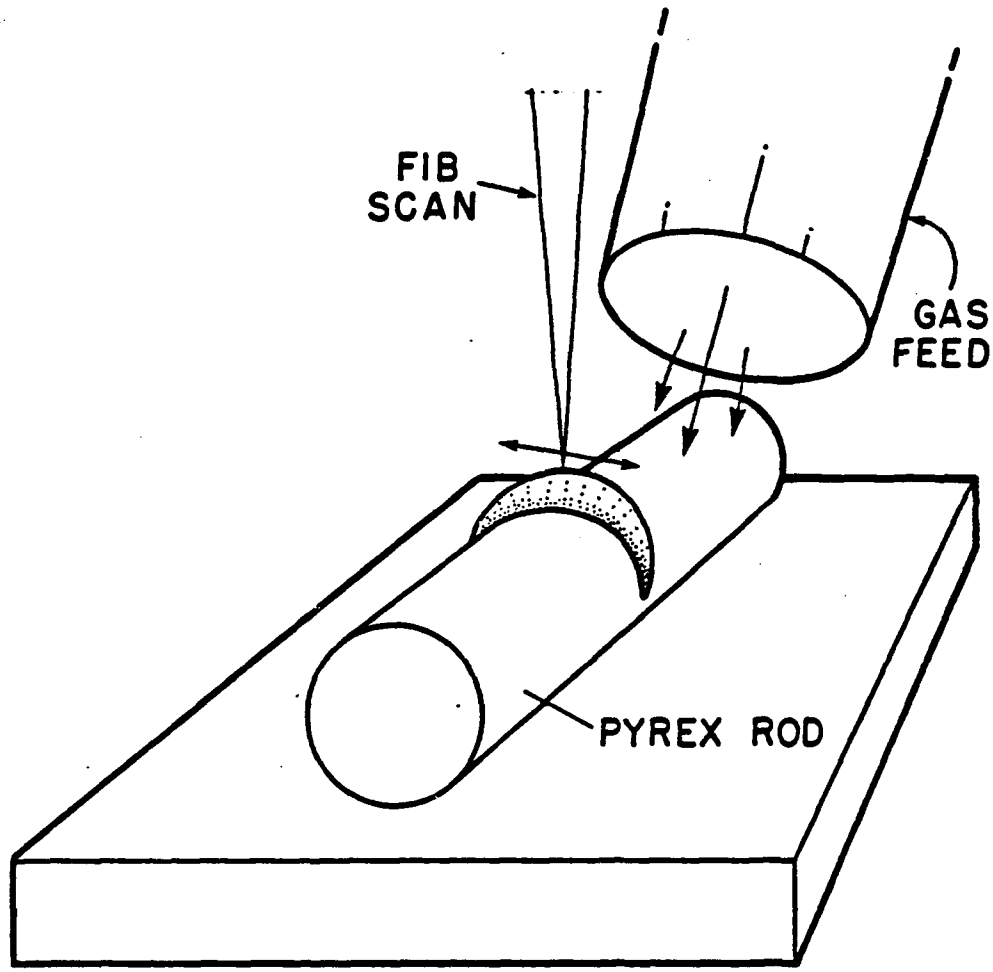

Fig. 3 Schematic of focused ion beam induced Pt deposition across a pyrex cylinder.

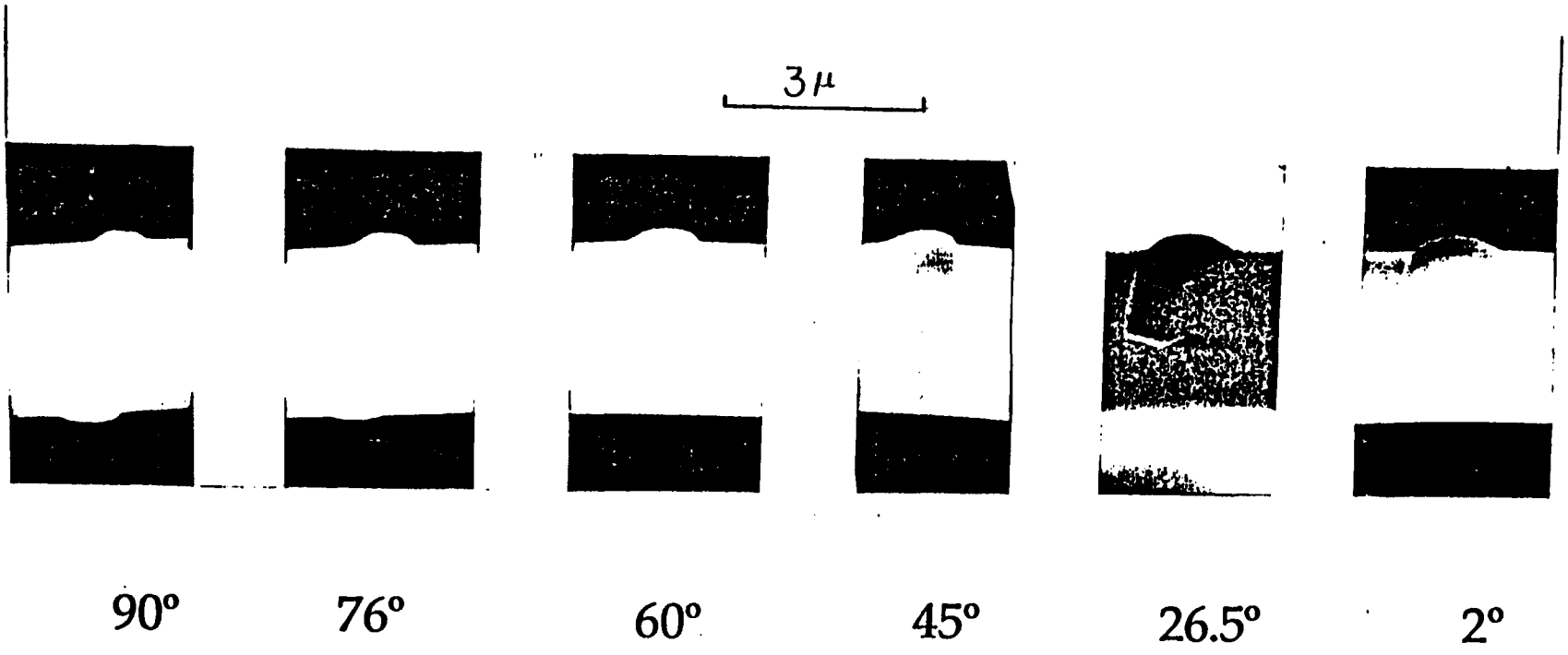

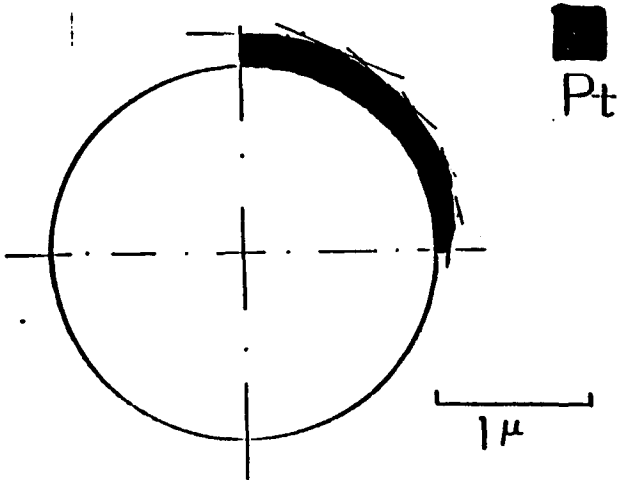

Fig. 4 SEM pictures of the Pt deposition on a 2.6 μm diameter pyrex fiber. The fiber is shown at various angles: 90° is top view where the profile of the depositon is seen in the case of glancing ion beam incidence, 0° shows the profile of the deposit at normal ion beam incidence. Lower figure shows a scale drawing of the measured Pt thickness. The deposition was carried out at 32 keV 25 Pa, with the beam scanned at 5 kHz over a length of 24 μm for8 minutes.

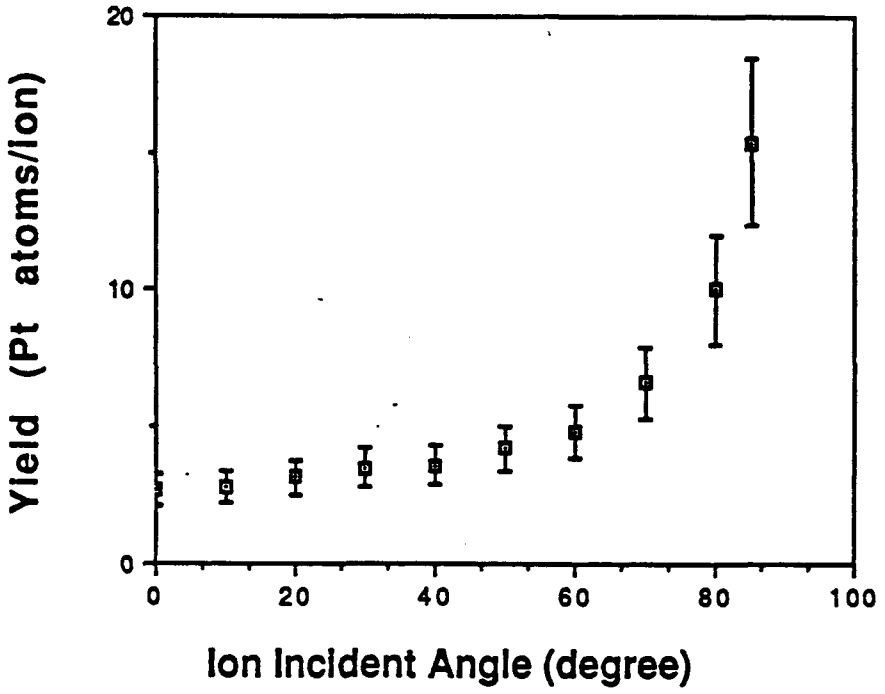

Fig. 5 Yield of the platinum deposition as a function of angle of incidence, θ, calculated by dividing the relative thickness of the deposit as measured in Fig. 4 by cosθ.

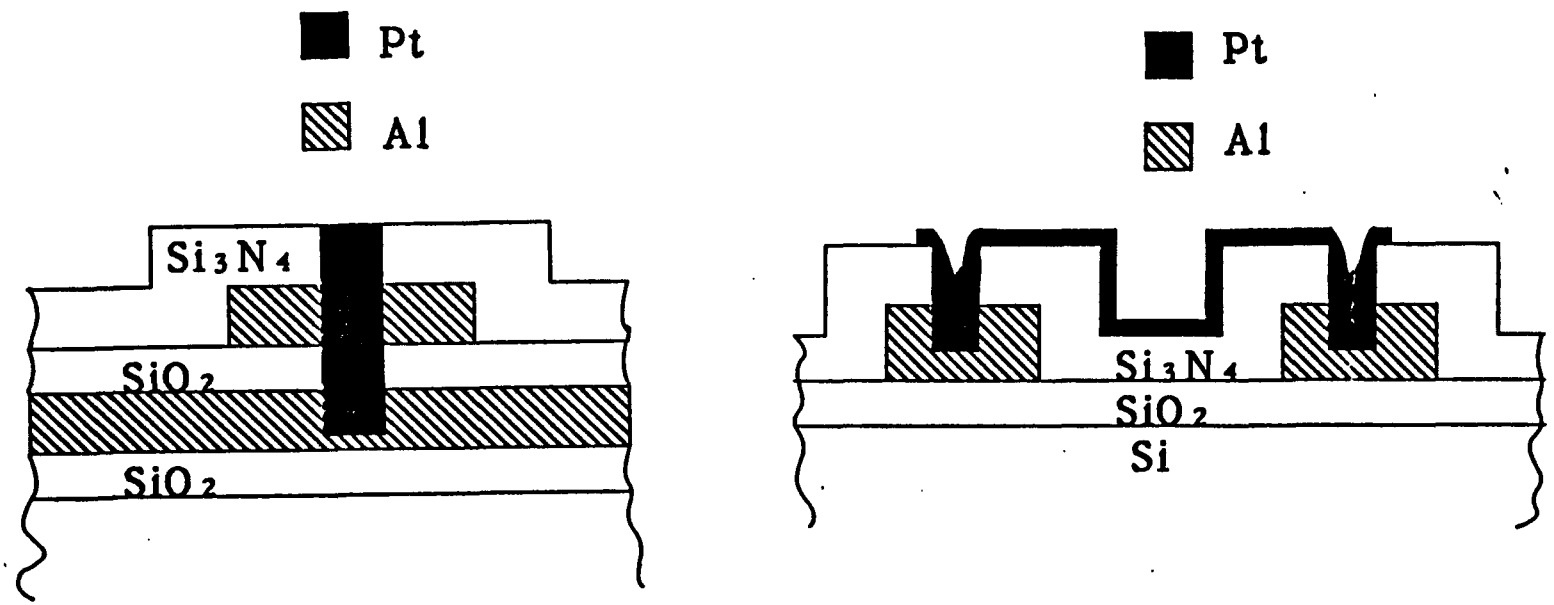

Fig. 6 On the left is shown a schematic of platinum plug in focused ion beam milled via connecting two intersecting conductors. On the right is a schematic of a Pt connection made between two adjacent conductors.

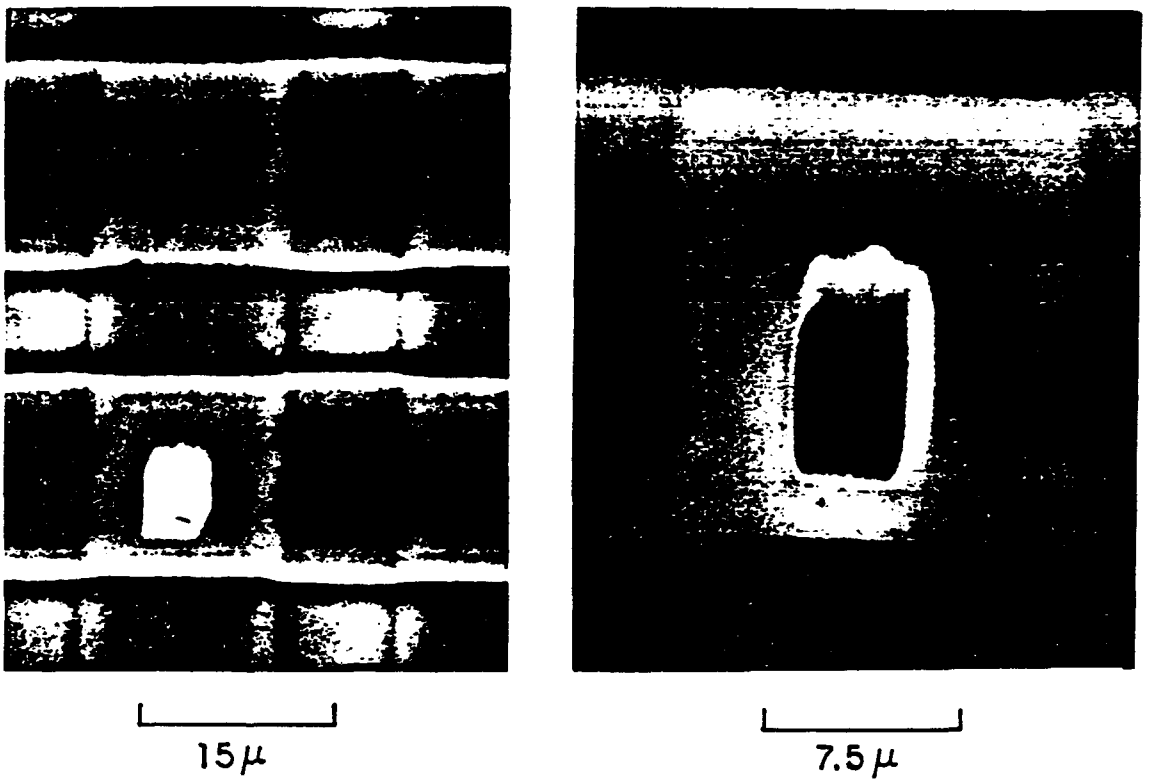

Fig. 7 On the right is an SEM of a rectangular via milled down to the second conductor. On the left is the same via filled with Pt.

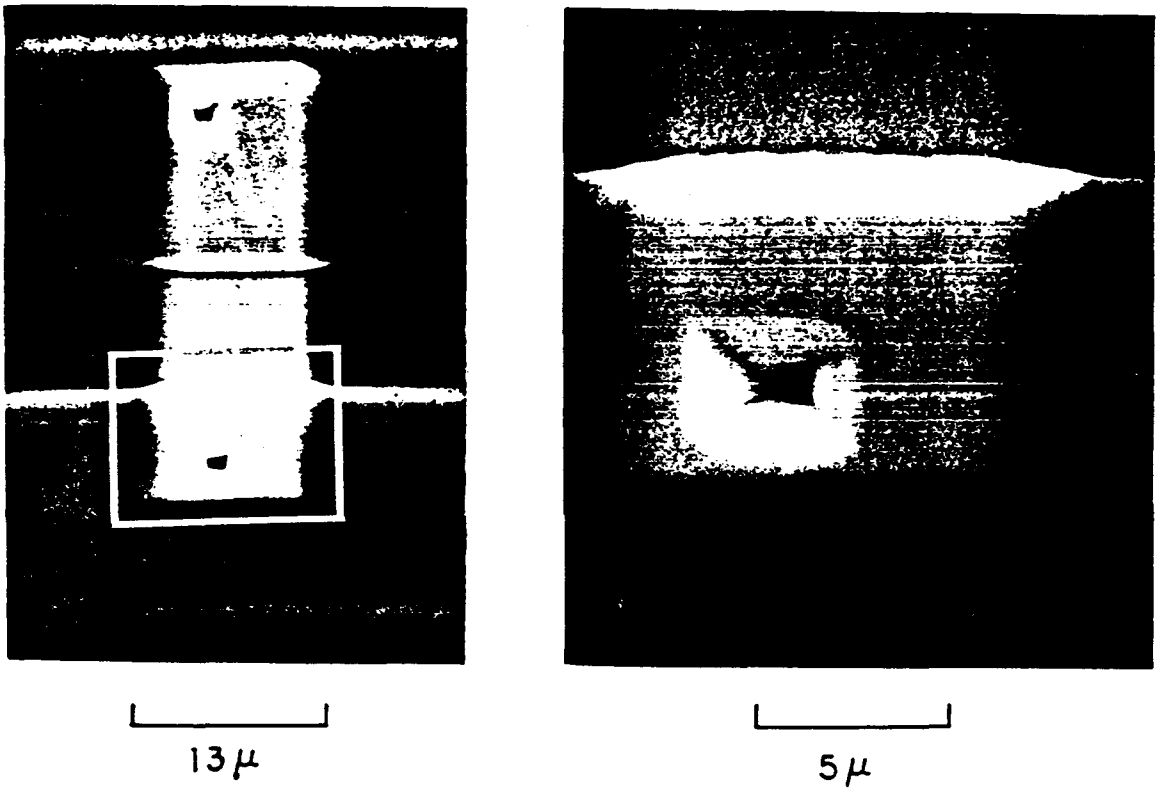

Fig. 8 SEM of a "jumper" of deposited Pt connecting two adjacent conductors. On the right is a closeup of one of the via milled and filled through the passivation.

Appendix IX - Oral Presentations at Scientific Conferences:

November 1987	"Ion Induced Deposition of Gold Films", J.S. Ro, A.D. Dubner, C.V. Thompson, and J. Melngailis, US/Japan Seminar on Focused Ion Beam Technology and Applications Osaka, Japan
December 1987	"Microstructure of Gold Films Grown by Ion Induced Deposition" J.S. Ro, A.D. Dubner, C.V. Thompson, and J. Melngailis MRS Symposium, Boston
March 1988	"Focused Ion Beam Microfabrication" J. Melngailis Invited paper SPIE Symposium on Microlithography, Santa Clara, CA
September 1988	"Focused Ion Beam Induced Deposition of Metals" P.G. Blauner, J.S. Ro, Y. Butt, C.V. Thompson, and J. Melngailis Microcircuit Engineering Conf. Vienna, Austria
October 1988	"Focused Ion Beam Induced Deposition" J. Melngailis Invited paper Amer. Vacuum Society National Symposium, Atlanta, GA
October 1988	"Focused Ion Beam Fabrication of Submicron Gold Structures" P.G. Blauner, J.S. Ro, Y. Butt, C.V. Thompson, and J. Melngailis Electrochemical Soc. Symp., Chicago
March 1989	"Focused Ion Beam Induced Deposition" J. Melngailis and P.G. Blauner Invited paper MRS Symp. San Diego, CA
May 1989	"Focused Ion Beam Induced Deposition of Low Resistivity Gold Films" P.G. Blauner, Y. Butt, J.S. Ro, C.V. Thompson, and J. Melngailis Electron Ion and Photon Beam Symposium Monterey, CA
March 1990	Short course given on "Focused Ion Beam Microfabrication" J. Melngailis, SPIE Symposium, Santa Clara, CA

May 1990 "Focused Ion Beam Induced Deposition"
J. Melngailis (Invited paper)
Electrochemical Soc. Meeting, Montreal, Canada

May 1990 "Focused Ion Beam Induced Deposition of Platinum"
T. Tao, J.S. Ro, J. Melngailis, Z. Xue, and H.D. Kaesz
Electron Ion and Photon Beam Technology Symposium,
San Antonio, TX